Nachweis eines neuartigen Tyrosyl–$Mn^{III}Mn^{III}$ gekoppelten Spinsystems in der Mn-Ribonucleotid-Reduktase von *Corynebacterium ammoniagenes* und *Corynebacterium glutamicum*

Von der Naturwissenschaftlichen Fakultät

der Gottfried Wilhelm Leibniz Universität Hannover

zur Erlangung des Grades

Doktor der Naturwissenschaften

Dr. rer. nat.

genehmigte Dissertation

von

Dipl.-Biol. Patrick Stolle

geboren am 30. April 1980 in Stadthagen.

2010

Referent:	Prof. Dr. rer. nat. Georg Auling
1. Korreferent:	Prof. Dr. rer. nat. Thomas Brüser
2. Korreferent:	Prof. Dr. rer. nat. Dr. h.c. Wolfgang Lubitz
Tag der Promotion:	10. August 2010

Zusammenfassung

Alle Organismen synthetisieren die für die DNA-Kettenverlängerung und Reparatur essentiellen Desoxyribonucleotid-triphosphate (*d*NTPs) mit Hilfe der Ribonucleotid-Reduktase (RNR) (EC1.17.4.1) über einen konservierten radikalischen Mechanismus. Die RNR von *C. ammoniagenes*, kodiert durch *nrdEF*-Gene (*n*ucleotide *red*uction), ist als Manganenzym mit einer $\alpha\beta_2$-Struktur beschrieben. Nach heterologer Expression in *Escherichia coli* wurde jedoch ein Fe-Metallocofaktor im R2F-Protein postuliert. In dieser Arbeit ermöglichte die homologe Expression des *nrdF*-Gens zusammen mit der Entwicklung eines effizienten Chromatographieprozesses die Bereitstellung beliebiger Mengen des Zielproteins, beispielsweise für dessen Kristallisation. Das so gereinigte, native R2F war ein Manganprotein frei von Eisen. Es zeigte hohe enzymatische Aktivität im Komplementationstest (69 µmol × mg^{-1} × min^{-1}) und hat ein für Tyrosylradikale ($Y^{\bullet}$) spezifisches Absorptionsmaximum bei 408 nm. Ein neu entwickelter Enzymtest ergab die direkte Beteiligung an der Ribonucleotidreduktion, indem 0,2 nmol 2'-Desoxycytidindiphosphat unter Beteiligung von 0,4 nmol $Y^{\bullet}$ gebildet wurde. Dieser neue Test erwies sich auch als geeignet für die Suche nach Inhibitoren der RNR, einem wichtigen Angriffspunkt für die Hemmung der Zellproliferation. Erste Hinweise auf eine Kopplung des Tyrosylradikals mit einem benachbarten Metallzentrum ergaben sich durch temperaturabhängige X- / Q-Band EPR-Studien am *C. ammoniagenes*-R2F. Die Röntgenkristallstruktur (PDB 3MJO) des R2F-Proteins zeigt, dass der Metallocofaktor aus einem oxo/hydroxo-verbrückten Mangandimer in einem Abstand von ~8 Å zum Tyrosylradikal (Y115) besteht. Dessen Oxidationszustand wurde mit Hochfeld-EPR (122 / 244 GHz) als $Mn^{III}Mn^{III}$ bestimmt. Es wird ein Mechanismus zur Generierung dieses Metalloradikal-Cofaktors in der Zelle unter Beteiligung von H_2O_2 diskutiert. Mit der vorliegenden Arbeit wird ein langjähriger Disput endgültig geklärt. Das neuartige Tyrosyl-$Mn^{III}Mn^{III}$ gekoppelte Spinsystem wird mit einer Kombination biochemischer Methoden, Röntgenkristallstrukturanalyse und Multifrequenz EPR-Spektroskopie umfassend vorgestellt. Die Manganenzyme von *C. ammoniagenes* und *C. glutamicum* sind im Ordnungssystem der RNRs der Klasse Ib zuzuordnen.

Schlagwörter: *Corynebacterium ammoniagenes*, Mn-Ribonucleotid-Reduktase, Metalloradical-Cofaktor.

Abstract

Deoxyribonucleic acid (DNA) - nature's universal information storage medium - is synthesized from deoxyribonucleotide monomers, which are in all organisms provided by a single enzyme, ribonucleotide reductase (RNR) (EC1.17.4.1). Ribonucleotide substrate conversion occurs via a radical reaction mechanism that is highly conserved. The RNR, encoded by the *nrdEF-genes* (*n*ucleotide *red*uction), is denoted as a manganese-enzyme comprising of a $\alpha\beta$2-structure. Onto heterologous expression in *E. coli*, however, a Fe-metallocofactor was postulated. In this study the homologous expression of the *nrdF*-gene combined with the development of an efficient chromatographic protocol enabled delivery of any quantities of the target protein, for example for its crystallization. The purified, native R2F was a manganese-enzyme free of iron. It showed high enzymatic activity in the standard complementation assay (69 µmol × mg^{-1} × min^{-1}) and had a distinct absorption at 408 nm, characteristic of a tyrosyl radical ($Y^{\bullet}$). A novel enzyme assay revealed a direct involvement of $Y^{\bullet}$ in the ribonucleotidenn reduction as 0.2 nmol 2'-deoxyribonucleotide were formed driven by 0.4 nmol $Y^{\bullet}$. This new test has also proved suitable for the search for inhibitors of RNR, a key target for inhibition of cell proliferation. First evidence for a coupling of the tyrosylradical with an adjacent metal center resulted from X-/ Q-Band temperature dependent EPR studies on *C. ammoniagenes*-R2F. The X-ray crystal structure analysis (PDB 3MJO) of the R2F-protein shows that the metallocofactor consists of an oxo / hydroxo-bridged manganese-dimer at a distance of ~8 Å to the tyrosylradical (Y115). Its oxidation state was determined using high-field EPR (122 / 244 GHz) as $Mn^{III}Mn^{III}$. An *in-vivo* mechanism of metalloradical-cofactor generation by participation of H_2O_2 is discussed. The present work, finally resolves a long dispute. The novel tyrosylradical-$Mn^{III}Mn^{III}$ coupled spin system is presented comprehensively with a combination of biochemical methods, X-ray crystal structure analysis and multi-frequency EPR spectroscopy. The manganese enzymes of *C. ammoniagnes* and *C. glutamicum* were assigned to the class Ib RNRs.

Keywords: *Corynebacterium ammoniagenes,* Mn-ribonucleotide reductase, metalloradical-cofactor.

Inhaltsverzeichnis

Abkürzungen

Abb.	Abbildung
ATCC	American Type Culture Collection
BSA	Bovines Serum Albumin
Bq	Becquerel
C.a., C.g.	*Corynebacterium ammoniagenes, C. glutamicum*
Cm, Cm^r	Chloramphenicol, Chloramphenicol-Resistenz
Da	Dalton
(*d*)ADP, (*d*)ATP	(Desoxy-)Adenosindi-, triphosphat
(*d*)CDP, (*d*)CTP	(Desoxy-)Cytidindi-, triphosphat
(*d*)GDP, (*d*)GTP	(Desoxy-)Guanidindi-, triphosphat
DNA	Desoxyribonukleinsäure
DTT	*DL*-Dithiothreitol
EDTA	Ethylendiamintetraessigsäure
EPR / ESR	Elektronenspinresonanz-Spektroskopie
Fur	Ferric uptake repressor
G	Gauss
HPLC	high performance liquid chromatography
HU	Hydroxyharnstoff
IPTG	Isopropyl-β-D-thiogalactopyranosid
K	Kelvin
KPP	Kaliumphosphatpuffer
M	Molar
Me	Metallion
Mn-RNR	Manganabhängige Ribonucleotid-Reduktase
MntR	Manganese uptake repressor
NADPH	protoniertes Nicotinamid-adenin-dinucleotid-phosphat
nrd	Operon für *n*ucleotide *r*e*d*uction
nrdA, E	Gen für die katalytischen UE der Klasse Ia-RNRs, Ib-RNRs
nrdB, F	Gen für die kleine Untereinheit der Klasse Ia-RNRs, Ib-RNRs
OD_{600}	Optische Dichte, gemessen bei λ = 600 nm
PCET	Proton coupled electron transfer

PS I / II	Photosystem I / II
R1, R1E	Katalytische Untereinheit der Klasse Ia-, Ib-RNRs
R2, R2F	Metallocofaktor der Klasse Ia-, Ib-RNRs
RNR	Ribonucleotid-Reduktase
ROS	Reactive oxygen species
SDS	Natriumdodecylsulfat
T	Tesla
Tab.	Tabelle
TCA	Trichloressigsäure
Y, $Y^{\bullet}$	Tyrosin, Tyrosylradikal
ZFS	Nullfeldaufspaltung (zero field splitting)

Einleitung

Obschon man bei biologischen Prozessen zuerst an organische Verbindungen wie Proteine, Enzyme und Lipide denkt, spielen oft anorganische Komponenten, insbesondere die Übergangsmetalle eine wichtige Rolle. Die Spannweite reicht von der Bindung eines einzelnen Metallions zur Strukturstabilisierung der Proteinmatrix (Rigby Duncan & Stillman, 2006) über die Beteiligung an der Proteinfaltung (vergl. 5.1.1) bis hin zu komplexen Multicenter-Redoxproteinen, wie sie beispielsweise im Photosystem II (vergl. 5.2) an mehrstufigen Elektronen-Transferprozessen beteiligt sind (Dau & Haumann, 2007; Sharp & Chapman, 1999). Die Tatsache, dass die Beteiligung von Metallionen in biologischen Systemen im Laufe der Evolution erhalten blieb legt den Schluss nahe, dass sie essentielle Eigenschaften besitzen, die von organischen Molekülen allein nicht oder nur unzureichend geleistet werden können. Die Verwendung spezifischer Metalle für bestimmte biologische Funktionen hat neben charakteristischen Faktoren, wie Größe, Geometrie und Valenz, auch weitere Gründe. Neben der Abundanz eines Metalls in Habitaten, ist auch die Bioverfügbarkeit, also die Zugänglichkeit eines Metalls für einen Organismus, ein entscheidender Faktor. Eisen zum Beispiel hat einerseits eine hohe Abundanz, mit 4,7 Prozent ist es das viert häufigste Element in der Erdkruste, andererseits liegt es aufgrund der oxischen Atmosphäre als schwer lösliches $Fe(OH)_3$ vor. Seine Bioverfügbarkeit ist daher mit durchschnittlich 10^{-18} M streng limitiert (Grotzinger et al., 2007) und liegt weit unter dem Bedarf proliferierender Zellen. Im Laufe der Evolution entwickelte sich eine Vielzahl effizienter Metall-Aufnahmesysteme, die eine Mobilisierung schwer löslicher Metalle durch sekretierte Chelatoren ermöglichten. Die komplexierten Ionen können anschließend über spezifische Rezeptoren durch die Zellmembran in das Zellinnere transportiert werden, wo das importierte Metallion direkt verwendet oder in Speicherformen gelagert wird (Drechsel & Winkelmann, 1997). Neben den essentiellen Eigenschaften von Metallen darf man ihre toxischen Wirkungen auf die Zelle jedoch nicht außeracht lassen. Metalle sind unterschiedlich toxisch, das bedeutet, dass ihre intrazellularen Konzentrationen streng kontrolliert und reguliert werden müssen. Zur Aufrechterhaltung dieser Homöostase (vergl. 5.1.3) haben Mikroorganismen eine Vielzahl von teils hochspezifischen Im- und Exportmechanismen durch die schützende Zellmembran entwickelt (Arino et al., 2010; Moore & Helmann, 2005).

5.1 Metalloproteine

Durch die ersten Untersuchungen an der Photosyntheserate von *Chlorella,* in Abhängigkeit der Zugabe verschiedener chemischer Elemente, zeigte Pirson, dass Mangan essentiell für das Wachstum dieser Algen ist (Pirson, 1937). Der biochemische Hintergrund blieb zu diesem Zeitpunkt aber ungeklärt (vergl. 5.2). Mit dem Nachweis eines proteingebundenen Übergangsmetalls, nämlich Nickel, in der katalytisch aktiven Urease von *Canavalia ensiformis,* die bereits 50 Jahre zuvor als erstes Protein kristallisiert worden war (Sumner, 1926), wurde das erste Metalloprotein beschrieben (Dixon et al., 1975). Mittlerweile geht man davon aus, das fast die Hälfte aller Proteine ein Metall für ihre biologische Funktion benötigen (Andreini et al., 2008). Es stellt sich die Frage, welche einzigartigen Eigenschaften die Bindung eines Metalls mit sich bringen. Im Zinkfingerprotein ist ein Zinkion (Zn^{2+}) koordinativ über zwei Histidine und zwei Cysteine in der Zn-Fingerdomäne gebunden. Hierdurch nimmt die Domäne eine schleifenförmige Struktur an, die spezifisch mit DNA und RNA interagieren kann. Es erscheint also nicht verwunderlich, das Zinkfingerproteine eine wichtige Rolle in der Funktion von Transkriptionsfaktoren spielen (Schleif, 1988). Ein weiteres Beispiel der Strukturfunktion eines Metalls ist das in der Pyruvatcarboxylase koordinierte Mangan (Jitrapakdee et al., 2002). Neben den einfachen, strukturgebenden Eigenschaften können Metalle direkt an katalytischen Prozessen beteiligt sein. Sie können als Lewis Säure/Base die Nucleo- oder Elektrophilie der Reaktionspartner modifizieren, als Elektronendonatoren oder Akzeptoren fungieren, zur Radikalerzeugung verwendet werden und am Elektronentransport beteiligt sein und (Waldron et al., 2009).

An der Wasseroxidation im Photosystem II (PSII) sind mehrere Mangan-Redoxenzyme beteiligt (siehe Kapitel 5.2). In diesem Zusammenhang ist die Mangan Katalase aus *Lactobacillus plantarum* zu nennen, deren Cofaktor einen putativen $Mn(III)_2$-(μ-oxo)-(μ-$O_2CR)_2$ Zustand durchläuft (Riggs-Gelasco et al., 1995). Die Rolle eines di-μ-carboxylato verbrückten $Mangan(II)_2$ als Cofaktor der Arginase (Kanyo et al., 1996) ist es, die die Degradation von Arginin zu Ornithin katalysieren. Ein zusätzlich am Metallzentrum koordiniertes Wassermolekül kann durch dieses leichter deprotoniert und das Substrat nucleophil angegriffen werden. Auch für das Enzym Glutamin-Ligase ist ein vergleichbarer nucleophiler Angriff durch zwei koordinierte Mn(II)-Ionen beschrieben (Yamashita et al., 1989). Eine nähere Betrachtung des Metallzentrums manganabhängiger Proteine zeigt, dass hier bevorzugt Asparaginsäure, Histidin und Glutaminsäure zur Koordinierung des Metalls

vorhanden sind (Christianson, 1997). In der Arginase der Rattenleber wird das Mn_2-Zentrum durch sechs dieser Aminosäuren koordiniert (Khangulov et al., 1998). Dieses Ligandenfeld findet sich nicht nur zur Koordination von Mangan, sondern ist auch beim Eisencofaktor der Klasse Ia RNR von *E. coli* konserviert (Högbom et al., 2002). Mononucleare Manganenzyme nutzen im Prinzip die gleichen Liganden, die Koordination des einzelnen Metalls erfolgt dann über vier Aminosäuren.

5.1.1 Biosynthese von Metalloproteinen

Grundsätzlich können Metalloproteine, anhand der Biosynthese ihres Metallocofaktors, in drei Gruppen eingeteilt werden. Bei Proteinen der ersten Gruppe, wird der Metallocofaktor durch Koordination mit funktionellen Gruppen der Polypeptidkette gebunden. *In-vitro* gelingt in vielen Fällen ein Metalleinbau ohne die Beteiligung eines zusätzlichen katalytischen Mechanismus, jedoch verläuft dieser oft sehr langsam und ohne charakteristische Metallselektivität, (Merchant & Dreyfuss, 1998) so dass die Beteiligung von Transportsystemen, den Metallochaperonen (vergl. Kapitel 5.1.4) wahrscheinlich wird. Die zweite Metalloproteingruppe besitzt anorganische Metallcluster, deren Synthese von der Proteinbiosynthese entkoppelt abläuft. Die Synthese eines Eisen-Schwefelclusters verlangt z.B. die gezielte Bereitstellung von Eisen aus Speicherkomplexen, wie Ferritin (Arosio et al., 2009) sowie die Desulfurylierung von Cystein als Quelle für Schwefel (Zheng et al., 1993). Unter Beteiligung von Gerüstproteinen (vergl. Abb. 1) wird dann die Assemblierung des anorganischen Clusters durchgeführt und. Der fertige Metallcluster wird dann in das aktive Zentrum des Zielproteins transportiert. Die Metalloenzyme der dritten Gruppe besitzen einen organischen Metallocofaktor, wie beispielsweise die Cytochrome. Die Biosynthese von Protein und Cofaktor läuft ebenfalls getrennt voneinander ab. Der anschließende Einbau des organischen Metallocofaktors erfolgt zum Teil nach weiteren Modifikationen, durch spezialisierte Metallochaperone. Neben der inzwischen gut verstandenen Assemblierung des Cytochrom c Oxidase-Komplexes *(Khalimonchuk & Rodel, 2005; Kranz et al., 2009)*, scheint die nach 30 Jahren intensiver Bearbeitung, mittlerweile exzellent verstandene Assemblierung des Eisen-Molybdän-Cofaktors (FeMo-Co) der Nitrogenase (NifDK), als Modell für die komplexe Biosynthese von Metalloproteinen (Curatti et al., 2007; Rubio & Ludden, 2008) gut geeignet und wird im Folgenden besprochen. Der größte Anteil der biologischen Stickstofffixierung wird durch die Nitrogenase katalysiert. Das in Abb. 1 präsentierte Schema der FeMo-Co Assemblierung wurde um das zentrale Gerüstprotein NifEN aufgebaut. In diesem werden die FeMo-Co-Vorläufer [Fe-S]-Cluster, Molybdän und Homocitrat zusammengebracht. (Corbett

et al., 2006; George et al., 2007; Hu et al., 2006a; Hu et al., 2006b; Soboh et al., 2006) Hierzu wird der Eisen-Schwefel Cluster unter Beteiligung einer Cystein-Desulfurase (NifS) und des NifU-Stützproteins, im S-Adenosylmethionin abhängigen NifB synthetisiert (Zhao et al., 2007) und anschließend von NifX auf NifEN transferiert (Hernandez et al., 2007). Das erforderliche Homocitrat wird durch die Homocitratsynthase NifV bereitgestellt und über NifH an NifEN gebunden. Der vollständig assemblierte FeMo-Cofaktor wird dann von einem Chaperon (NafY) gebunden und auf das apo-NifDK transferiert (Rubio & Ludden, 2008).

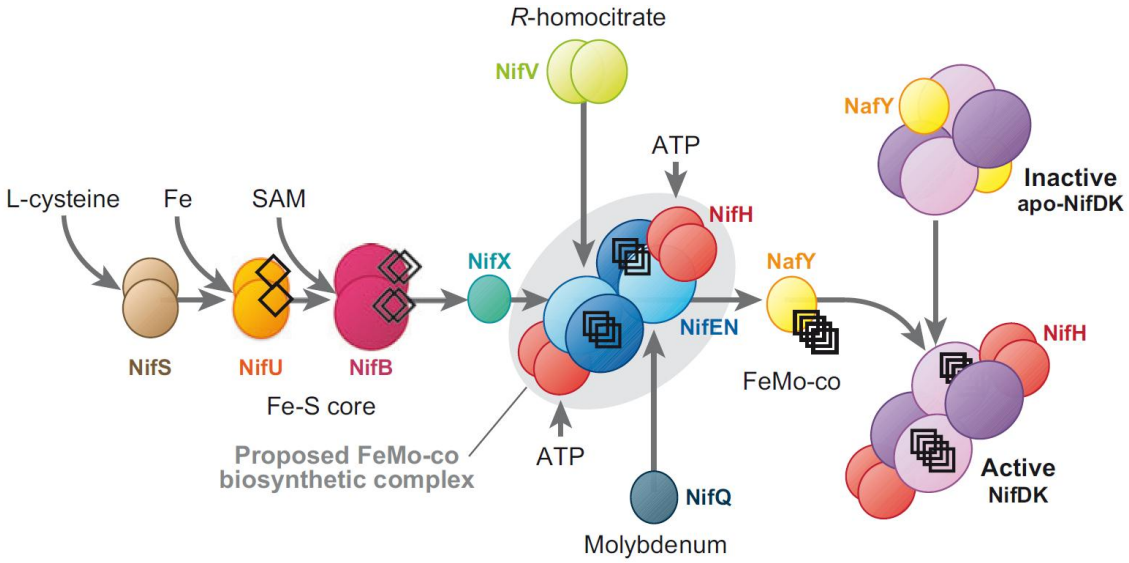

Abb. 1: Schematische Darstellung der Eisen-Molybdän Cofaktor (FeMo-Co) Biosynthese der Nitrogenase. Die Assemblierung der FeMo-Co Vorläufer zum fertigen Cofaktor wird im NifEN/NifH Enzymkomplex abgeschlossen. *De-novo* synthetisierte FeMo-Co wird in apo-NifDK zur Generierung der katalytisch aktiven Nitrogenase inseriert. An dem hier gezeigten FeMo-Co Biosyntheseweg sind Enzyme, Stützproteine sowie Chaperone für die komplexen Metallocluster beteiligt. Die schwarzen Rechtecke stellen die strukturelle Komplexität der FeMo-Co Vorläufer dar. Abbildung aus (Rubio & Ludden, 2008).

5.1.2 Metallspezifität & Metallochaperone

Jedes Metalloprotein muss die korrekte Aufnahme von Metallen sicherstellen. Die Stabilität von Metallionen (vergl. Irving-Williams Reihe) wird auch in der proteingebundenen Form beibehalten. Mit steigender Kernladungszahl sinkt die Abschirmung der 3d-Orbitale und der Ionenradius nimmt ab, wodurch die Lewis-Säurestärke zunimmt. Daraus resultiert, das Kupfer und Zink die stabilsten Komplexe bilden, gefolgt von Ni < Co < Fe < Mn < Ca und Mg, das die labilsten Komplexe bildet (Irving & Williams, 1948). Die Metallspezifität der reaktiven Zentren sowie die Eigenschaften der gebundenen Metalle werden durch die jeweiligen Liganden und die umgebende Proteinstruktur beeinflusst. So können Ionen falscher Ladung

oder durch die vorgegebene Koordinationsgeometrie von der Bindung im Apoprotein oder sogar schon früher während der Faltung, ausgeschlossen werden. Diese Spezifität ist insbesondere bei naszierenden Polypeptiden noch nicht vollständig ausgebildet, so dass hier der größte Anteil der Ligandenstabilisierungsenergie vom Metall selbst ausgeht und somit die Affinität für ein Metall der Irving-Williams Reihe folgen würde. Das Proteine allein aufgrund ihrer Affinität (Liganden, Koordinationsgeometrie) in einem einzigen Schritt das benötigte Ion aus dem inhomogenen cytosolischen Metallmix binden können, ist unwahrscheinlich. Hierfür bedarf es weiterer Mechanismen, die nachfolgend beschrieben werden.

5.1.3 Metallhomöostase

Um den Metallbedarf der Zelle zu gewährleisten, muss die schützende Zellmembran, die eine freie Diffusion von Metallionen in das Zytosol verhindert, kontrolliert überwunden werden. Metalloregulatorische Proteine erkennen intra- und extrazelluläre Konzentration von Metallionen, und können entsprechend die Expression an der Homöostase beteiligter Systeme regulieren (Finney & O'Halloran, 2003). Unter Metall limitierten Bedingungen werden Metallionen und chelatierte Metallkomplexe aktiv in die Zelle transportiert (Hantke, 2001). In *Bacillus subtilis* werden Metall-Influxsysteme durch den spezifischen „ferric uptake repressor" (Fur) (Bsat et al., 1998), sowie die Paraloge Zur (Zink) (Gaballa & Helmann, 1998; Gaballa et al., 2002), CueR (Kupfer)(Changela et al., 2003), MntR (Mangan)(Que & Helmann, 2000) und den Peroxidstresssensor PerR reguliert (Bsat et al., 1998; Herbig & Helmann, 2001). Durch die Beschreibung eines nickel-uptake regulators" (Nur) in *Streptomyces coelicolor* wurde die Fur-Familie um ein weiteres Paralog erweitert (Ahn et al., 2006). Übersteigt die cytosolische Konzentration hingegen den Normbereich werden Metalleffluxsysteme (ArsR, CzrA, NixA und SmtB) durch die Bindung eines (teilweise unspezifischen) metallischen Effektors, Me(II) / Me(III) induziert, so dass nach Translation der Systeme, ein aktiver Export aus der Zelle ermöglicht wird.

In diesem Zusammenhang wurde ein erstes Mn(II)-reguliertes Effluxsystem (MntE) bei *Streptococcus pneumoniae* beschrieben (Jakubovics & Valentine, 2009). Tab. 1 fasst die an der Homeostase beteiligten Systeme und ihre Orthologe zusammen.

Tab. 1: Metall Transporter - Genetische Kodierung und Regulation, modifiziert nach (Moore & Helmann, 2005).

Familie	Operon(s)	Regulatoren	Import	Export
ABC-Transporter	*feuABC yusV*	Fur	Fe(II)-Siderophor	
	fhuBGCD	Fur	Ferrichrom	
	fhuBGC yxeB	Fur	Ferrioxamin	
	yfiZ yfhA yusV	Fur	Fe(II)-Siderophor	
	yfmCDEF	Fur	Fe(II)-citrat	
	mntABCD	MntR	Mn(II)	
		MntE		Mn(II)
	PsaBCA	PsaR	Mn(II)	
	ycdHI yceA	Zur	Zn(II)	
	yvrCBA	Riboswitch	Cobalamin	
CDF	*czcD*	CzrA MntE		Zn(II), Cd(II), Mn(II)
NRAMP	*mntH*	MntR	Mn(II)	
P-Typ ATPase	*zosA*	PerR	Zn(II)	
	cadA	CzrA		Cd(II)
	copA	CueR		Cu-CopZ
	yloB	n.n.	Me(II)	
FTS3	*ywbLMN*	Fur	Fe(III)	
ACR3	*arsB*	ArsR		As(III)
ArsB	*aseA ydfA*	ArsR		As(III)
MeCit	*citH*	---	Ca(II)-citrat	
	citM	CitST TCS	Me(II)-citrat	
CorA	*yqxL*	n.n.	Mg(II)	
MgtE	*ykoK*	n.n.	Mg(II)	

Das Fur Regulon von *B. subtilis* (Fur_{BS}) umfasst 39 Gene, organisiert in 20 Operons, die in erster Linie für Enzyme der Siderophorsynthese sowie Eisen-Siderophoraufnahmesysteme kodieren (Baichoo et al., 2002). Fur_{BS} ist ein DNA-bindendes Protein, das pro Monomer einen strukturellen Zn(II)-Kern, sowie die regulatorisch aktive Fe(II)-Bindestelle enthält. In der Fe(II) besetzten Form bindet Fur_{BS} als Dimer an einer 19 bp Konsensussequenz der DNA, die ein konserviertes 14 bp Fur-Bindemotiv (GATAATnATTATAC) trägt, und repremiert sämtliche Promotoren an der Eisenaufnahme beteiligter Systeme (Baichoo & Helmann, 2002). Es folgt die Translationsinhibierung der Gene des *dhb Operons (May et al., 2001),* zuständig für die Dihydroxybenzoat-Siderophor (Corynebactin) Biosynthese, sowie vier weiterer ABC–Transporter für Corynebactin, Hydroxamatsiderophore, Eisencitrat und Fe(III)-Permeasekomplexe (Baichoo et al., 2002; Schneider & Hantke, 1993). Die Inaktivierung des Fur Repressors, und somit der Translation der Eisenimportsysteme, kann neben Eisenmangel auch durch weitere externe Bedingungen ausgelöst werden. Stickstoffmonoxid, oder davon abgeleitete radikalische Verbindungen wie Peroxynitrit, führen zur Nitrosylierung des Fur

Fe(II)-Kerns und folglich zu dessen Inaktivierung (Moore et al., 2004). Bei Fur_{Ec} wird Derepression auch durch erhöhte Mn(II)-Ionen Konzentrationen erzielt, die anstelle von Fe(II) im Repressor strukturell gebunden werden (Guedon et al., 2003). Neben den hier besprochenen regulatorischen Mechanismen wurde auch eine Beteiligung von Fur an der Virulenz von Mikroorganismen beschrieben (Delany et al., 2001; Delany et al., 2004). Kürzlich wurde auch die Beteiligung von Glutaredoxinen, primär katalysieren sie die Oxidoreduktion von Glutathion, in der intrazellularen Eisenregulation von *Saccharomyces cerevisiae* gezeigt (Rouhier et al., 2010). Glutaredoxine sind im Gegensatz zu Fur nicht direkt an der Mobilisierung oder dem Transport von Fe(II) beteiligt. Ihre Aufgabe ist es, als Gerüstproteine für die *de-novo* Synthese von Eisen-Schwefel-Clustern oder als temporäre Speicher von generierten Fe-S Clustern zu dienen, wodurch die Konzentration freier Eisenionen in der Zelle herabgesetzt wird und sie somit einen Beitrag in der Eisenhomöostase leisten (Rouhier et al., 2010). In Gram-positiven Bakterien reguliert DtxR, ein funktionelles Fur-Ortholog, einen Mn(II)-ABC-Transporter (*mntABCD*) sowie das Homolog (*mntH*) eines eukaryotischen „natural resistance-associated macrophage protein" kurz Nramp Transporters (Guedon et al., 2003; Hantke, 2001). Nickel dient als Cofactor einiger mikrobieller Enzyme, wie z.B. der Hydrogenase (Mulrooney & Hausinger, 2003b). Der Nickelimport erfolgt mit Hilfe eines ABC-Transporters (NikABCDE), gebunden als Metallophor, sowie mittels einer HoxN Permease (NixA). Die Regulation dieses Transporters erfolgt mit Hilfe des Nickel-Responsive Repressor (NikR), einem 15 kDa Protein, das eine N-terminale DNA sowie C-terminalen Nickelbindedomäne besitzt (Chivers & Sauer, 2000). Dieser Repressor reguliert die Translation des Nickel ABC-Transporters (*nikABCDE*) (Mulrooney & Hausinger, 2003b). In Gegenwart gesteigerter cytoplasmatischer Nickelkonzentrationen, bindet NikR an eine palindromische Sequenz der *nikA* Promotorregion (GTATGA-16N-TCATAC) (Chivers & Sauer, 2002) und inhibiert die Translation des *nikABCDE*-Genclusters (Ahn et al., 2006). In *E. coli* wurde neben NikR, RcnR als ein weiterer Regulator der Nickel-Homöostase beschrieben (Iwig et al., 2006). Er reguliert die Expression des Nickel-Effluxproteins (RcnA) (Rodrigue et al., 2005). Die intrazellulare Speicherung erfolgt über das Hpn Protein, einem histidinreichen Protein ähnlich dem Metallothionin, dessen Expression durch NikR hochreguliert wird (Ge et al., 2006). Darüber hinaus ist NikR von auch an der Regulation der Cofaktorsynthese einer Superoxiddismutase (SOD) beteiligt. Die Bindung von NikR an die Promotorregion inhibiert die Expression des *sodF*Gens und induziert die Expression einer Ni-abhängigen SOD.

5.1.4 Metallochaperone

Ein weiterer Mechanismus sicherzustellen, dass ein korrektes Metall in das zu assemblierende Metalloprotein gelangt, ist die Verwendung von Metallochaperonen. Diese Hilfsproteine binden zunächst ein spezifisches Metallion und transferieren es dann auf das spezifische Zielprotein mittels Liganden-Austauschreaktionen (Furukawa et al., 2004; Pufahl et al., 1997). Die Art (Geometrie, Ladung, Hydrophobizität) des Protein-Proteinkontakts sorgt ebenfalls dafür, dass nur die korrespondierenden Proteine Zugriff auf das zu transferierende Metall erhalten. Ein Sonderproblem stellt freies Kupfer dar, da es für Zellen äußerst toxisch ist und in der Zelle ausschließlich in gebundener Form vorliegen darf. Die strikte Verwahrung des einerseits benötigten, andererseits toxischen Metalls muss durch einen effektiven Kupfertransports, der auch während der Protein-Proteinübergabe eine sichere gebundene Form sicherstellt, gewährleistet sein. Der cytosolische Kupferdetektor CueR reguliert die Translation einer Typ P_1 ATPase (CopA) und einer Multikupfer-Oxidase (CueO). Letztere bindet vier Kupferionen, wodurch sich ihre Konformation ändert. In diesem gefalteten Zustand wird sie anschließend über den TAT-Weg ins Periplasma exportiert (Finney & O'Halloran, 2003).

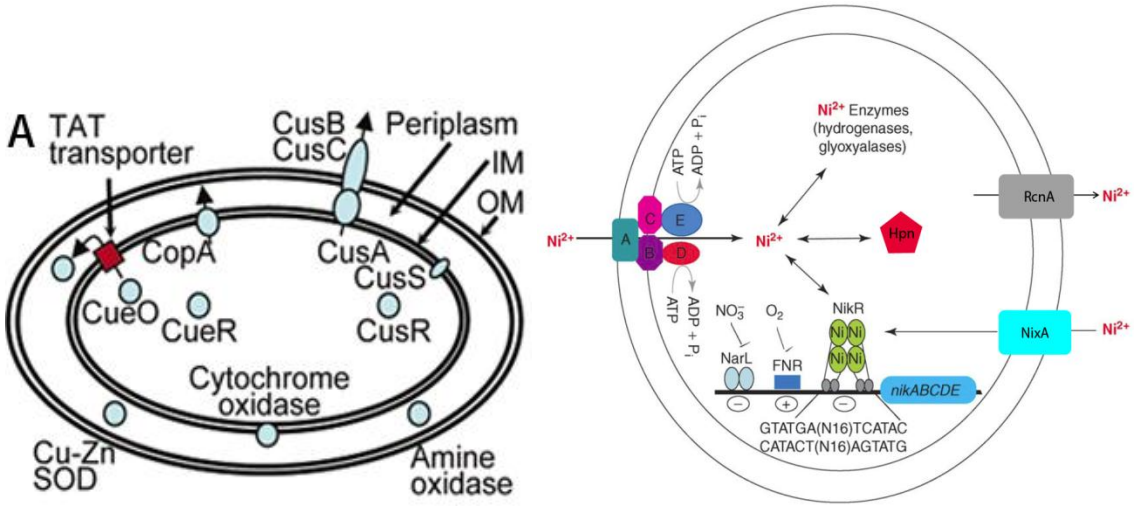

Abb. 2: A) Kupferhomöostase von *E. coli*, aufgrund der toxischen Wirkung darf Kupfer zu keiner Zeit in freier Form in der Zelle vorliegen, sondern bedarf eines strikten Transports; IM = Innere Membran, OM = Äußere Membran aus (Tottey et al., 2005). B) Schematische Darstellung der Nickel-Homöostase in *E. coli*, modifiziert nach (Dosanjh & Michel, 2006).

5.2 Der Superkomplex des Photosystems II

Cyanobakterien, photoautotrophe Mikroorganismen, erschlossen sich die Oxidation von Wasser unter der Nutzung von Lichtenergie als nahezu unlimitierte Elektronenquelle. Für die Oxidation des Sauerstoffs im Wasser, bedarf es jedoch eines Oxidationsmittels mit einem Potential größer +0,82 V. Der Aufbau organischer Verbindungen aus Kohlenstoffdioxid hingegen verlangt Reduktionsäquivalente mit einem elektronegativen Potential von -0,32 V. Für den Prozess der lichtvermittelten ATP-Synthese bedarf es folglich eines Carrier-vermittelten Elektronentransports, mit einer Kaskade von elektropositiven bis hin zu elektronegativen Redoxpotentialen. Beide Äquivalente werden in den Lichtreaktionen der Photosysteme (PS) II und I erzeugt. Die cofaktorhaltigen Untereinheiten der beiden Proteinkomplexe sind über Polypeptide zu einer Elektronentransportkette zusammengeschalten. Im PS II werden in einer lichtgetriebenen Reaktion dem Wasser Elektronen entzogen und entlang einer e^--Transportkette zum PS I Komplex übertragen (McEvoy et al., 2005). In einer zweiten lichtabhängigen Reaktion reduzieren diese Elektronen dann, katalysiert durch das PS I und dessen assoziierter Ferredoxin-$NADP^+$-Reduktase, $NADP^+$ zu NADPH (Nelson & Ben-Shem, 2005).

Das funktionelle Photosystem II ist aus 25 Untereinheiten, die den PS II-*Core*komplex, die Lichtsammelkomplexe (LHC) sowie (redoxaktive) Hilfsproteine bilden, mit einer molekularen Masse von insgesamt ~700 kDa aufgebaut (Boekema et al., 1995),. Diese Systeme setzen mehrere proteingebundene Metalle ein um ihre vielfältigen Funktionen durchführen zu können. Porphyrine des Chlorophylls tragen Magnesiumionen und das Cytochrom b_{559} eine Hämgruppe. Neben diesen werden auch Cu^{2+}, Ca^{2+}, sowie Mangan in unterschiedlichen Oxidationszuständen (Mn^{2+}, Mn^{3+}, Mn^{4+}) in den Metallocofaktoren verwendet (Barber et al., 1997; Renger & Renger, 2008). Die Spaltung zweier Wassermoleküle unter Freisetzung des vierfach oxidierten Produkts O_2 wird über den Mn_4Ca-Komplex, dem „Oxygen Evolving Complex" (OEC) des PS II katalysiert (Kok et al., 1970). Dazu wird ein Photon über ein komplexiertes Chlorophyll (P680) absorbiert und ein Elektron von diesem primären Donor über ein Phäophytin zu einem Plastochinon (Q_A) direkt zu einem sekundären Chinon (Q_B) übertragen, das sobald es zweifach reduziert und protoniert wurde, abgespalten wird (siehe Abb. 3**A**). Die für die Wasserspaltung zugrunde liegenden Reaktionen am Mn_4Ca-Komplex, nämlich alternierende Deprotonierungen und Oxidationen des Metallocofaktors sind im *I*-Zyklus (Abb. 3**B**) dargestellt (Dau & Haumann, 2007). Die paramagnetischen Spezies der hierbei auftretenden unterschiedlichen Valenzen des Mangantetramers, können mittels der

Elektronenspinresonanz Spektroskopie detektiert und im Vergleich zu (synthetisierten) Modellkomplexen interpretiert werden (Haddy, 2007).

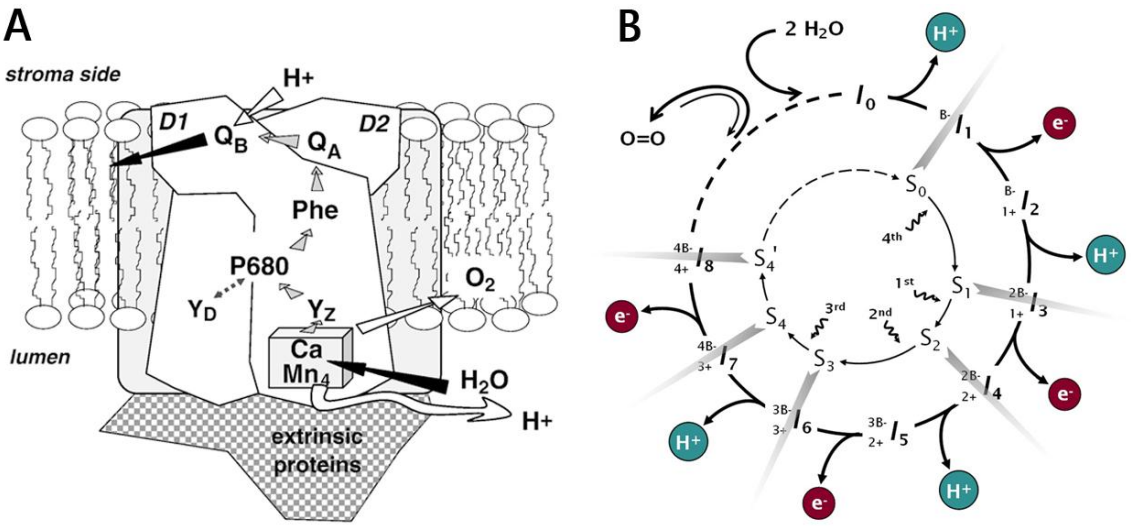

Abb. 3: A) Schema der Elektronentransferkette sowie des Sauerstoff generierenden Komplexes (OEC) im Photosystem II; B) Reaktionszyklus des Mn_4Ca-Komplexes während der Wasseroxidation. P680, primäres Chlorophyll; $Y_{Z/D}$, Tyrosin; Phe, Pheophytin; Q_A, Plastochinon; Q_B, sekundäres Chinon; I_{0-8}, Übergangszustände des Mn_4Ca-Cofaktors, die linksseitig tief-/ bzw. hochgestellten Angaben spiegeln die Anzahl akkumulierter Redoxequivalente wieder. Modifiziert nach (Dau & Haumann, 2007).

5.3 Radikale in biologischen Systemen

Radikale werden vorwiegend negativ oder als gefährlich wahrgenommen, da sie allgemein mit unerwünschten und schädlichen Effekten in Verbindung gebracht werden. Die Abb. 4 liefert einen kurzen Überblick über Angriffspunkte und Auswirkungen unkontrollierter radikalischer Reaktionen. Die Neutralisation zellschädigender, reaktiver Sauerstoffspezies (ROS) erfolgt intrazellular über das Enzym Superoxiddismutase (SOD). In den meisten Bakterien ist für diese katalytische Funktion Mangan, als Cofaktor der manganabhängigen SOD, über drei Histidine und ein Aspartat gebunden (Abreu & Cabelli, 2010). Einige SODs haben eine gewisse Toleranz für das gebundene Metall, so dass sie neben Mangan auch Eisen unter Beibehaltung ihrer enzymatischen Aktivität gebunden werden kann.

Mn^{III}-SOD + $O_2^{\bullet -}$ → Mn^{II}-SOD + O_2

Mn^{II}-SOD + $O_2^{\bullet -}$ $2H^+$ → Mn^{III}-SOD + H_2O_2

Unter oxidativem Stress steigt der für die Mn-SOD Assemblierung benötigte Manganbedarf und eine Hochregulation des Manganimports wird erforderlich (Whittaker, 2010). Während die Regulation der entsprechenden Gene schnell auf Änderungen der Redoxumgebung reagiert, scheinen auch trägere, posttranslationelle Kontrollsysteme für die Bacillibactin oder Siderophor Biosynthese zu existieren. In den Gattungen *Deinococcus* und *Lactobacillus* werden intrazellular sehr hohe Mn(II)-Konzentrationen angehäuft, die dem Schutz vor ionisierender Strahlung und reaktiven Sauerstoffspezies dienen. (Jakubovics & Jenkinson, 2001) *D. radiodurans* ist extrem resistent gegenüber ionisierender Strahlung (Daly et al., 2004). Die Reparatur strahlungsinduzierter DNA-Doppelstrangbrüche wird durch homologe Rekombination durchgeführt (Daly et al., 1994). Als Folge dieser Maßnahme steigt der Bedarf an Desoxyribonucleotiden drastisch an, die allein durch das Metalloenzym Ribonucleotid-Reduktase bereitgestellt werden können.

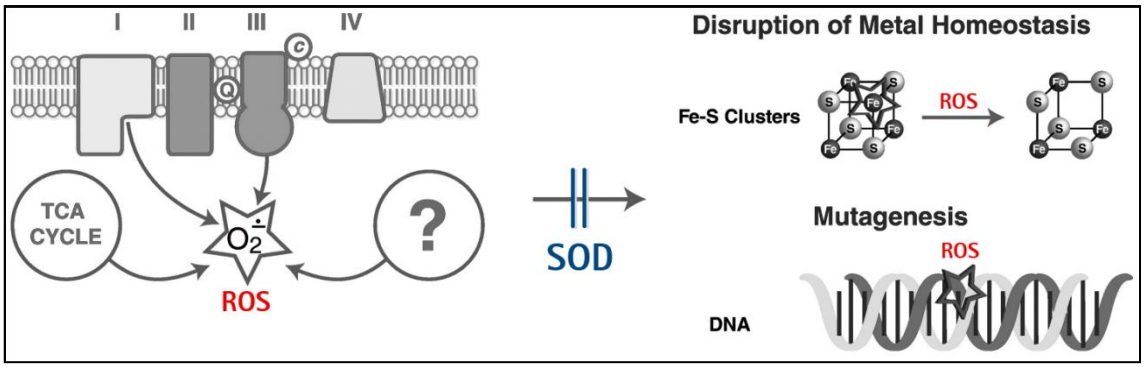

Abb. 4: Ursprung und Wirkung reaktiver Sauerstoffspezies (ROS). Lebende Organismen generieren in zahlreichen Stoffwechselprozessen, zum Beispiel in der Atmungskette und im Calvinzyklus, als Nebenprodukt freie Superoxidradikale ($O2^{-\bullet}$). Eine Auswahl potentieller ROS-Schadensorte ist in der rechten Hälfte dargestellt. Abbildung modifiziert nach (Whittaker, 2010).

Im Fokus dieser Arbeit stehen nicht die negativen Effekte sondern im Gegenteil die essentiellen Funktionen von Radikalen. Viele Teilschritte biologischer Prozesse können ausschließlich unter Einbeziehung proteingebundener Radikale durchgeführt werden, da diese wirksame Oxidationsmittel für eine Vielzahl von Reaktionen sind, und ihr Oxidationsdationspotential in Abhängigkeit des Protonierungsgrades des umgebenden Ligandenfeldes festgelegt wird (Stubbe & van Der Donk, 1998). Diese Radikale müssen bereits vor Beginn der Reaktion im Protein erzeugt und bis zur Verwendung gespeichert werden (Frey et al., 2006; Stubbe & van Der Donk, 1998). Während die Halbwertszeit freier Radikale

in Lösung im Bereich von Micro- bis Millisekunden liegt, weisen proteingebundene Radikale Halbwertszeiten von Stunden (Stubbe & Riggs-Gelasco, 1998) bis hin zu mehreren Wochen (Stolle et al., 2010a) auf. Diese ungewöhnliche Stabilität wird durch eine effiziente Abschirmung des Radikals über eine dichte Proteinstruktur erreicht, die den Zugang des umgebenden Mediums zum Radikal zuverlässig verhindert.

5.4 Ribonucleotid-Reduktasen (RNR)

Alle Organismen synthetisieren die für die DNA Kettenverlängerung und Reparatur essentiellen Desoxyribonucleotid-triphosphate (*d*NTPs) mit Hilfe der Ribonucleotid-Reduktase (EC1.17.4.1). Dieses Enzym katalysiert die Reduktion der Ribose in den Ribonucleotid-di-/triphosphaten zur 2`C-Desoxyribose (vergl. Abb. 5) über einen radikalischen Mechanismus, vergl. Abb. 10 (Jordan & Reichard, 1998). Die Elektronen für diese Reduktion werden durch kleine thiolhaltige Proteine (Thioredoxine / Glutaredoxine) geliefert. Die essentielle Funktion der RNR stellt die einzige Möglichkeit zur *de-novo* Synthese von DNA-Bausteinen dar. Daher wird ihre Inaktivierung als potenter Angriffspunkt betrachtet, sei es zur Tumorbekämpfung, zur Wachstumsinhibierung pathogener Organismen, oder zur Unterdrückung der Vermehrung von eukaryotischen DNA-Viren. Die Ausnahme macht *Bacillus subtilis* mit seinem hochentwickelten „salvage pathway". Dieses Gram-positive Bakterium kann über die Wiederverwertung von Abbauprodukten des Nukleinsäurekatabolismus eine Blockade der Ribonucleotid-Reduktion umgehen (Nygaard, 1993). Jeder Organismus hat in seinem Genom ein bestimmtes GC Verhältnis. Die dafür benötigte Balance zwischen den vier *d*NTP-Pools können die RNRs über eine allosterische Regulation der Substratspezifität aufrecht halten (Brown & Reichard, 1969a). Allen RNRs ist ferner gemeinsam, dass sie die Katalyse über ein transientes Thiylradikal, welches das Substrat durch Abstraktion des 3´-Wasserstoffs aktiviert, initiieren (Nordlund & Reichard, 2006).

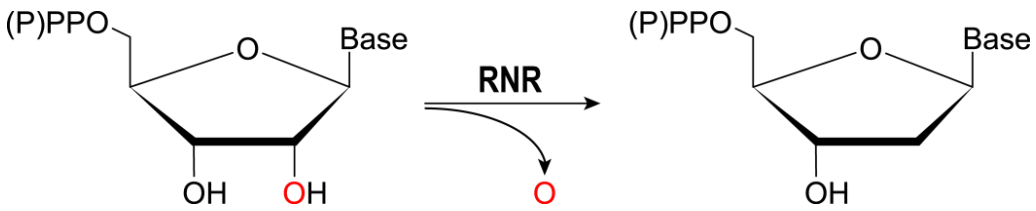

Abb. 5: Ribonucleotid-Reduktasen katalysieren über einen radikalischen Mechanismus (vergl. Abb. 10) die Reduktion von Ribonucleotid-di-/triphosphaten zu den korrespondierenden Desoxyriboseprodukten.

Die Fähigkeit, Ribonucleotide zu reduzieren, gilt als einer der entscheidenden Schritte von der RNA- zur DNA-Welt (Reichard, 1993). Die 2-Desoxyribose ist aufgrund ihrer geometrischen und chemischen Pentofuranosestruktur, die die heterozyklischen Basen über

N-glykosidische Bindungen, sowie dem 3'-5'-Phosphodiester am Polynucleotidstrang verknüpft, besonders geeignet für ein Molekül, das als langfristige Speichermatrix verwendet wird. Das Fehlen einer Hydroxylgruppe am C2-Atom der Desoxyribose zwischen Base und Phosphodiester, sorgt, verglichen mit Ribose, für eine höhere Stabilität gegenüber chemischer sowie enzymatischer Hydrolyse. Die Aktivität der RNR ist zellzyklusabhängig, d.h., sie ist am höchsten in der exponentiellen Wachstumsphase der Prokaryoten sowie der S-Phase von Eukaryoten, genau dann, wenn der Bedarf an Desoxyribonucleotiden für die Replikation am größten ist. Eine Einordnung der RNRs in eine von drei Klassen wird über die folgenden Eigenschaften vorgenommen. Wichtigstes Kriterium für die Einteilung ist die Art, wie das transiente Thiylradikal ($R\text{-}S^{\bullet}$) in der katalytischen α Untereinheit generiert und das hierfür benötigte Äquivalent gespeichert und transferiert wird (vergl. Abb. 8).

5.4.1 Klasse I

Ribonucleotid-Reduktasen der Klasse I bestehen aus zwei unterschiedlichen Untereinheiten. Die größere, katalytische α-Untereinheit (R1), hat neben der Substratbindungsstelle auch zwei Bindungsstellen für allosterische Effektoren (siehe Kap. 5.4.5). Die kleinere β-Untereinheit (R2) trägt den Metallocofaktor (Reichard, 1993; Sjöberg, 1997). Auf Grund der allosterischen Regulation, der Organisation der *nrd*-Gene (*n*ucleotide *red*uction) sowie des Vorhandenseins eines organischen Speicherradikals in R2 wird eine weitere Unterteilung in Ia, Ib und Ic vorgenommen (Nordlund & Reichard, 2006). Den Prototyp einer Klasse Ia-Reduktase, kodiert durch *nrdAB*-Gene, stellt die RNR von *Escherichia coli* mit ihrer bekannten Struktur dar (vergl. Abb. 6). Sie besteht aus jeweils zwei homodimeren Untereinheiten ($\alpha_2\beta_2$). Der Metallocofaktor des R2 Proteins besteht aus einem μ-oxo verbrückten $Fe(III)_2$-Kern, der das proteingebundene Tyrosylradikal stabilisiert. Dieses Eisenzentrum wird unter Beteiligung von molekularem Sauerstoff von $Fe(II)_2$ über $Fe(III)_2$ zu einem transienten Fe(III)-Fe(IV) Zustand oxidiert, der seinerseits über Oxidation des Tyrosins (Y122) das Tyrosylradikal generiert und selbst in den $Fe(III)_2$ Zustand geht (Jordan & Reichard, 1998).

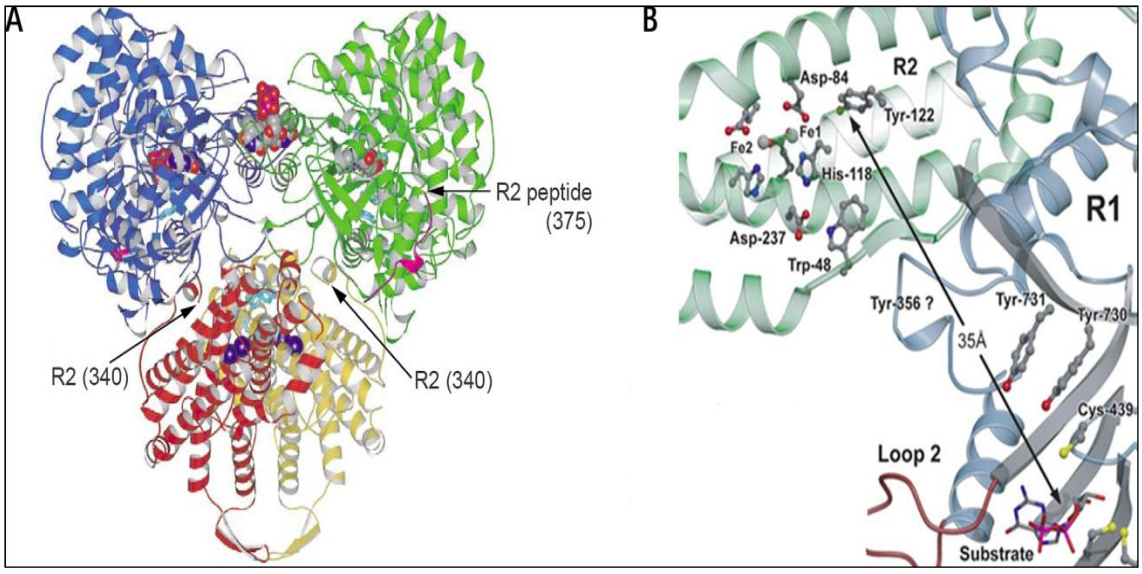

Abb. 6: A) Dockingmodel der *E. coli* Klasse Ia RNR, bestehend aus zwei R1 und zwei R2 Homodimeren (Stubbe, 2003). Das Di-Eisenzentrum in R2 ist durch rote Kugeln dargestellt. Die R2 C-Termini sind mit (340-375) gekennzeichnet. Die am proton coupled electron transfer (PCET) zwischen R1 und R2 beteiligten Aminosäuren sind hier türkisfarben dargestellt. B) Schema des PCET zwischen R1 und R2, der Klasse Ia RNR von *E. coli*, modifiziert nach (Eklund et al., 2001).

Die RNR von *Salmonella typhimurium* wurde als Prototyp einer Klasse Ib RNR vorgeschlagen (Jordan et al., 1994) und als Fe-Protein kristallisiert (Eriksson et al., 1998). Die für die Nucleotidreduktion notwendigen Elektronen stellt NrdH als glutaredoxinähnliches Protein mit einer thioredoxinähnlichen Funktion Elektronen aus den redoxaktiven Cysteinen bereit (Jordan et al., 1996). Ein Flavoprotein (NrdI) wurde als weiteres akzessorisches Protein von Cotruvo & Stubbe (Cotruvo & Stubbe, 2008) für die Regeneration des $Fe(III)_2$-Tyrosyl Radikalcofaktors der Klasse Ib RNR von *E. coli* beschrieben. Die α und β Untereinheiten der Reduktasen dieser Klasse werden über die *nrdEF*-Gene kodiert. Die fakultativ anaerobe, Gram-negative Spezies *E. coli* besitzt RNRs der Klassen Ia, Ib und III (vergl. 5.4.3). Unter Standardbedingungen der aeroben Anzucht werden die *nrdAB*-Gene für die Klasse Ia RNR stark, die *nrdEF*-Gene für die Klasse Ib RNR nur schwach exprimiert. Eisenmangel sowie oxidativer Stress führen zu einer Induktion der *nrdEF*-Gene (McHugh et al., 2003; Monje-Casas et al., 2001). Die Aktivierung des Metallocofaktors bedarf nach der Assemblierung einer einmaligen Aktivierung durch die akzessorischen Faktoren NrdI und NrdH (Cotruvo & Stubbe, 2008; Cotruvo & Stubbe, 2010). Die RNRs der Gram positiven Bakterien *C. ammoniagenes* und *C. glutamicum* sind ebenfalls in den *nrdEF*-Genen (vergl. Abb. 7) organisiert und teilen viele der Eigenschaften einer Klasse Ib Reduktase, unterscheiden sich aber in der Art des

verwendeten Metallocofaktors. Unter Manganmangel zeigen diese Bakterien Symptome einer beeinträchtigten DNA-Synthese (Auling et al., 1980). Infolge einer Hemmung der Zellteilung weisen die Zellen ein ungewöhnliches Längenwachstum auf (unbalanciertes Wachstum) und reichern Nucleotide im umgebenden Medium an. Dieser Effekt wurde auf die Manganabhängigkeit der Ribonucleotid-Reduktion in diesen coryneformen Bakterien zurückgeführt (Auling & Follmann, 1994).

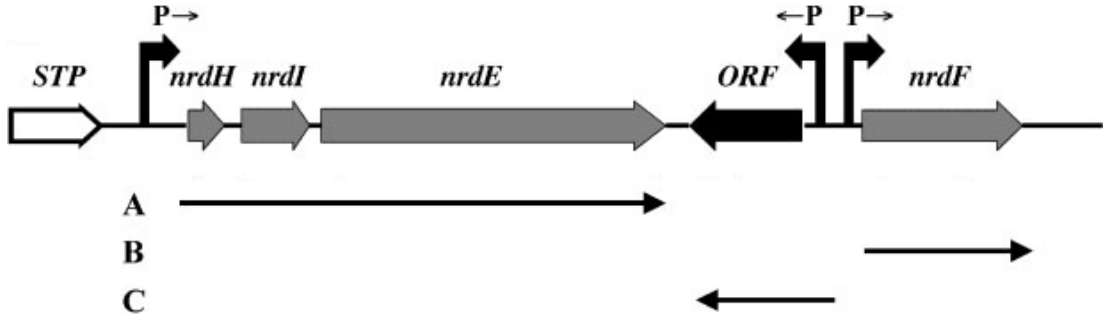

Abb. 7: Organisation des 71 kb *nrd*-Clusters von *C. ammoniagenes*. Die Pfeile stellen die Lokalisation sowie Orientierung der *nrd*-Gene dar. Die Transkription der Gene für das NrdH-Redoxin (*nrdH*), das NrdI-Protein (*nrdI*) und die katalytische R1E-Untereinheit der RNR (*nrdE*), steht unter der Kontrolle eines gemeinsamen, putativen Promotors (P). Die Transkriptionskontrolle der kleinen, Metallocofaktor tragenden Untereinheit (*nrdF*) erfolgt über einen eigenen Promotor. Die Funktion des open reading frames (ORF) ist bisher ungeklärt. Abbildung modifiziert nach (Torrents et al., 2003).

Eine weitere Klasse, Ic, wurde für die RNR aus dem Gram-negativen, obligat parasitären Bakterium *Chlamydia trachomatis* beschrieben (Högbom et al., 2004). Hier fehlt das in den Klasse I RNRs konservierte Tyrosin (Y115) im R2-Protein, welches nach den Standardvorstellungen (Nordlund & Reichard, 2006) für die Oxidation zum Tyrosylradikal benötigt wird. Damit kann nicht der übliche Metallocofaktor gebildet werden. Dessen Funktion zur Erzeugung des initiierenden Thiylradikals wird hier durch einen Mn(IV)-Fe(IV) Metallcluster ersetzt (Jiang et al., 2007a; Jiang et al., 2007b). Trotz der besonderen Eigenschaften der Chlamydien-RNR, werden die Gene als *nrdAB* bezeichnet (Roshick et al., 2000).

5.4.2 Klasse II

Klasse II Ribonucleotid-Reduktasen sind besonders unter den anaeroben Mikroorganismen, wie den Lactobacillen sowie bei Cyanobakterien und Archaea weit verbreitet. Als Prototyp dieser Klasse gilt die monomere, Cobalamin-abhängige RNR von *Lactobacillus leichmannii* (Panagou et al., 1972). Reduktasen dieser Klasse besitzen eine im Vergleich zu anderen RNRs einfachere Struktur, die nur aus der katalytischen Untereinheit, entweder als Monomer (α) oder Dimer (α_2) besteht, und vom *nrdJ*-Gen kodiert wird (Booker & Stubbe, 1993). Das für die Ribonucleotidreduktion benötigte Thiylradikal (Licht et al., 1996), wird hier über ein 5´-Desoxyadenosylradikal unter Beteiligung von Cobalt(II) initiiert. Dies entsteht nach Bindung des 5´-Desoxyadenosyl-Cobalamins an die katalytische Untereinheit durch homolytische Spaltung der metalloorganischen Co(III)-C Bindung (Follmann, 2004).

5.4.3 Klasse III

Die Klasse III RNRs sind die Sauerstoff empfindlichen Enzyme strikt anaerober Bakterien, wie den methanogenen Archaea aber auch in fakultativ anaeroben Bakterien wie *E. coli*. Sie sind heterogen aufgebaut, aus der *nrdD* kodierten katalytischen α / α_2 Untereinheit sowie der aktivierenden *nrdG* kodierten β_2 Untereinheit (Logan et al., 1999). Dabei trägt der Metallocofactor NrdG einen Eisen-Schwefelcluster des Typs [4Fe-4S] (Tamarit et al., 2000), welcher zusammen mit S-Adenosyl-Methionin (SAM) und einem reduzierten Flavodoxin ein sauerstoffsensitives Glycylradikal in der katalytischen Untereinheit erzeugt. Dieses Glycylradikal, ist es erst einmal unter Beteiligung der Aktivase NrdG erzeugt, generiert kontinuierlich das für die Substratreduktion essentielle Thiylradikal in NrdD. Im Unterschied zu den aeroben Reduktasen wird nach der erstmaligen Glycylradikalgenese die Aktivase NrdG nicht weiter benötigt und das katalytische NrdD-Protein behält als Monomer / Homodimer seine Aktivität (Stehr et al., 2001). Anaerobe Klasse III Reduktasen verwenden als finalen Elektronenakzeptor Formiat und nicht wie in den anderen RNR-Klassen üblich Dithiole (Mulliez et al., 1995).

Die anaerobe RNR von *E. coli*

Wechseln die äußeren Bedingungen zu mikroaerophilen, bzw. anaeroben Bedingungen, findet eine Hochregulation der *nrdDG*-Gene für die Klasse III RNR statt. Die Regulation der Genexpression wird über den Tanskriptionsfaktor NrdR gesteuert, der an eine spezifische

16 bp Region, der NrdR-Box, innerhalb der nrd-Promotorregion bindet (Boston & Atlung, 2003; Torrents et al., 2007). Diese Regulation gewährleistet eine effiziente Versorgung des Organismus mit reduzierten DNA Bausteinen, auch unter wechselnden äußeren Bedingungen. Eine Fähigkeit, die auch pathogenen Organismen die Proliferation innerhalb von Sauerstoffarmen Geweben infizierter Wirte ermöglicht (Torrents & Sjöberg, 2010).

5.4.4 Evolution der RNRs

Leben, wie wir es kennen, benötigt mindestens zwei grundlegende Voraussetzungen, Selbstreplikation und Katalyse, die durch drei Makromoleküle gewährleistet werden. DNA dient hierbei als Informations-Speichermatrix, Proteine übernehmen vielfältige katalytische Funktionen und RNA dient als Schnittstelle der erstgenannten angesichts der katalytischen Funktion von RNA (Cech, 2004), zusammen mit ihrer Fähigkeit zur Selbstreplikation. Eine ursprüngliche RNA-Welt erscheint denkbar (Watson, 1987). Ein zweites Argument für diese These liefert das Enzym Ribonucleotid-Reduktase, welches die benötigten Bausteine für DNA Moleküle während des Übergangs zur DNA-Welt zu produzieren begann, selbst. Diese radikalgetriebene katalytische Funktion bedarf der Einbettung in einer schützenden Struktur, einem Reaktionskomplex, der ausschließlich aus Proteinen besteht. Hieraus lässt sich ebenfalls ableiten, dass auch die Entstehung von Proteinen der von DNA vorausgegangen sein muss. Da heute drei Klassen von RNRs bekannt sind, stellt sich die Frage ob sich diese Klassen eigenständig oder ausgehend von einem gemeinsamen Urahn entwickelten. Sequenzvergleiche zeigen eine begrenzte Homologie zwischen Klasse I und II RNRs. Beschränkt man den Vergleich auf das katalytische Reaktionszentrum, zeigt sich das dieses aus einer stark konservierten Region aus 10 α/β Barrels mit einem Thiylradikal an der Spitze einer Proteinschleife besteht. Diese konservierte Struktur, die interessanterweise auch in der Pyruvat-Formiatlyase (Becker et al., 1999) vorhanden ist, sowie die unterschiedliche allosterische Regulation der RNRs (siehe unten) deuten auf eine divergierende Entwicklung, ausgehend von einem gemeinsamen Vorfahren hin. Da DNA vor der Wandlung von einer anaeroben zu einer aeroben Atmosphäre entstanden sein muss, scheiden Klasse I RNRs als Vorfahr aus. Das für Klasse II essentielle Kobalt war auf der frühen Erde nur spärlich verfügbar, Minerale mit Eisen-Schwefel Anteil hingegen waren weit verbreitet, so dass die anaerobe Klasse III RNR als Urahn wahrscheinlich ist (Huber & Wachtershauser, 1997; Sofia et al., 2001). Die unterschiedlichen Mechanismen der Thiylradikalgenerierung (vergl. Abb. 8) entstanden vermutlich erst im späteren Verlauf der Evolution.

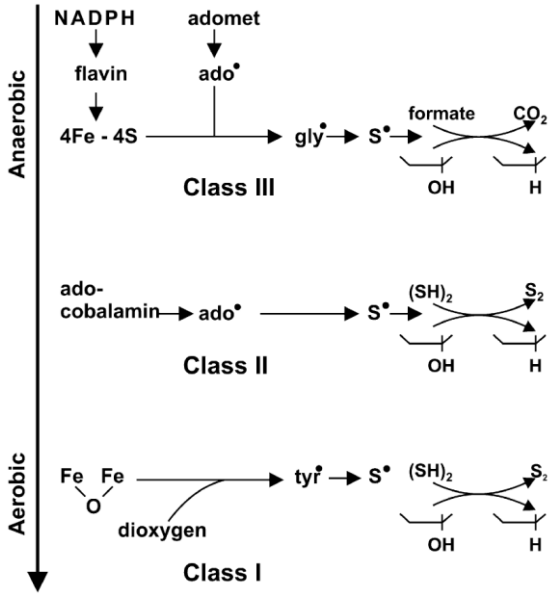

Abb. 8: Generierung des Reaktionsinitiierenden Thiylradikals im Klassenvergleich. Klasse III RNRs nutzen ein Adenosylmethionin (adomet) und ein reduziertes Eisen-Schwefelzentrum um ein Adenosylradikal (ado$^{\bullet}$) zu erzeugen, das über ein Glycyl- das initiierende Thiylradikal (S$^{\bullet}$) generiert. Klasse II Enzyme verwenden stattdessen Adenosylcobalamin zur Generierung eines Thiylradikals. In Klasse I RNRs erzeugt die R2 Untereinheit unter Verwendung eines Metallocofaktors ein stabiles Tyrosylradikal (Y$^{\bullet}$) welches das initiierende Thiylradikal in der katalytischen R1 Untereinheit erzeugt. Abbildung aus (Reichard, 2010).

Die NrdEF Proteine sind untereinander sehr ähnlich. Ein molekularer Vergleich der abgeleiteten RNR Primärstrukturen (vergl. Abb. 9) spiegelt die Verwandtschaft der Gram-positiven Bakterien mit hohem (Actinobacteria) und niedrigem GC-Gehalt (Firmicutes) wieder (Torrents et al., 2002). Daneben wird *nrdEF* in *E. coli* und *S. typhimurium,* aber sonst in keinem weiteren Gram-negativen Bakterium gefunden (Fieschi et al., 1998). Das deutet darauf hin, dass *nrdEF* ursprünglich bei den Gram-positiven Bakterien entstand und erst im Lauf der Evolution über horizontalen Gentransfer, von einer mit den *Corynebakterien* oder *Mycobakterien* nah verwandten Spezies, in die *Enterobacteriaceae* übertragen wurde (Torrents et al., 2002).

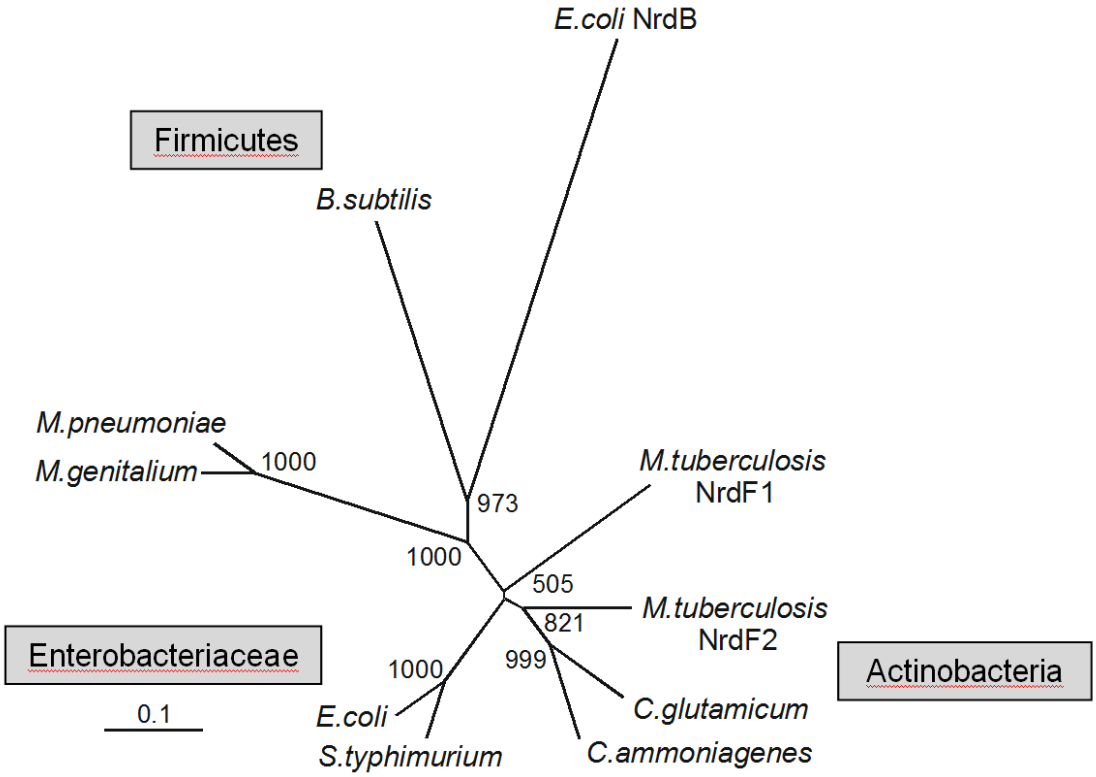

Abb. 9: Evolutionäre Verwandtschaft der Klasse Ib RNRs, modifiziert nach (Oehlmann, 1998).

5.4.5 Der katalytische Mechanismus

Der Mechanismus der Ribonucleotidreduktion ist an den Reduktasen der Klasse I am besten untersucht und wird hier exemplarisch für das Klasse Ia Enzym von *E. coli* beschrieben. Die Reaktion beginnt mit Van der Waals Wechselwirkungen zwischen C439, welches auch das initiierende Thiylradikal trägt, und dem 3´-C des Ribosesubstrats (vergl. Abb. 10). Die gegenüberliegenden Cysteine, C225 proximal sowie C462 distal, liefern hierfür die benötigten Reduktionsäquivalente. Die konservierten Aminosäuren E441, N437 und C134 sind nah an der 3´-Hydroxylgruppe des Substrats positioniert. Sie dienen in diesem Mechanismus als Base und bilden die katalytisch wichtigen Wasserstoffbrücken zum Substratmolekül aus. Die eigentliche Reaktion wird durch das in C439 lokalisierte Thiylradikal initiiert (Licht et al., 1996), welches durch Abstraktion des koordinierten Wasserstoffs am 3´-C der Ribose (Stubbe et al., 1983) ein Substratradikal generiert (S1) (Stubbe et al., 2003).

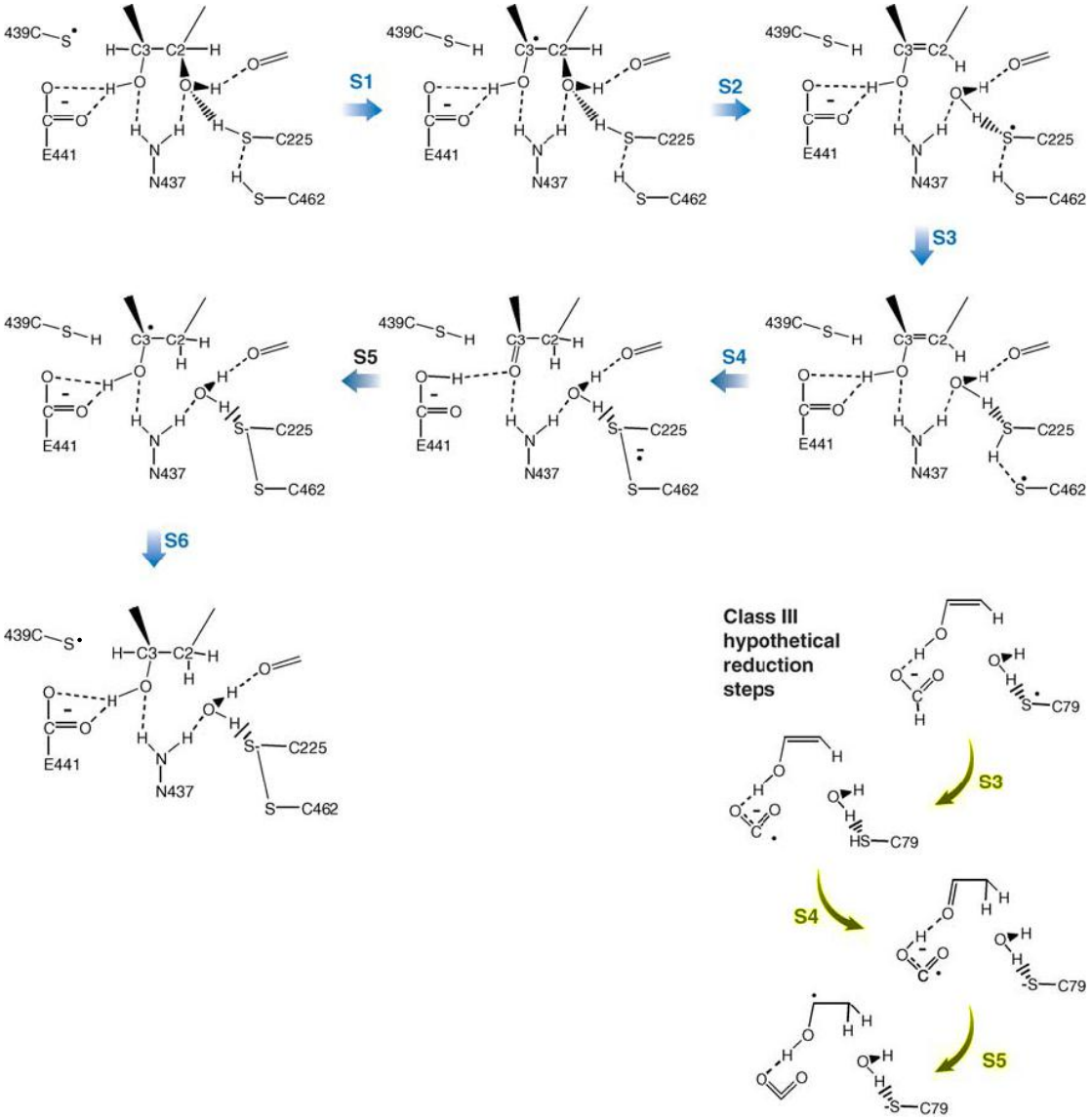

Abb. 10: Der katalytische Mechanismus der Klasse I & II RNRs (S1-S6), sowie der hypothetische Reduktionsschritt der Klasse III RNR (S3–S5). Schema modifiziert nach (Nordlund & Reichard, 2006). Die Annotation der Aminosäuren folgt der Klasse Ia RNR von *E. coli*.

Es folgt die Spaltung der 2´-C-O Bindung unter Bildung eines Cysteinylradikals in Position C225 (S2) sowie die Protonierung und Abgang eines Wassermoleküls. Begünstigt durch die Deprotonierung der 3´-Hydroxylgruppe, erfolgt die Protonierung des 2´-Kohlenstoffs (S3) einhergehend mit der Bildung eines Disulfidradikals zwischen den Reduktionsequivalenten C225 und C426 (S4). Das hierfür benötigte Proton stammt aus C462, dessen Transfer durch das zuvor abgespaltene Wassermolekül ermöglicht wird (Pelmenschikov et al., 2004). In einem letzten Reaktionsschritt reoxidiert das entstehende Desoxyriboseradikal (S5) das

initiierende Thiylradikal (S6) und die Reaktion ist abgeschlossen. Die Regeneration der oxidierten Cysteine C225 und C462 erfolgt durch spezifische Redoxine und NADPH (vergl. Abb. 11).

In der Reduktion der korrespondierenden Cysteine der *C. ammoniagenes* Klasse Ib RNR ersetzt das NrdH–Protein die Funktion des Thioredoxins. NrdH hat thioredoxinähnliche Eigenschaften (Willing et al., 1988a) weist aber eine glutaredoxinähnliche Struktur auf (Stehr et al., 2001).

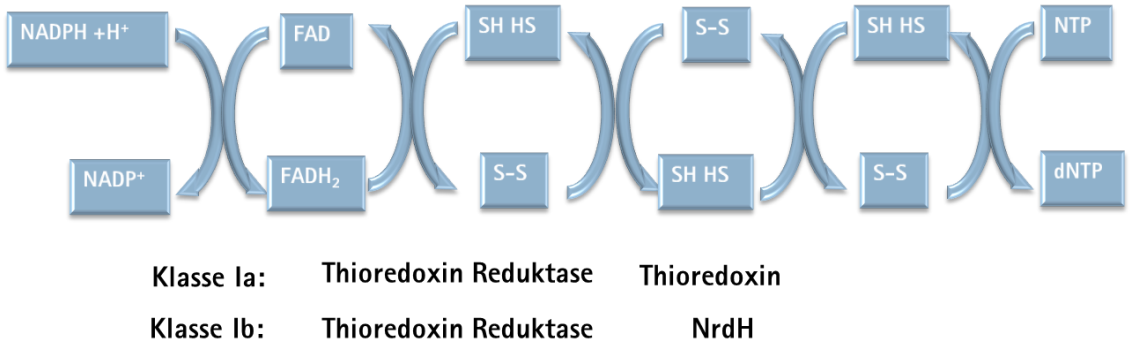

Abb. 11: Schematische Darstellung der Reduktion der an der Katalyse beteiligten Cysteine in den R1-*E. coli* Klasse Ia, bzw. R1E-*C. ammoniagenes* Ib-Untereinheiten der Ribonucleotid-Reduktase.

5.4.6 Allosterische Regulation

Die DNA Replikation benötigt eine ausgeglichene Versorgung mit allen vier dNTPs. Störungen würden zu erhöhten Mutationsraten führen und ggf. zum Absterben der betroffenen Organismen führen. Die bisher am besten untersuchte Klasse Ia RNR besitzt für diesen Zweck zwei allosterische Effektorbindestellen, eine regulatorische und eine Spezifitätsbindestelle. An die regulatorische können ATP, was zu einer Steigerung der Aktivität führt, sowie dATP mit einem aktivitätssenkenden Effekt binden. Die zweite allosterische Regulation bewirkt eine Änderung der Substratspezifität durch Bindung eines Desoxyribonucleotides. Dabei führt die Bindung eines dNTPs zu Konformationsänderungen in der Substratbindestelle, so dass diese eine höhere Affinität für eines der drei weiteren Nucelotide erhält und somit über eine Feedbackregulation die Produktbalance aufrechterhalten wird (Brown & Reichard, 1969a; Brown & Reichard, 1969b).

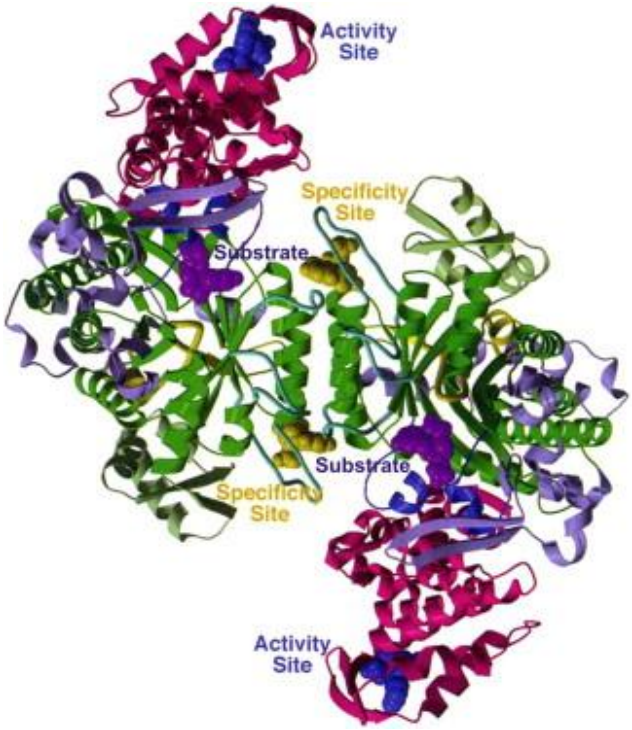

Abb. 12: Struktur des R1 Homodimers von *E. coli*, modifiziert nach (Eriksson et al., 1997). Jedes Monomer besitzt eine Substratbindestelle (violett), eine Bindestelle für einen allosterischen Effektor (blau) sowie für einen Spezifitätseffektor (gelb). Der allosterische Effektor bindet am N-Terminus der Monomere, der Spezifitätseffektor verbrückt die Monomere. Dabei wird die Phosphatgruppe des Substrats an die eine, die Base an die zweite Untereinheit der RNR gebunden (Reichard, 2010).

Zielsetzung dieser Dissertation

Die Beteiligung von Mangan an der Ribonucleotid-Reduktion von *C. ammoniagenes* ATCC 6872 wurde erstmals 1980 postuliert (Auling, 1980) und durch Anreicherung einer Mangan-Ribonucleotid-Reduktase im Labor H. Follmann belegt (Willing et al., 1988b). Mangan ist essentieller Bestandteil im Metallocofaktor der kleinen Untereinheit (R2F). Erste EPR-spektroskopische Untersuchungen an teilgereinigten R2F-Fraktionen ergaben ein putatives Tyrosylradikal im X-Band (Griepenburg et al., 1996) und eine Mangansignatur (hyperfine sextet) im Q-Band (Griepenburg et al., 1998). Dieses Modell einer manganabhängigen RNR wurde zunächst von der Gruppe um B.-M. Sjöberg bestätigt (Fieschi et al., 1998). Wurde aber von demselben Labor nach heterologer Expression des *nrdF*-Gens aus *C. ammoniagenes* in genetisch leicht zugänglichen Stämmen der phylogenetisch entfernten Spezies *E. coli* sowie zusätzlicher *in-vitro* Manipulation des erhaltenen R2F und dessen nachfolgender Kristallisation mit einem di-Eisen-Metallocofaktor verworfen (Högbom et al., 2002; Huque et al., 2000). Ein erster Versuch zur homologen Expression des *nrdF*-Gens in der Arbeitsgruppe Auling erbrachte mit dem Stamm *C. ammoniagenes* pWCAX keine ausreichenden Proteinmengen für physikalische Analysen (Follmann, 2001). Barckhausen (2004) entwickelte den Stamm *C. ammoniagenes* pOCA2 und detektierte ein ungewöhnliches Tyrosylradikal in einer nachweislich eisenfreien Mn-RNR, lieferte jedoch keine Enzymaktivität. Nachteilig waren auch die hohen Verluste an Tyrosylradikal (Spin) bei der Reinigungsprozedur.

Hauptziel der vorliegenden Arbeit war es daher, das bisherige Reinigungsverfahren mit Schwerpunkt auf Erhalt der Spinkonzentration weiterzuentwickeln, um große Menge der kleinen RNR-Untereinheit mit hoher Aktivität zu präparieren. Mit diesem nativen R2F-Protein sollte der Metallstatus mit chemischen und physikalischen Methoden aufgeklärt werden. Die Aufnahme einer hochaufgelösten Kristallstruktur kombiniert mit Multifrequenz-EPR Spektroskopie die Koordination des nativen Metallzentrums sowie dessen Oxidationsstatus klären. Ein biochemischer Ansatz könnte neue Einsichten in den Tyrosyl-Mangancofaktor liefern, indem ein geeignetes Redoxäquivalent zur Generierung des Tyrosylradikals eingesetzt wird. Die an *C. ammoniagenes* gewonnenen Erkenntnisse sollten ferner zur Anreicherung einer aktiven R2F-Untereinheit bei einem Wildtyp des Aminosäureproduzenten *C. glutamicum* genutzt werden.

Ergebnisse

7.1 Zusammenfassende Darstellung der Einzelarbeiten

Ein bisher praktiziertes Reinigungsschema für die *C. ammoniagenes* Mn-RNR aus homologer Expression war durch hohe Verluste des Tyrosylradikals charakterisiert und eine Aktivität des R2F-Proteins wurde lediglich über die Absorption des 408 nm-Radikalsignals postuliert (Barckhausen, 2004). Schon zu Beginn dieser Arbeit fielen aber bestimmte Schwächen auf:

1.) Keine Inhibierung proteolytischer Aktivität beim Zellaufschluss,
2.) mögliche Abreicherung des löslichen Zielproteins durch unerwünschte Wechselwirkungen mit ungelösten Zellkomponenten / Membranen,
3.) keine spezifischen Maßnahmen zur Stabilisierung des Tyrosylradikals,
4.) ungünstige Durchführung der Anionenaustauschchromatographie.

Die übliche Inhibierung des proteolytischen Abbaus durch Standard-Inhibitorcocktails mit hoher Dosierung von Ethylendiamintetraessigsäure (EDTA) zur Inaktivierung von Metalloproteasen schien ungeeignet. Eine Komplexierung des im R2F-Protein koordinierten Mangans würde den Metallocofaktor der Mn-RNR zerstören. Formulierungszusätze wie Imidazol, die einen Metallfremdeintrag zur Folge haben können, waren ebenfalls auszuschließen, sollte die Darstellung des nativen R2F-Proteins das Ziel sein. Als zur Vermeidung von Artefakten geeigneter Zusatz erwies sich der Protease Inhibitor Sigma-Aldrich Art.-Nr. P2714-1BTL (in 2,5-facher Verdünnung). Verluste beim Aufschluss und den ersten Zentrifugationsschritten wurden durch Zusatz von 0,1 % Tween 80 und 100 mM KCl zum Aufschlusspuffer minimiert. Eine geringe Halbwertszeit des Tyrosylradikals (5 h bei 4°C) war von Griepenburg (Griepenburg et al., 1996) beschrieben. Durch Zusatz von Glycerin, Detergens und Erhöhung der Ionenstärke (Fig. 4, (Stolle et al., 2010a)) wurde eine drastische Stabilisierung des mit Mangan gekoppelten Tyrosylradikals erreicht, der die Halbwertszeit auf ~200 h bei 4 °C erhöhte. Ferner war das bisherige Protokoll der ersten Anionenaustausch-chromatographie (Uno™sphere Q) völlig ungeeignet für die Zielsetzung dieser Arbeit. Deshalb wurde zunächst der Elutionsbereich des R2F Proteins in Abhängigkeit des modifizierten Puffersystems mit einem flachen, linearen Gradienten als 334 ±10 mM KCl bestimmt. Die präparative Elution erfolgte mit einem vierstufigen Gradienten. Zusätzlich wurde die spezifische R2F-Ladekapazität erhöht, indem der Auftragspuffer mit 150 mM KCl dotiert wurde, um eine unerwünschte Bindung von Begleitproteinen zu unterdrücken. Durch die hier

genannten Modifikationen konnten die dramatischen Verluste an Radikal bereits während der ersten Anreicherungsstufen von ca. 80 % auf 15 % gesenkt werden. In der sich anschließenden Größenausschlußchromatographie wurde der Elutionsbereich des monomeren 38 kDa R2F-Proteins auf 32 – 45 kDa begrenzt.

Für Hochfeld EPR Messungen (122 und 244 GHz) an biologischen Materialien sind entscheidende Hürden in der Probenvorbereitung zu überwinden: Inhomogenes Protein, zu geringe Menge, zu geringe Aktivität. Für diese Erfordernisse, wurde die zweite Anionenaustauschchromatographie an Mono Q® mehrfach optimiert. Für die Applikation auf die Säule wurde die Proteinprobe mit 375 mM KCl zur Verringerung unspezifischer Adsorption versetzt. Die weitere Elution unspezifischer Proteine erfolgte in einer Gradientenstufe mit 515 mM KCl, gefolgt von einem steilen linearen KCl-Gradienten, wobei die Elution des homogenen R2F-Proteins im Bereich von 520 bis 535 mM KCl recht konzentriert erfolgte. Eine Echtzeiterfassung (online) des R2F-Proteins während der Elution würde eine engere Fraktionierung erlauben und damit die Abreicherung von Fremdproteinen maximieren. Sie würde auch die Voraussetzung für eine Automatisierung der R2F-spezifischen Fraktionierung liefern.

Die Detektion des Tyrosylradikals von R2F erfolgte bisher off-line über Differenzspektren und wurde durch kontinuierliche Messverfahren ersetzt. Dafür wurde auf Grundlage des in Fig. 3a (Stolle et al., 2010a) präsentierten R2F Absorptionsspektrums die maximale Absorptionsbreite des proteingebundenen Tyrosylradikals auf 8 nm (404 – 412 nm) bestimmt. Eine kontinuierliche Messung der Absorption an den Wellenlängen 408 nm (Maximum) sowie 413 nm (Baseline) generierte ein virtuelles Differenzspektrum, welches als Fraktionierungsparameter in der angestrebten Automatisierung eingesetzt wurde. Durch die beschriebenen Modifikationen, die Verwendung von Superloops zur Probenladung und Zwischenspeicherung von Eluaten, konnte die Teilautomatisierung des hier beschriebenen Chromatographieprozesses erfolgreich umgesetzt werden. Die vorherigen Verluste, die zu einer geringen Gesamtausbeute von 16,1 nmol aktivem Protein aus 60 g Zellen führten konnten drastisch minimiert werden, so dass aus der modifizierten Proteinreinigung 30 mal mehr aktives, homogenes Protein, also insgesamt 0,52 µmol pro Batch präpariert werden konnten.

Ein Hauptziel dieser Arbeit war es, den Metallstatus des Metallocofaktors im R2F-Protein zu klären. Nach homologes Expression des *nrdF*-Gens in *C. ammoniagenes* wurden vier

voneinander unabhängige Metallanalysen (i) Graphitrohr-Atomabsorptionsspektrometrie (GF-AAS), (ii) Massenspektrometrie mit induktiv gekoppeltem Plasma (ICPMS), (iii) chemische Metallbestimmungen und (iv) Totalreflexions-Röntgenfluoreszenzspektrometrie (TXRF) durchgeführt (Stolle et al., 2010a). Übereinstimmend wurde Mangan, mit einer Stöchiometrie von 0,74 ±0,04 Mol Mn pro 1 Mol R2F-Monomer im Metallocofaktor nachgewiesen. Durch diese Methoden wurde die Gegenwart signifikanter Mengen von Eisen im nativen R2F-Protein endgültig ausgeschlossen. Die Spezifität des R2F-Metallocofaktors für Mangan wurde durch eine Versuchsreihe geklärt. Hierzu wurden gezielt zweiwertige Metalle, deren Beteiligung in RNRs anderer Klassen beschrieben wurde, dem Fermentationsmedium während der Anzucht von *C. ammoniagenes* zugesetzt. Die Zugabe äquimolarer Mengen (100 µM) von Mangan(II)-chlorid, Zink(II)-chlorid und Eisen(II)-chlorid veränderte weder den Status noch die Menge an aktivem Metallocofaktor. Wurde dem Fermentationsmedium hingegen ausschließlich Eisen(II)-chlorid während der Induktionsphase zugesetzt, blieb die Bildung des organischen Radikals aus. Darüber hinaus wurde nach Reinigung dieses R2F-Proteins ebenfalls kein Eisen im Metallocofaktor nachgewiesen und der größte Anteil des Proteins verblieb in der inaktiven Apoform.

Nachdem die Art des Metallocofaktors, sowie dessen Beteiligung an der Ribonucleotidreduktion in dieser Arbeit geklärt werden konnte, war es attraktiv, eine Modellvorstellung zur Entstehung des neuartigen Tyrosyl-Mn_2 gekoppelten Spinsystems des Metallocofaktors der RNR von *C. ammoniagenes* zu entwickeln. Entscheidende Hinweise für die Generierung des aktiven Metallocofaktors wurden in ausführlichen Reaktivierungsversuchen, nach gezielter Reduktion des Tyrosylradikals mit Hydroxyharnstoff, erarbeitet. Nach vollständiger Entfernung von HU mittels Ultrafiltration wurde eine vollständige Regeneration des Metalloradikalcofaktors durch Zugabe von 10 µM H_2O_2 und 2,5 µM 1,1'- Dimethyl- 4,4'- bipyridinium als Mediator erreicht, die über eine zeitaufgelöste Aufnahme der $Y^{\bullet}$-Absorption bei 408 nm verfolgt werden konnte. Dabei ist anzumerken, dass die Konzentration des regenerierten Tyrosylradikals die der Anfangskonzentration um 30 % übertraf (siehe Diskussion).

Erstmals wurde hier im Standardassay für RNRs Aktivität (69 µmol × mg^{-1} × min^{-1}) für das R2F-Protein nach homologer Expression gemessen. Dieses bisher unerreichte hohe Niveau (Stolle et al., 2010a), übertraf nicht nur bei weitem für das *C. ammoniagenes* R2F publizierte Aktivitäten (Griepenburg et al., 1998), sondern auch die in der Literatur für Klasse Ia RNRs

berichteten Aktivitäten (Huque et al., 2000). Damit und mit der hier erreichten hohen Spinkonzentration des R2F-Proteins waren die Voraussetzungen für weiterführende Arbeiten geschaffen. Die Idee, eine direkte Beteiligung des Tyrosylradikals (Y115) an der Ribonucleotidreduktion nachzuweisen, lag nahe. Dafür wurde ein neuartiger Enzymtest entwickelt, in dem unter Ausschluss von standardmäßig verwendeten *in-vitro* Reduktionsmitteln das Verhalten des Tyrosylradikals (Fig. 3a, Stolle et al.) optisch zeitaufgelöst verfolgt werden konnte. Ein für die RNR-Forschung üblicher Komplementationsassay (R1E + R2F) wurde durch Zugabe des Substrats CDP gestartet und die zu erwartende Löschung des charakteristischen 408 nm Radikalsignals über die Zeit verfolgt (Fig. 3b, Stolle et al., 2010a). Das mit Beteiligung des Tyrosylradikals gebildete Produkt wurde über eine modifizierte HPLC-Methode (Pal et al., 1975) mit einem Referenzstandard validiert und die Ausbeute quantifiziert. Auf diese Weise konnte gezeigt werden, dass 0,2 nmol dCDP unter Beteiligung von 0,4 nmol $Y^{\bullet}$ gebildet werden.

Der hier neu entwickelte alternative Enzymtest könnte als Screeningverfahren für Inhibitorstudien verwendet werden, weil die Ribonucleotid-Reduktasen aufgrund ihrer essentiellen Funktion einen lukrativen Angriffspunkt zur Bekämpfung proliferierender Zellen, insbesondere pathogener Mikroorganismen sowie Tumorzellen, bieten. Für diesen Zweck wurde exemplarisch als zu testender Inhibitor ein von der Sequenz des C-Terminus des R2F Proteins abgeleitetes Heptapeptide synthetisiert. Eine Vorinkubation der katalytischen R1E Untereinheit mit diesem Peptid führte zur Inaktivierung der Ribonucleotid-Reduktion, erkennbar am Erhalt des charakteristischen $Y^{\bullet}$-Absorptionsmaximums (Stolle et al., 2010b).

Die Adaption des optimierten Reinigungsschemas zur Anreicherung des R2F-Proteins aus *C. glutamicum* (Wildtyp) konnte in dieser Arbeit ebenfalls erfolgreich umgesetzt werden. Erstmals wurde für dieses Enzym eine hohe enzymatische Aktivität im Komplementationstest gemessen und das spezifische 408 nm $Y^{\bullet}$-Absorptionssignal dargestellt (Abbouni et al., 2009).

7.2 Publikation I: Homologous Expression of the *nrdF*-Gene of *Corynebacterium ammoniagenes* Strain ATCC 6872 generates a Manganese-Metallocofactor (R2F) and a Stable Tyrosyl Radical ($Y^{\bullet}$) involved in Ribnucleotide Reduction

Eigenanteil:

Das *nrdF*-Gen von *Corynebacterium ammoniagenes* wurde in einer vorhergehenden Dissertation (Barckhausen, 2004) zwar homolog exprimiert und das Genprodukt angereichert, jedoch ohne Nachweis der spezifischen Aktivität. Ein stark modifizierter Reinigungsprozess führte zu einem hochaktiven R2F-Protein, das mit seiner im biochemischen Komplementationsassay gemessenen spezifischen Aktivität sämtlicher in der Literatur beschriebener Ribonucleotid-Reduktasen übertrifft. Zur Aufklärung des Reaktionsmechanismus wurde ein präparativer Enzymtest entwickelt, für den die benötigten Proteinmengen über Teilautomatisierung bereitgestellt wurden. Mit diesem neuartigen Test konnte eine direkte Beteiligung des in der R2F-Untereinheit lokalisierten Tyrosylradikals in der Ribonucleotid-Reduktion gezeigt werden. Die Eignung dieses neu entwickelten Tests für RNR-Inhibitorstudien im Echtzeit-Screeningverfahren wurde vorgestellt (Stolle et al., 2010b).

the FEBS Journal

Homologous expression of the *nrdF* gene of *Corynebacterium ammoniagenes* strain ATCC 6872 generates a manganese-metallocofactor (R2F) and a stable tyrosyl radical (Y•) involved in ribonucleotide reduction

Patrick Stolle[1], Olaf Barckhausen[1,*], Wulf Oehlmann[1], Nadine Knobbe[2], Carla Vogt[2], Antonio J. Pierik[3], Nicholas Cox[4], Peter P. Schmidt[4,†], Edward J. Reijerse[4], Wolfgang Lubitz[4] and Georg Auling[1]

1 Institut für Mikrobiologie, Leibniz Universität Hannover, Germany
2 Institut für Analytische Chemie, Leibniz Universität Hannover, Germany
3 Institut für Zytobiologie, Philipps Universität Marburg, Germany
4 Max-Planck-Institut für Bioanorganische Chemie, Mülheim, Germany

Keywords
Corynebacterium ammoniagenes; EPR; homologous expression; manganese-tyrosyl; metallocofactor; ribonucleotide reductase

Correspondence
G. Auling, Institut für Mikrobiologie, Leibniz Universität Hannover, Schneiderberg 50, D-30167 Hannover, Germany
Fax: +49 511 762 5287
Tel: +49 511 76 5241
E-mail: auling@ifmb.uni-hannover.de

***Present address**
Olaf Scheibner, Thermo Fisher Scientific GmbH, Bremen, Germany

†Deceased 2008

(Received 21 February 2010, revised 7 September 2010, accepted 17 September 2010)

doi:10.1111/j.1742-4658.2010.07885.x

Ribonucleotide reduction, the unique step in the pathway to DNA synthesis, is catalyzed by enzymes via radical-dependent redox chemistry involving an array of diverse metallocofactors. The nucleotide reduction gene (*nrdF*) encoding the metallocofactor containing small subunit (R2F) of the *Corynebacterium ammoniagenes* ribonucleotide reductase was reintroduced into strain *C. ammoniagenes* ATCC 6872. Efficient homologous expression from plasmid pOCA2 using the *tac*-promotor enabled purification of R2F to homogeneity. The chromatographic protocol provided native R2F with a high ratio of manganese to iron (30 : 1), high activity (69 μmol 2′-deoxyribonucleotide·mg^{-1}·min^{-1}) and distinct absorption at 408 nm, characteristic of a tyrosyl radical (Y•), which is sensitive to the radical scavenger hydroxyurea. A novel enzyme assay revealed the direct involvement of Y• in ribonucleotide reduction because 0.2 nmol 2′-deoxyribonucleotide was formed, driven by 0.4 nmol Y• located on R2F. X-band electron paramagnetic resonance spectroscopy demonstrated a tyrosyl radical at an effective *g*-value of 2.004. Temperature dependent X/Q-band EPR studies revealed that this radical is coupled to a metallocofactor. Similarities of the native *C. ammoniagenes* ribonucleotide reductase to the *in vitro* activated *Escherichia coli* class Ib enzyme containing a dimanganese(III)-tyrosyl metallocofactor are discussed.

Introduction

The ribonucleotide reductase [1] enzymes (RNR) catalyze the formation of deoxyribonucleotides from ribonucleotides. It is the only biological pathway for deoxyribonucleotide (DNA monomer) production and thus regulates the rate of DNA synthesis within all cells [2]. The reduction of ribonucleotides to 2′-deoxyribonucleotides proceeds via a free radical reaction mechanism, which is initiated by an organic radical [3] and conserved in all organisms. RNR enzymes do differ with respect to the methodology used to generate

Abbreviations
GF-AAS, graphite furnace atomic absorption spectroscopy; HU, hydroxyurea; ICP-MS, inductively coupled plasma MS; IPTG, isopropyl thio-β-D-galactoside; *nrdF*, nucleotide reduction gene; R1E, large catalytic subunit; R2F, small subunit of the RNR; RNR, ribonucleotide reductase; Y•, tyrosyl radical.

the initial free radical and, as such, are divided into three classes, based on the metallocofactor required for the radical initiation process.

The RNR enzyme of the Gram-positive species *Corynebacterium* (formerly *Brevibacterium*) *ammoniagenes* was originally described as a manganese analogue [4] of the iron containing class I RNR of *Escherichia coli*. This assignment was based on an analysis of its metal composition and similarity of its absorption spectrum to di-manganese(III) model complexes [5]. This Mn-RNR was considered as a prototype of an enzyme category of its own [3,6,7]. The manganese metallocofactor, contained in the small subunit (R2F) of this Mn-RNR, was further studied by EPR spectroscopy. These early studies suggested the metal site contained a manganese [8] and a stable free radical centred at $g = 2.004$ [9]. The organic radical was assigned to Y115 of the NrdF protein [10,11]. An independent study by Fieschi *et al.* [11] confirmed that the RNR 'as isolated' from the wild-type strain *C. ammoniagenes* ATCC 6872 contained manganese instead of iron metallocofactor. Subsequently, the same group revised this assignment, and suggested instead that RNR of *C. ammoniagenes* contained an iron metallocofacor. In their latter study, they used an R2F preparation originating from heterologous expression of the *C. ammoniagenes nrdF* gene in *E. coli* and subsequent *in vitro* activation of the apo-R2F with iron ascorbate [12,13]. Such a heterologous expression approach may have its limitations. To operate correctly, any introduced gene (cis-acting DNA) must comply with unknown (trans-acting factors) (e.g. chaperones or cofactors) in the host cell [14]. An increasing awareness of these limitations has encouraged research aiming to construct new vectors for homologous expression and thus improve the functional screening of phenotypes not detectable in *E. coli*.

It is essential to the field of RNR research that the long outstanding dispute over the metal content of the RNR of *C. ammoniagenes* is resolved. In the present study, our strategy was to establish the homologous expression of the *C. ammoniagenes nrdF* gene and enrich the native R2F within its original genetic background. A first obstacle was the low rate of gene transfer into *C. ammoniagenes* [15,16], which is not a model organism, notwithstanding previous intensive studies on the production of taste-enhancing nucleotides [7,17,18]. In the present study, the tool box for genetic manipulation of the related species *Corynebacterium glutamicum* [19–22] was successfully adapted (C.-H. Luo, unpublished results) to the nucleotide-producer *C. ammoniagenes* [10]. The present strategy of reintroducing the *nrdF* gene into the genetic background of corynebacteria comprised an initial transfer into the accessible species *C. glutamicum* and the performance of a second, final gene transfer into *C. ammoniagenes* strain ATCC 6872, which is the original source of the Mn-RNR [4]. The intermediate use of the restriction-deficient strain *C. glutamicum* R163 [23], a derivative of the wild-type strain *C. glutamicum* ATCC 13059, as an initial corynebacterial recipient allowed us to develop an efficient electroporation protocol for *C. ammoniagenes* ATCC 6872 as the final recipient.

In the present study, we report data on homologous expression of the *nrdF* gene of *C. ammoniagenes* strain ATCC 6872. This is the first report of the successful purification of high amounts of the native *C. ammoniagenes* R2F as a manganese- and tyrosyl radical-containing metallocofactor, which was recently crystallized as a manganese protein [24]. Furthermore, the application of this R2F in a novel enzyme assay revealed the quenching of its tyrosyl radical concomitant with product formation.

Results

Purification of *C. ammoniagenes* R2F from homologous expression using plasmid pOCA2 by promotorless insertion of *nrdF* under the control of the *tac*-promotor

The *E. coli/C. glutamicum* shuttle vector, pXMJ19 [21], was used for subcloning of the *nrdF* gene under the control of the hybrid *tac* promotor. The resulting expression vector, plasmid pOCA2, contained the complete *nrdF* gene in the right orientation. It was first introduced into *E. coli* XL1-Blue to control the isopropyl thio-β-D-galactoside (IPTG)-inducible expression of *nrdF* in the *E. coli* (*lacIq*) background. Regulation of NrdF (R2F) synthesis by the expression vector pOCA2 was confirmed by SDS/PAGE of extracts from induced cells. A distinct band at 38 kDa, the expected size of R2F, reacted specifically with R2F-antibody (data not shown).

Gene transfer into *C. ammoniagenes* strain ATCC 6872, the original source of the Mn-RNR [4], was achieved by an improved electroporation protocol described in the Materials and methods. The enhanced expression of the *nrdF* gene should generate higher titres of functional R2F harbouring a tyrosyl radical (see Discussion). Transformants from reintroduction of the *nrdF* gene via plasmid pOCA2 were selected by their resistance towards chloramphenicol and an acquired tolerance towards the radical scavenger hydroxyurea (HU) [4,9]. Following this protocol, single colonies of *C. ammoniagenes* pOCA2 tolerated

12 mM HU (when induced). By contrast, the growth of the wild-type strain ATCC 6872 was completely suppressed by the addition of 3 mM HU (Table 1). In liquid medium, strain *C. ammoniagenes* pOCA2 produced increased levels of R2F after 5 h of incubation in the presence of 0.6 mM IPTG. This amounted to 5% of the total cellular protein as assessed by SDS/PAGE and immunodetection (see above).

The high expression of the *nrdF* gene led to detection of an absorption maximum of 408 nm in enriched fractions of *C. ammoniagenes* pOCA2 for the first time when Mn^{2+} was added during induction (Fig. 1). No radical signal at 408 nm was observed upon addition of Fe^{2+} during induction and no iron was found in the respective R2F preparation as assessed by the phenantroline method.

Absorption at 408 nm, characteristic of tyrosyl radicals in RNR [25], was used in conjunction with SDS/PAGE and R2F-antibody as a marker to assist in the purification of the R2F-protein. In the new purification strategy that was developed (see Materials and methods), an increase in the putative radical signal, relative to the overall protein concentration, was observed with each purification step (Fig. 1). This correlated with an increase of specific activity (Table 2) and an increase in the manganese to iron content (Fig. 1) as determined by graphite furnace atomic absorption spectroscopy (GF-AAS) and inductively coupled plasma MS (ICP-MS).

The best resolution of protein fractions was achieved by gel filtration using a Superdex 200 column. Two major fractions were observed: an iron-rich fraction of molecular mass 81 ± 12 kDa and a manganese-rich fraction of molecular mass 38 ± 4 kDa. Only the manganese-rich fraction displayed the radical signal at 408 nm and contained the R2F protein as determined using R2F-antibody. The iron-rich fraction did not show any RNR activity. Similarly, no reaction was observed with R2F-antibody for this fraction. RNR activity and R2F-antibody response were also not observed for all additional high- and low-molecular weight fractions. Interestingly, the R2F protein eluted as a monomer for the *C. ammoniagenes* pOCA2 strain. The opposite is observed for preparations sourced from the wild-type [4,8,9].

The manganese-rich fraction was further purified using a Mono Q® column. This allowed purification of R2F to homogeneity (Fig. 2). The identity of the purified R2F protein was confirmed by complete sequencing and comparison with the published reference data (UniProtKB: O68555_CORAM). The R2F protein displayed a molecular extinction coefficient (ε_{280}) of 76280 $M^{-1} \cdot cm^{-1}$. This value was calculated using the molecular mass of the R2F monomer, the absorption at 280 nm and protein quantification, and is consistent with the theoretical ε_{280}. It should be noted that, if a dimer is assumed, the value of ε_{280} would decrease by one half. The manganese content was determined spectroscopically by oxidation of the protein bound manganese to MnO_4^- [26]. This yielded a manganese concentration of 0.74 ± 0.04 mol $Mn \cdot mol^{-1}$ monomer.

Table 1. Tolerance towards HU exposure.

	HU concentration (mM)				
Strain, condition	1.0	3.0	6.0	9.0	12.0
Corynebacterium ammoniagenes ATCC 6872	+++	+	–	–	–
Corynebacterium ammoniagenes pOCA2	+++	+	+	–	–
Corynebacterium ammoniagenes pOCA2[a]	+++	+++	+++	++	++

[a] Induced, 1 mM IPTG.

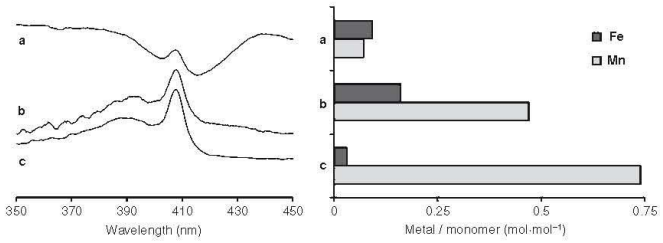

Fig. 1. Enrichment of the 408 nm radical signal (left) and manganese (right) in fractions of the Mn-RNR from *C. ammoniagenes* pOCA2 during chromatography using UNO™ sphere Q (a), Superdex 200 (b) and Mono Q® (c). The radical intensities were assessed from absorption difference spectra, which was generated by subtraction of HU-treated data from native protein data. All spectra were adjusted in position on the *y*-axis. Metal content was determined as described in the Materials and methods.

Table 2. Enrichment of the radical-containing R2F from expression of the *nrdF* gene using *C. ammoniagenes* pOCA2. AS, precipitation by ammonium sulfate; QS, chromatography using UNO™ sphere Q; S, Superdex 200 gel filtration; MQ, chromatography using Mono Q®. The radical concentration was calculated using the 408 nm tyrosyl radical signal as described in the Materials and methods. As a result of the presence of oligonucleotide inhibitors, enzymatic activity (standard assay) cannot be determined before the AS step, which reduces the protein concentration by one half. Therefore, the data refer only to the different steps during enrichment.

Step	Radical concentration ($\mu mol \cdot mL^{-1}$)	Recovery (%)	Protein (mg)	Specific activity ($\mu mol \cdot mg^{-1} \cdot min^{-1}$)	Enrichment of R2F
AS	0.11	100	5525	14.3	2.0
QS	0.18	84	2610	24.2	4.2
S	0.31	61	640	41.2	17.2
MQ	0.52	52	291	69.0	36.0

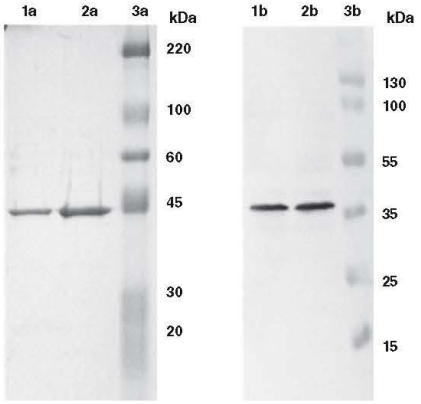

Fig. 2. Homogeneity of purified R2F eluted from a Mono Q® HR 5/5 column as assessed by SDS/PAGE (left) and western blotting with R2F-antibody (right); from left to right: 1, R2F from Mono Q®; 2, same, concentrated; 3, molecular weight standard.

Thus, 300 mg of R2F with a specific activity of 69 μmol 2′-deoxyribonucleotide·mg^{-1}·min^{-1} (see Discussion) were usually obtained from 70 g wet weight of biomass.

Spectroscopic characterization of the R2F protein from *C. ammoniagenes*

The optical absorption spectrum of the purified R2F contained a sharp absorption centred at 408 nm, characteristic of tyrosyl radical seen in RNR (Fig. 3A), such as that reported for the manganese containing RNR in *C. glutamicum* (wild-type) [27]. The radical content was determined as 0.18 mol tyrosyl radical (Y•) per mol R2F monomer. The short half-life (only 5 h at 4 °C) posed a significant experimental challenge. This problem was overcome by the addition of glycerol and/or detergents. These helped to stabilize the radical. In the final protocol that was developed, the addition of glycerol and detergent combined with an enhanced ionic strength (Fig. 4) extended the half-life of the radical in the purified *C. ammoniagenes* R2F to 2 weeks at 4 °C or 6 days at 21 °C.

The X-band EPR spectrum (9.46 GHz) measured at 77 K revealed an organic radical positioned at a *g*-value of 2.004 (Fig. 5). The intensity of this EPR signal correlated with the 408 nm maximum, as seen in the optical absorption spectra. The EPR signal could not be saturated with the available microwave power (200 mW). The simulation shown in Fig. 5B was generated using the parameters of a typical isolated tyrosyl radical. This simulation reproduces the centre of the experimental spectrum reasonably well. It cannot, however, explain the remarkably broad wings of the signal. The broad lineshape and the enhanced relaxation properties of the signal at 77 K indicate that the Y• is coupled to a paramagnetic centre, presumably the metallocofactor. It should be noted that the EPR spectra and their temperature dependence as observed for the current radical-manganese species differ from that reported for the metallocofactor of R2F from *C. glutamicum* [27]. However, the EPR properties of both species are consistent with a tyrosyl radical. Differences in lineshape and temperature dependence between the two species may be related to subtle changes in the structure of the manganese cofactor, which will affect its effective zero-field splitting and therefore also the lineshape of the coupled radical; a full discussion is provided elsewhere [28].

A similar radical species was observed at Q-band (5 K). Under these conditions, the signal resolved additional structures with peak splittings in the range 2–4 mT (Fig. 6A). In addition, a superimposed weak six-line signal from Mn(II) with peak spacings in the range 8–10 mT was also detected. The lineshape of the radical-like EPR signal is strongly temperature-dependent, as is apparent from the comparison of the spectra recorded at 5 K (Fig. 6A) and 77 K (Fig. 6B). The radical type central line of the EPR spectrum is present at all temperatures. The total spectral breadth of the signal, as defined by the broad wings at X-band (Fig. 5) and the additional peaks at Q-band (Fig. 6A), does not change with the external field. This behaviour is indicative of an $S = 1/2$ spin system (i.e. the tyrosyl) coupled to a metal centre with integer spin as

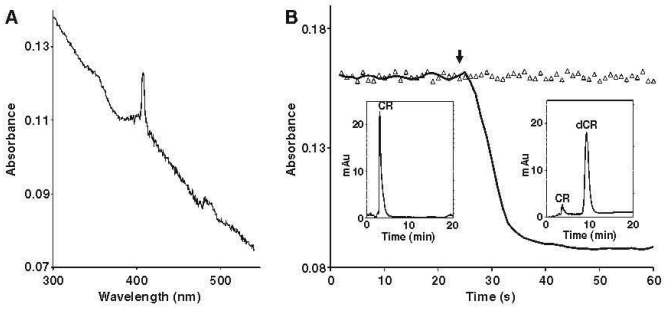

Fig. 3. Involvement of the R2F tyrosyl radical in 2′-deoxyribonucleotide product formation, noticeable as depletion of its 408 nm absorption signal. The wavescan (A) was run with 0.67 nmol R2F. The change of the absorption at 408 nm during the reaction was tracked in a time-scan (B) of a novel enzyme assay; continuous black line, course of enzyme reaction; arrow, time point of substrate addition; triangles, control (reaction by addition of BSA instead of substrate). The assay contained 2.36 nmol R2F (with 0.40 nmol Y•) complemented in the ratio 2:1 with R1E in the usual 85 mM potassium phosphate buffer (pH 6.6) in a total volume of 10 μL, and reaction was started by addition of 0.25 nmol CDP to the holoenzyme. After 0.5 min, the reaction was stopped by boiling and the mixture was digested by alkaline phosphatase treatment and analyzed by HPLC at the nucleoside level [51]. The left inset shows the starting condition with the substrate peak cytidine (CR), whereas the formation of product peak 2′-deoxycytidine (dCR) is shown in the right inset. The product after 0.5 min of reaction was confirmed by identical retention compared to a commercial 2′-deoxycytidine reference (AppliChem GmbH, Darmstadt, Germany). The data presented in (B) are the mean of triplicate runs. Addition of BSA instead of CDP kept Y• stable, excluding mere dilution.

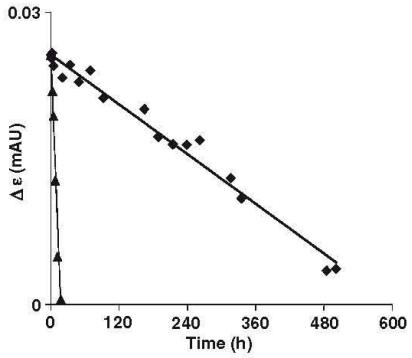

Fig. 4. Enhanced longevity of the R2F tyrosyl radical by buffer optimization. R2F was incubated at 4 °C in 85 mM potassium phosphate buffer, 2 mM dithiothreitol (pH 6.6) as standard buffer (▲) or supplemented with 100 mM KCl, 15% glycerol and 0.5% Tween 80 (♦). Time resolved UV-visible spectra, based on the wavescan in Fig. 3A, were recorded and Δε values were generated by subtraction of absorbance at 413 nm from the 408 nm maximum of Y• by a drop line approach.

suggested for class Ib of *E. coli* [29]. A full analysis of this signal is provided elsewhere [28].

To verify the assignment of the coupled signal, the sensitivity of the *C. ammoniagenes*-RNR towards the radical scavenger hydroxyurea [4,10] was investigated. Our putative coupled 'radical signal' at 77 K (Fig. 6B) disappeared after the addition of 10 mM HU (final concentration) to R2F. Only the Mn(II) artefact was observed after the addition of HU (Fig. 6C). This signal is similar to that of a control solution of free Mn(II) in the same buffer, except for the linewidth (50 mM Tris/HCl, pH 7.5 with 10 mM HU; Fig. 6D).

Because the EPR spectra of the active R2F protein are indicative of a radical coupled to an integer Mn_2 spin system, we assume that the Mn(II) species is a reduced or inactivated form of the metal complex. Similar experiments at X-band (Fig. S1) did not resolve a Mn(II) type EPR spectrum after HU treatment. It is assumed that the amount of inactive Mn(II) varies slightly in the preparations. After denaturation of R2F with HU and trichloroacetic acid, a Mn(II) type EPR spectrum was observed, similar to that of $MnCl_2$ in Tris buffer (Fig. S1E). Denaturation presumably liberates all bound manganese species from their protein environment. A quantification of this signal indicated a manganese content of 1.4 ± 0.2 Mn per R2F dimer, similar to that seen by chemical oxidation to MnO_4^- [26].

The stable tyrosyl radical (Y•) of the *C. ammoniagenes* R2F is involved in ribonucleotide reduction

An activity assay was developed to examine the enzymatic reaction of the RNR of *C. ammoniagenes*. The aim was to identify potential differences between this

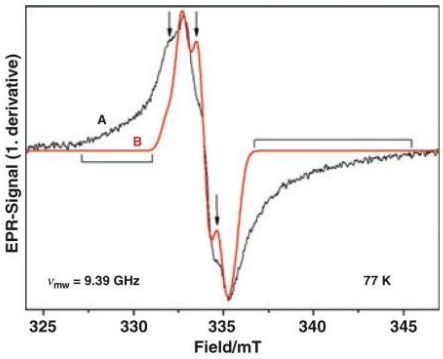

Fig. 5. X-band EPR signal of the 38 kDa R2F-monomer (270 μM in 50 mM Tris/HCl at pH 7.5) from *C. ammoniagenes* pOCA2 (A) in comparison with a simulation (B) typical for a class Ib RNR tyrosyl radical [54]. The simulation parameters are: linewidth 0.4 mT, *g*-tensor, g_x = 2.0090, g_y = 2.0044, g_z = 2.0022, one β-^{1}H-hyperfine-tensor (1.18, 1.11, 1.11 mT) and two α-^{1}H-hyperfine tensors (−0.32, −1.00, −0.66 mT) rotated by 60° and 300° around the *z*-axis of the *g*-tensor. This rotation corresponds to the hydrogen bonding angles in the planar tyrosyl radical. The positions of the hyperfine splittings are indicated by arrows. The brackets indicate the signal wings, which could not be simulated. Experimental conditions: 9.39 GHz, 2 mW, 77 K, modulation amplitude 0.16 mT, modulation frequency 100 kHz, nine scans of 84 s, time constant 82 ms.

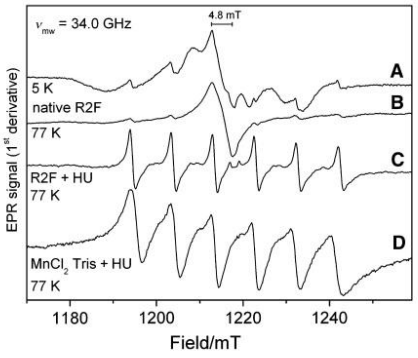

Fig. 6. Q-band EPR of R2F-protein (6.75 μM in 50 mM Tris/HCl, pH 7.5) from *C. ammoniagenes*-RNR; general experimental conditions unless stated otherwise: microwave frequency 34.0 GHz, field modulation 1.0 mT, 100 kHz, ten scans; accumulation time 84 s; time constant 82 ms; (A) native at 5 K and 12.2 μW power; (B) native at 77 K, 122 μW power, the 4.8 mT line width of the first derivative of the inner ($Y^\bullet$) signal is indicated by a bar; (C) after adding 10 mM (final concentration) hydroxyurea (HU) at 77 K, 122 μW power; (D) for comparison, 300 μM $MnCl_2$ in 50 mM Tris/HCl (pH 7.5) and 10 mM HU at 77 K, 244 μW power, 25 scans; field modulation 0.5 mT; 100 kHz; accumulation time 84 s; time constant 41 ms.

species and that of *E. coli*, the archetypal model system of class I RNR. Briefly, the catalytic mechanism of ribonucleotide reduction *in vivo* seen in *E. coli* [29] can be described in four steps: (a) substrate ribonucleotide binding and radical transfer from the tyrosyl radical (Y122) of the R2 subunit to the cysteine (C439) found in the active site of the R1 subunit; (b) the abstraction of two protons and water release, with the concomitant formation of a disulfide cysteine; (c) radical transfer from the R1 subunit back to the tyrosine Y122 of the R2 subunit; and (d) dedocking of the product deoxyribonucleotide and reduction of the disulfide cysteine by NADPH. In *in vitro* studies, the reductant dithiothreitol is often added to facilitate reduction of the disulfide cysteine. In the assay reported in the present study, a reductant is omitted so that only one enzyme turnover is allowed. Similarly, no attempt was made to reconstitute the sample with NrdI, an accessory flavodoxin-like protein. A recent study identified this protein as an important component in the *in vitro* assembly of a Mn-R2F-$Y^\bullet$ cofactor [30]. Importantly, however, it is not required for normal enzyme function once the metallocofactor is assembled.

Enzyme assays were started upon addition of the nonlabelled substrate CDP. In samples that contained both the large catalytic (R1E) and R2F subunit, product formation was observed using HPLC. The highest product yield (0.18 nmol 2′-deoxyribonucleotide) was achieved by 0.4 nmol $Y^\bullet$ and 0.2 nmol CDP. The ratio of R1E to R2F was 2 : 1. Thus, almost complete product formation could be achieved. In samples in which R1E was omitted, no product formation was observed. Similarly, when a mimic of the C-terminal peptide of the R2F subunit, the heptapeptide (*N*-acetyl-TDDDWDF) was added, no product formation was observed. It is considered that the R1E and R2F subunits interact via this protein domain. Thus, these results confirm that product formation requires both the R1E and R2F subunits for catalysis, as expected.

The tyrosyl radical of the R2F subunit was also monitored during the course of the enzyme assay. Curiously, under conditions where the product was formed, the tyrosyl radical, as measured by the absorption maximum of 408 nm, decreased in magnitude. Complete disappearance of the absorption maximum could be achieved using the same conditions described above for maximum product formation (Fig. 3B) and the residual absorbance observed in this sample was not further affected by the addition of HU. The tyrosyl radical completely decayed within 10 s of substrate addition. The degree of tyrosyl radical loss was dependent on the concentration of substrate added. Tyrosyl

radical ($Y^{\bullet}$ = 0.4 nmol) decay was observed if the substrate concentration was in excess of 0.15 nmol. The reasons for this suprising drop in the radical concentration during substrate conversion are given in the discussion.

Discussion

There is a growing body of evidence suggesting that the heterologous expression of genes encoding metalloproteins can lead to incorrect metal ion incorporation. This is observed in rubredoxin and desulforedoxins where zinc, instead of native metal iron, is taken up when heterologously expressed in *E. coli* [31]. Similarly, a thermophilic manganese-catalase, which failed to be synthesized in an active form in *E. coli*, was ultimately enriched only by using its original source, *Thermus thermophilus*, as a cell factory for expression [32]. Thus, avoidance of the use of surrogate hosts for expression reflects an increasing awareness of the requirement of genus- or species-specific metal chaperones in microorganisms. Even a demand for a simultaneously increased level of accessory protein(s) may be considered [33].

In the present study, we aimed to examine the RNR enzyme of *C. ammoniagenes* in its native species. Here, the source of the native R2F-protein of the *C. ammoniagenes* ribonucleotide reductase were transformants from the reintroduction of the *nrdF* gene into the strain of its origin description [4] after the development of an efficient electroporation protocol. Acquired resistance towards the radical scavenger HU (Table 1) identified clones with increased levels of radical-bearing R2F. The breakthrough for high expression of R2F came from the construction of the plasmid pOCA2 using the *C. glutamicum/E. coli* shuttle vector pXMJ19 [21]. High amounts of R2F were synthesized from the inserted promotorless *nrdF*-gene under tight control of the IPTG-inducible *tac* promotor. This finding corroborates another study [34] reporting that the hybrid *tac* promotor from *E. coli* is a strong promotor in *C. ammoniagenes* as well. Because of high expression from the *tac* promotor, the proposed function of manganese in the transcriptional regulation of the *nrd* operon [35] may not be considered in the light of the results obtained in the present study. Rather, the involvement of manganese in the *in vivo* assembly of the metallocofactor of *C. ammoniagenes* R2F is envisaged. This is based: (a) on the parallel enrichment of manganese (Fig. 1); (b) the radical signal at 408 nm (Fig. 1); and (c) the 38 kDa R2F protein confirmed by both R2F-antibody (Fig. 2) and protein sequencing. In addition, this R2F displayed a molecular extinction coefficient at 280 nm (see Results), near the theoretical value of 71280 $M^{-1} \cdot cm^{-1}$. Taken together, these observations demonstrate conclusively that the purified protein was R2F and that it contained a manganese metallocofactor. The decisive step for purification of the manganese cofactor containing R2F-protein came from gel filtration (Superdex 200) in which the 38 kDa monomer of R2F eluted in a manganese rich pool and was thus separated from the bulk of larger iron proteins. In summary, our protocol led to the enrichment of highly active R2F, in which at least 50% of the original radical concentration of the metallocofactor was retained (Table 2).

Previous purification efforts and those of an independent laboratory resulted in elution of a dimeric R2F from gel filtration [4,8,9,11]. Both of these previous studies used the *C. ammoniagenes* wild-type. The disparate elution behaviour observed may be a result of the enhanced expression of *nrdF* alone using the strain *C. ammoniagenes* pOCA2. The resulting imbalance between the small and the large subunit indicates that stoichiometric amounts of both appear to be necessary for dimerization of R2F, which has a distinct C-terminal region for contact with R1E (see below). However, the data do not suggest an enzymatically active $Y^{\bullet}$- and manganese-containing R2F monomer. Rather, the specific activity was assayed after biochemical complementation with R1E and subsequent formation of a dimeric R2F in the holoenzyme.

The specific activity of the *C. ammoniagenes* R2F, as isolated (69 $\mu mol \cdot mg^{-1} \cdot min^{-1}$) is remarkably high compared to other class I RNRs: *E. coli* R2, 6.0 $\mu mol \cdot mg^{-1} \cdot min^{-1}$ [36]; *E. coli* Mn-R2F, *in vitro* activated with the accessory factor NrdI, 0.6 $\mu mol \cdot mg^{-1} \cdot min^{-1}$ [30]; *Salmonella typhimurium* Fe-R2F, 0.85 $\mu mol \cdot mg^{-1} \cdot min^{-1}$ [37]; and *C. ammoniagenes* Fe-R2F, 0.05 $\mu mol \cdot mg^{-1} \cdot min^{-1}$ [12]. The recently described *C. glutamicum* RNR, 32 $\mu mol \cdot mg^{-1} \cdot min^{-1}$ [27] is an exception. The NrdI protein has recently been identified as an important component in the *in vitro* assembly of a Mn-R2F-$Y^{\bullet}$ cofactor [30] seen in class Ib RNR. The *nrdI* gene is located in the *nrd* operon of *C. ammoniagenes* [11] and other organisms [38,39]. In the present study, the R2F, as isolated, did not contain NrdI, as assessed by ESI-QTOF-MS.

In our view, *C. ammoniagenes* restricts the incorporation of iron into R2F *in vivo*, even in the absence of manganese, and it is the availability of manganese that is the limiting factor determining the amount of functional metalloradical cofactor obtained. In addition, relatives of corynebacteria belonging to the genus *Arthrobacter* were ineffective with respect to compensating for the effects of manganese limitation by iron

and other divalent metal ions [40]. In our opinion, continuous metal determination of the native R2F during enrichment from its original source *C. ammoniagenes* (Fig. 1) has resolved the long-standing debate over the metal speciation of the *C. ammoniagenes* RNR, conclusively demonstrating that it uses only manganese. For this challenge, sensitive methods, which measure elemental concentrations in the range of $ng \cdot L^{-1}$, were indispensable. The methods applied here for quantitative metal analysis (GF-AAS, ICP-MS) required adaptation (see Materials and methods) as a result of problems with the protein matrix in analysis of metalloproteins [41]. Thus, approximately the same values for the purified R2F protein as those obtained by the chemical determination were achieved (Fig. 1c; Mono Q®-step). A finding of 1.4 Mn per R2F dimer appears consistent with the assigment of *C. ammoniagenes* RNR as a class Ib enzyme. The consensus is that all class I RNRs use binuclear metallocofactors, although substoichiometric amounts of metals are found in the purified proteins. In addition, sequence alignment of the corynebacterial NrdF protein reveals that the residues required for a binuclear metal centre are conserved [10,11]. The absence of iron in the *C. ammoniagenes* R2F 'as isolated' suggests that iron does not play an important role in this species. The diferric metallocofactor, obtained after heterologous expression in the phylogenetically distant Gram-negative species *E. coli* [12], is thus considered an experimental artefact. In addition, a unique additional solvent water molecule [13] was identified as part of the hydrogen bonding network about the Y115 in Fe-R2F, indicating easier solvent access to the tyrosyl. The same water molecule is not observed when the protein contains an active manganese metallocofactor [28]. This feature appears to correlate with the relative activities of the R2F subunit when manganese or iron is bound. The solvent accessable Fe-R2F has a much lower activity than the solvent inaccessable Mn-R2F. Solvent inaccessability of the Mn-R2F was indicated by its high inhibition constant (I_{50}) of 10 mM towards EDTA [4], which suggested that the metal centre is burried within the protein. This feature is also observed in its crystal structure [28]. A binuclear manganese cluster is consistent with a recent report for the *E. coli* RNR Ib [30]. The lower than expected manganese and radical content of the Mn-RNR reported in the present study is easily explained when considering that we are dealing with a mixture of fully occupied (2 Mn), radical-containing R2F monomers and apoprotein free of both. The manganese and radical content per mol R2F monomer found in the present study (0.74 and 0.18, respectively) suggest that only 25% of the manganese would be present in a binuclear form of the active metallocofactor (i.e. 0.185 Mol Mn_2 per Mol R2F), given that both sites would have equal affinity for manganese. Possibly, manganese loading is enhanced when *nrdF* is coexpressed with *nrdI* [30].

The absorption spectrum obtained for the tyrosyl radical of the R2F subunit (Fig. 3A) matches those of other RNR [12,37] and is detectable even in partially enriched fractions. Furthermore, the increase of the concentration of the organic radical in response to added manganese indicates an obligatory role of this metal during *in vivo* generation of the radical. It is expected that the tyrosyl radical is directly involved in 2′-deoxyribonucleotide product formation via radical transfer to the catalytic site of the R1E subunit. As reported in the Results, upon completion of substrate conversion, the radical is then rapidly passed back from the R1E subunit to the tyrosyl of the R2F subunit. Subsequently, the dicysteine unit is re-reduced by an exogenous reductant and catalytic activity is restored. By not adding the reductant, the expectation is that only one turnover of the enzyme is possible. However, it is still expected that tyrosyl radical should be restored upon the completion of substrate conversion. It is unclear from our results obtained in the present study whether this is the case. In our modified activity assay (without reductant), tyrosyl radical decay was clearly observed and the extent of its decay matched the level of substrate conversion. Control measurements without R1E, and under conditions where R1E and R2F could not specifically interact, showed that no substrate conversion or radical loss was observed. Thus, the results clearly demonstrate the tyrosyl radical is a participant in enzymatic function, as expected. It is unclear, however, why tyrosyl radical recovery is not observed. At present, we lack the temporal resolution to distinguish whether tyrosyl radical decay is related to a single turnover event and thus represents a fundamental difference in the reaction mechanism of this RNR and that of other class 1 RNRs or, instead, is a result of the interaction of the R2F with the inactivated (oxidized) form of the R1E. We consider the first option unlikely. Under these circumstances, the Mn-Y• metalloradical cofactor would have to be reassembled upon each turnover of the enzyme to provide the radical species. This process is likely to be slow relative to the kinetics of substrate conversion observed when an exogenous reductant is present (dithiothreitol). Instead, we favour the latter option. Radical transfer from the R2F subunit to the R1E subunit is considered to be commensurate with substrate binding. Thus, a protein conformational change of R1E somehow facilitates electron transfer.

Here, we suggest that R2F and the oxidized form of R1E are also capable of radical transfer. The R1E (in its oxidized, dicysteine state) may still have the product deoxyribonucleotide weakly associated with the substrate binding pocket and, as such, in a protein conformation conducive to radical transfer. Thus, multiple electron transfer events between the R1E catalytic site and the R2F tyrosyl could lead to the progressive loss of the radical species. It is noted that the kinetics of radical loss (over many seconds) are consistent with this mechanism. Similarly, because the proposed radical decay occurs as a result of product (formally substrate) association with R1E, a correlation between its decay and substrate concentration could be expected.

In conclusion, the EPR properties of the Y•-Mn R2F cofactor described in the present study, as well as the ability of hydroxyurea to reduce both Y• and the manganese cluster, are consistent with the proposed di-Mn(III) cofactor in *E. coli* NrdF recently described by Cotruvo and Stubbe [30]. A companion study by Cox *et al.* [28] involving X-ray analysis and multifrequency EPR provides additional support for this assignment.

Materials and methods

Chemicals

2′,5′-ADP Sepharose (self packed XK 16/20), UNO™ sphere Q (self packed XK 16/20) and Superdex 200 prep grade (prepacked) chromatography media and columns were obtained from Pharmacia LKB (Freiburg, Germany). HiTrap™ desalting columns and Mono Q® HR 5/5 were obtained from GE Healthcare Europe GmbH (München, Germany). Visking® dialysis tubes were obtained from Serva Feinbiochemica GmbH & Co., KG (Heidelberg, Germany). Amicon® Ultra-4 Centrifugal Filter Units were purchased from Millipore Corporation (Billerica, MA, USA), [5-^{3}H]CDP, ammonium salt (10 30 Ci·mmol^{-1}) and [8-^{3}H]GDP, ammonium salt (10 15 Ci·mmol^{-1}) were obtained from Amersham-Buchler (Braunschweig, Germany). The inhibitory peptide *N*-acetyl-TDDDWDF was synthesized by Genosphere Biotechnologies (Paris, France).

Bacterial strains, plasmids and general culture conditions

Bacterial strains and plasmids used in the present study are listed in Table 3. *C. ammoniagenes* ATCC 6872 was cultivated at 30 °C in LB medium which contains: 10 g·L^{-1} peptone from casein, 5 g·L^{-1} yeast extract and 5 g·L^{-1} NaCl. The pH was adjusted to 7.2 with 3 M NaOH before sterilization. Agar plates were prepared by addition of 15 g·L^{-1} Difco agar (Difco, Franklin Lakes, NJ, USA). For growth of *C. ammoniagenes* pOCA2, 15 mg·L^{-1} chloramphenicol was added to the medium. The same antibiotic was used for assaying tolerance of corynebacterial transformants against increasing concentrations (1 15 mM) of the radical scavenger hydroxyurea by checking for growth on LB agar plates in the presence of IPTG (1 mM) at 30 °C.

E. coli XL1-Blue was grown at 37 °C in LB medium [42] supplemented with ampicillin (100 μg·mL^{-1}), chloramphenicol (30 μg·mL^{-1}) and either D-glucose (0.5%, w/v) or IPTG (1 mM) as required. Single colonies of the recombinant *E. coli* strain were cultured overnight in 5 mL of LB medium containing chloramphenicol (30 μg·mL^{-1}) and D-glucose (0.5%, w/v). For induction of the *nrdF* gene, cells from liquid cultures were harvested by low-speed centrifugation, transferred into 5 mL of fresh LB medium, containing 1 mM IPTG instead of D-glucose, and incubated for another 3 h before expression analysis.

Large-scale growth of *C. ammoniagenes* pOCA2

C. ammoniagenes pOCA2 was grown aerobically in LB medium in the presence of chloramphenicol (15 μg·mL^{-1}) in a 10 L bioreactor (8 L air·min^{-1}; agitation at 350 r.p.m.;

Table 3. List of strains and plasmids.

Strain or plasmid	Genotype or description	Source or reference
Bacteria		
Corynebacterium ammoniagenes ATCC 6872	Wild-type	Willing *et al.* [4]
Escherichia coli XL1-Blue	*end*A1, *gyr*A96, *hsd*R17 (r_k^- m_k^+), *rec*A1, *rel*A1, *sup*E44, *thi*-1, F′(*pro*AB, lacI^q ZΔM15, Tn10)	Stratagene GmbH (Waldbronn, Germany)
Plasmids		
pXMJ19	Cm^r P_{tac}, lacI^q	Jakoby *et al.* [21]
pCR® 2.1-TOPO®	*amp*^{r} and *km*^{r}	Invitrogen GmbH (Karlsruhe, Germany)
pOCA2	pXMJ19 with *nrdF* (+ribosome binding site) insert from *C. ammoniagenes* ATCC 6872 using the *Xba*I/*Eco*RI sites	Barckhausen [43]; present study

Biostat V, B-Braun Biotech. International, Melsungen AG, Germany) at 30 °C until the midlogarithmic growth phase (D_{578} = 7.5). Expression of *nrdF* was then induced by 0.6 mM IPTG and 0.185 mM Mn^{2+} for 3 h before harvesting cells. Induction omitting this Mn-supplementation did not lead to RNR activity above the wild-type level [43].

Plasmid construct for *nrdF* expression

Standard DNA techniques and isolation of corynebacterial DNA were carried out as described previously [22]. For construction of plasmid pOCA2, the *C. glutamicum/E. coli* shuttle vector pXMJ19 [21] was used. The *nrdF* gene of *C. ammoniagenes* ATCC 6872 (and 24 bp upstream of the start codon containing the putative ribosome binding site but not the promotor) was amplified by PCR using primers OB1 (5′-TTT TTC TAG AGC AGG GTA GGT TGA TTT CAT GTC GAA TG-3′; additional *Xba*I site underlined) and OB 3 (5′-AAA AGA ATT CTT AGA AGT CCC AGT CAT CGT C-3′; additional *Eco*RI site underlined).

The amplified PCR fragment (Taq polymerase; Qiagen, Valencia, CA, USA) was purified using the QiaEX purification Kit (Qiagen) for Topo® cloning into plasmid vector pCR® 2.1-TOPO® (Invitrogen, Karlsruhe, Germany). The cloned $nrdF^{+}$ gene was sequenced by a primer walking approach. For DNA analysis, DNASTAR software (DNASTAR Inc., Madison, WI, USA) and CLONE MANAGER 5.0 (Scientific & Educational Software, Cary, NC, USA) were used. Alignments of the cloned *nrdF* gene with available *nrdF* sequences of *C. ammoniagenes* ATCC 6872 [10,11], GeneBank accession number CAA70766) were performed using CLUSTAL_W [44]. The confirmed *nrdF* gene was digested with *Eco*RI and *Xba*I and ligated into pXMJ19. The resulting expression vector pOCA2 was introduced into the *E. coli* host strain XL1-Blue as described previously [45] for quality control of the plasmid construct.

Transformation/electroporation

To increase transformation frequencies, recipients were grown in the presence of glycine, Tween 80 and isoniazide as described previously [46] in 10 mL of LB broth at 30 °C until D_{578} in the range 0.4 0.6 was reached. The cells were kept on ice for 5 min and harvested by a 10 min of centrifugation in a polypropylene tube at 7500 ***g*** at 4 °C. After three-fold washing in cold distilled water, cells were resuspended in 80 μL of an ice-cold glycerol (10%) solution. For electroporation, 40 μL of these fresh electro-competent cells were mixed with plasmid DNA (1 μg) in a cold sterile electroporation cuvette (2 mm electrode gap; Biotechnologies and Experimental Research, BTX; San Diego, CA, USA) and pulsed immediately with a BTX Electro Cell Manipulator ECM®600. The cell manipulator was usually set at a voltage of 2.5 kV. Subsequently, cells were resuspended in 1 mL of BHI (Oxoid, Wesel, Germany), withdrawn immediately for recovery by 3 h of incubation at 37 °C and then plated for selection of transformants.

Protein techniques

Protein was determined by protein-dye binding with BSA as a standard [47]. Whole cell protein of *C. ammoniagenes* cells was isolated from 2 mL of induced culture. After centrifugation (20 000 ***g*** for 8 min), cells were washed in phosphate-buffered saline and subsequently incubated in 100 μL of lysis buffer (10 mM Tris-HCl, pH 6.8, 25 mM $MgCl_2$, 200 mM NaCl), containing 5 $mg{\cdot}mL^{-1}$ lysozyme, for 60 min at 37 °C. Finally, 10 μL of SDS (10%) and 100 μL of loading buffer [48] were added and the sample was heated at 95 °C for 5 min before SDS/PAGE [48] in a mini-gel system (Biometra GmbH, Göttingen, Germany). Coomassie stained protein bands were compared with protein molecular weight standards (Amersham Pharmacia, Piscataway, NJ, USA). Polyclonal rabbit antiserum specific against the *C. ammoniagenes* RF2 protein served for immunostaining in a western blot [49]. This R2F-antibody was obtained by peptide immunization using the C-terminal oligopeptide SSYVIGKAEDTTDDDWDF translated from the *nrdF* sequence of *C. ammoniagenes* ATCC 6872 [10] and subsequent purification of the IgG fraction. In-gel digestion of the R2F band and protein identification by Q-TOF MS-MS was performed as described previously [50].

Preparation of the native R2F-protein

For enrichment of R2F from *C. ammoniagenes* pOCA2, cells were disrupted by two passages in a French Press at 1500 p.s.i. The resulting homogenate was submitted to fractionated ammonium sulfate precipitation. Active RNR was found in the precipitate at 40 60% saturation. This fraction was applied to HiTrap™ desalting columns and RNR was further enriched on a UNO™ sphere Q column using 85 mM phosphate buffer (pH 6.6) containing 2 mM dithiothreitol and 2 mM $MgCl_2$ as buffer A, and by the addition of 1.0 M KCl as buffer B. Applying 10 mL of protein solution and a stepwise gradient (0%, 15%, 35% and 100% buffer B), RNR subunits co-eluted in the third step at ≤ 350 mM KCl. The active fractions were collected by ammonium sulfate precipitation with 70% saturation, dissolved, and 1 mL aliquots were applied for Superdex 200 gel filtration using 85 mM phosphate buffer (pH 6.6) containing 2 mM dithiothreitol.

The three manganese- and radical-positive fractions eluting from the Superdex 200 gel filtration at 38 kDa were pooled for an additional anion exchange chromatography on a Mono Q® column. After dialysis against 25 mM Tris-HCl buffer (pH 7.5) containing 2 mM dithiothreitol, 8 mL of protein solution was loaded onto the column. Final elution was carried out with a linear gradient of 1.0 M KCl.

Homogeneously purified R2F resulting from enrichment using *C. ammoniagenes* pOCA2 was used for studying the metallocofactor. Each step of this protein purification was examined by metal quantification and monitoring of a tyrosyl signal at 408 nm (see below). For certain experiments, the final Mono Q® eluates were concentrated using Amicon® Ultra-4 centrifugal devices (cut-off 10 kDa).

Ribonucleotide reductase assay

Neither the large catalytic R1E, nor the radical- and metal-containing R2F alone is proficient in ribonucleotide reduction. Therefore, formation of the active RNR holoenzyme is required by biochemical complementation through binding of the small to the large subunit. For this purpose, R2F enriched as described previously and R1E obtained by affinity chromatography [9] were combined in a 2 : 1 ratio at 30 °C for 5 min of incubation before the standard assay (see below), whereas their concentrations were estimated by SDS/PAGE, western blotting analysis and protein-dye binding.

The 100 μL standard assay for Mn-RNR activity [4] contained 50 μM CDP and 0.25 μCi [5-^{3}H]-CDP (10 30 Ci·mmol^{-1}) as substrate, 50 μM dATP as positive allosteric effector, 6 mM dithiothreitol, serving as hydrogen donor *in vitro*, and 1 mM $MgCl_2$ in 85 mM potassium phosphate buffer (pH 6.6). The reaction was started by addition of the catalytically active holoenzyme for 5 min of incubation at 30 °C and stopped by boiling for 3 min. Only crude or poorly purified protein fractions were additionally treated with pronase [4] at 37 °C for 90 min to destroy the intrinsic heat-stable nucleoside *N*-glycosylase of *C. ammoniagenes* ATCC 6872, followed by brief boiling to destroy the pronase. The nucleotides in the reaction mixture were converted to the corresponding nucleosides by alkaline phosphatase [4]. Deoxyribonucleosides were separated from ribonucleosides by a modified HPLC method of Pal *et al.* [51] with 0.1 M borate buffer at pH 8.2 on a EUROKAT-H ion exchange column (Knauer, Berlin, Germany). Three different fractions were collected in the order: substrate (cytidine coeluting with nonreacted CDP), product (deoxycytidine) and by-product (cytosine) for analysis by liquid scintillation counting (Wallac 1410; Pharmacia, Freiburg, Germany). Positive reactions were confirmed by sensitivity to the radical scavenger HU. Blank values were obtained by 3 min of boiling. For certain experiments, controls were extended by the omission of either subunit or substrate. The error of this HPLC approach, including alkaline phosphatase treatment, was 5%.

An alternative enzyme assay without addition of reductant or accessory factors (see Results) was developed by monitoring the signal at 408 nm to track the activity of the tyrosyl- and manganese-containing small subunit. Here, the reaction was started by addition of CDP. Data are given as the mean of triplicates.

Inhibitory effects of the synthetic heptapeptide *N*-acetyl-TDDDWDF (Genosphere Biotechnologies, Paris, France) were studied in the above alternative assay. Before carrying out the assay, 10 μL of peptide solution (1 mg dissolved in 100 μL of 85 mM potassium phosphate buffer, pH 6.6) was added to R1E for 5 min of preincubation.

Spectroscopy

An Ultrospec TM 3300 pro UV/VIS spectrophotometer (GE Healthcare Europe GmbH) was used for recording of absorption spectra in the range 300 600 nm (resolution = 0.2 nm, scan speed = 1161 nm·min^{-1}) in a 100 μL cuvette. The average of three records was taken. For production of difference spectra, native samples were recorded first, then 5 μL of 200 mM hydroxyurea solution were added to the same cuvette for another recording under identical conditions. Spectra of HU-treated samples were subtracted from the corresponding native samples. The radical concentration was calculated by determining the area of the radical signal in the absorption spectrum by cubic spline interpolation [52] in the range 403 413 nm using the coefficient 3200 M^{-1}·cm^{-1} calculated as $\Delta\varepsilon$ ($\varepsilon_{\lambda red} - \varepsilon_{\lambda ox}$) as described previously [53].

X-band EPR spectroscopy

Freshly prepared samples of R2F (180 μL, 100 μM) were loaded into EPR-tubes (Ilmasil-PN high purity quartz; outer diameter 4.7 ± 0.2 mm, wall thickness 0.45 ± 0.05 mm, length 13 cm; Quarzschmelze Ilmenau GmbH, Langewiesen, Germany) and immediately frozen in liquid nitrogen. EPR Spectra were recorded with a Bruker Elexsys 500 EPR spectrometer (Bruker, Rheinstetten, Germany) equipped with an Oxford 930 flow cryostat (Oxford Instruments Ltd, Abingdon, UK). Data acquisition and processing (determination of *g*-values, baseline subtraction, integration and conversion) was carried out using Bruker spectrometer software XEPR, version 2.3.1. For *g*-value determination, the microwave frequency was measured with the built-in ER-041-1161 counter. The minor offset of the magnetic field as measured by the EMX-032T Hall probe was corrected using a strong pitch standard (g = 2.0028). A solution of 10 mM $CuSO_4$ in 2 M $NaClO_4$ and 10 mM HCl was used as the standard for spin integration. Further EPR conditions are provided in the legend to Fig. 5.

Q-band EPR spectroscopy

CW-Q-band EPR spectra were recorded using concentrated samples of R2F (60 μL, 100 μM). The samples were loaded into EPR-tubes (outer diameter 3 mm, inner diameter 2 mm) as described above and the measurements were

performed on a Bruker ESP300 EPR-Spectrometer (Bruker), equipped with a CF 935 Oxford helium flow cryostat. The microwave frequency was measured with an HP 5352B counter (Agilent Technologies Inc., Santa Clara, CA, USA). Data acquisition was performed using the Bruker software, as described above.

Analysis of metals

Manganese and iron have been determined by GF-AAS and ICP-MS. [As a result of problems with the protein matrix in the analysis of metalloproteins, both methods applied in the present study for quantitative metal analysis (GF-AAS, ICP-MS) required adaptation by using L-tryptophan-containing standards to simulate the protein background. For example, in GF-AAS, high contents of the organic matrix will generate microscopic particles in the gas phase inside the graphite furnace as a result of incomplete combustion, causing an increase of the background signal and thus a significant deterioration of the signal-to-noise ratio. Although the temperature time programme was improved for atomization of manganese and iron, slightly higher concentrations were measured in comparison with ICP-MS.] Both techniques were operated under clean laboratory conditions, thus giving the opportunity to measure elemental concentrations in the range of $ng \cdot L^{-1}$. The detection limit for the most abundant iron isotope, ^{56}Fe, was 0.08 $\mu g \cdot L^{-1}$ and, for ^{55}Mn, was 0.03 $\mu g \cdot L^{-1}$, which is well below the expected concentrations of both elements in the protein samples. All ICP-MS determinations were performed with a quadrupole Elemental-X7 (Thermo Fisher Scientific Inc., Waltham, MA, USA). Very low iron concentrations cannot be determined with the quadrupole mass spectrometer because isobaric interferences from argon molecule ions, introduced into the system as plasma gas in great excess (e.g. $^{40}Ar^{14}N^+$, $^{40}Ar^{15}N^+$, $^{40}Ar^{16}O^+$ or $^{40}Ar^{16}O^1H^+$), are observed on all isotopes of iron (^{54}Fe, ^{56}Fe and ^{57}Fe) and the monoisotopic manganese (^{55}Mn). Therefore, precise determination of iron reported in the present study was achieved by using a hexapole collision cell which operated with a collision gas of 8% H_2 and 92% He. Rhodium was used as internal standard for all measurements.

For GF-AAS measurements, an AAS5 EA system (Carl Zeiss GmbH, Jena, Germany) was used. Manganese was determined at a wavelength of 279.8 nm and iron at 248.3 nm; for each analysis, 20 μL of sample were injected and the background correction was performed with a deuterium lamp. The temperature time programme was optimized for samples with high protein content, resulting in atomization temperatures of 2300 °C and 2150 °C for manganese and iron, respectively. L-tryptophan-containing standards were used to simulate the protein background.

In certain purification protocols, iron was determined spectroscopically from triplicates by the phenantroline method using a Fe standard (Merck, Darmstadt, Germany) and manganese by oxidation to MnO_4^- as described previously [26]. Fractions from ammonium sulfate precipitation and UNO™ sphere Q chromatography were desalted via HiTrap™ columns (GE Healthcare Europe GmbH) before metal analysis, whereas protein fractions from Superdex 200 gel filtration were used directly. Buffer aliquots identically treated as the samples were used for the subtraction of background throughout.

Acknowledgements

This paper is dedicated to Hans Diekmann who identified manganese in the control of growth in *C. ammoniagenes* and in the industrial production of nucleotides as prospective fields of study, as well as Hartmut Follmann who established research on ribonucleotide reductase in Germany. The authors thank I. Reupke for providing technical assistance, F. Büttner for total sequencing and A. Burkowski for the plasmid pXMJ19. G. Auling and P. Stolle appreciate the help of J. Stubbe and J. Cotruvo with respect to improving the manuscript. The work was supported in part by the grant Au 62/4-3 of the Deutsche Forschungsgemeinschaft to G. Auling and by the Max Planck Society.

References

1 Jordan A & Reichard P (1998) Ribonucleotide reductases. *Annu Rev Biochem* **67**, 71 98.
2 Reichard P (1993) From RNA to DNA, why so many ribonucleotide reductases? *Science* **260**, 1773 1777.
3 Follmann H (2004) Deoxyribonucleotides: the unusual chemistry and biochemistry of DNA precursors. *Chem Soc Rev* **33**, 225 233.
4 Willing A, Follmann H & Auling G (1988) Ribonucleotide reductase of *Brevibacterium ammoniagenes* is a manganese enzyme. *Eur J Biochem* **170**, 603 611.
5 Wieghardt K (1989) Die aktiven Zentren in manganhaltigen Metalloproteinen und anorganische Modellkomplexe. *Angew Chem Weinheim* **101**, 1179 1198.
6 Hogenkamp HP (1983) Nature and properties of the bacterial ribonucleotide reductases. *Pharmacol Ther* **23**, 393 405.
7 Auling G & Follmann H (1994) Manganese-dependent ribonucleotide reduction and overproduction of nucleotides in coryneform bacteria. In *Met Ions Biol Syst* (Sigel H & Sigel A eds), pp 132 161. Marcel Dekker Inc, New York.
8 Griepenburg U, Blasczyk K, Kappl R, Hüttermann J & Auling G (1998) A divalent metal site in the small subunit of the manganese-dependent ribonucleotide reductase of *Corynebacterium ammoniagenes*. *Biochemistry* **37**, 7992 7996.

9 Griepenburg U, Lassmann G & Auling G (1996) Detection of a stable free radical in the B2 subunit of the manganese ribonucleotide reductase (Mn-RRase) of *Corynebacterium ammoniagenes*. *Free Radic Res* **24**, 473 481.

10 Oehlmann W, Griepenburg U & Auling G (1998) Cloning and sequencing of the *nrdF* gene of *Corynebacterium ammoniagenes* ATCC 6872 encoding the functional metallo-cofactor of the manganese-ribonucleotide reductase (Mn-RRase). *Biotechnol Lett* **20**, 483 488.

11 Fieschi F, Torrents E, Toulokhonova L, Jordan A, Hellman U, Barbe J, Gibert I, Karlsson M & Sjöberg BM (1998) The manganese-containing ribonucleotide reductase of *Corynebacterium ammoniagenes* is a class Ib enzyme. *J Biol Chem* **273**, 4329 4337.

12 Huque Y, Fieschi F, Torrents E, Gibert I, Eliasson R, Reichard P, Sahlin M & Sjöberg BM (2000) The active form of the R2F protein of class Ib ribonucleotide reductase from *Corynebacterium ammoniagenes* is a diferric protein. *J Biol Chem* **275**, 25365 25371.

13 Högbom M, Huque Y, Sjöberg B-M & Nordlund P (2002) Crystal structure of the di-iron/radical protein of ribonucleotide reductase from *Corynebacterium ammoniagenes*. *Biochemistry* **41**, 1381 1389.

14 Angelov A, Mientus M, Liebl S & Liebl W (2009) A two-host fosmid system for functional screening of (meta)genomic libraries from extreme thermophiles. *Syst Appl Microbiol* **32**, 177 185.

15 Schäfer A, Kalinowski J & Pühler A (1994) Increased fertility of *Corynebacterium glutamicum* recipients in intergeneric matings with *Escherichia coli* after stress exposure. *Appl Environ Microbiol* **60**, 756 759.

16 Wohlleben W, Muth G & Kalinowski J. (1993) Genetic Engineering of Gram-positive bacteria. In *Genetic Engineering of Microorganisms* (Pühler A ed), pp 83 133. Wiley-VCH, Weinheim.

17 Elhariry H, Kawasaki H & Auling G (2004) Recent advances in microbial production of flavour enhancers for the food industry. In *Recent Research Developments in Microbiology* (Pandalai SG ed), pp. 15 39. Research Signpost, Trivandrum, India.

18 Teshiba S (1989) *Production of Nucleotides and Nucleosides by Fermentation*, Vol. 3, 1st edn. Gordon and Breach Science Publishers, Routledge, New York.

19 Schäfer A, Kalinowski J, Simon R, Seep-Feldhaus AH & Pühler A (1990) High-frequency conjugal plasmid transfer from gram-negative *Escherichia coli* to various gram-positive coryneform bacteria. *J Bacteriol* **172**, 1663 1666.

20 Eikmanns BJ, Kleinertz E, Liebl W & Sahm H (1991) A family of *Corynebacterium glutamicum/Escherichia coli* shuttle vectors for cloning, controlled gene expression, and promoter probing. *Gene* **102**, 93 98.

21 Jakoby M, Ngouoto-Nkili C-E & Burkovski A (1999) Construction and application of new *Corynebacterium glutamicum* vectors. *Biotechnol Tech* **13**, 437 441.

22 Oehlmann W & Auling G (1999) Ribonucleotide reductase (RNR) of *Corynebacterium glutamicum* ATCC 13032 genetic characterization of a second class IV enzyme. *Microbiology* **145**, 1595 1604.

23 Liebl W & Schein B (1990) Isolation of restriction deficient mutants of *Corynebacterium glutamicum*. *DECHEMA Biotechnology conference* **4**, 323 327, VCH Verlagsgesellschaft, Weinheim.

24 Ogata H, Stolle P, Stehr M, Auling G & Lubitz W (2009) Crystallization and preliminary X-ray analysis of the small subunit (R2F) of native ribonucleotide reductase from *Corynebacterium ammoniagenes*. *Acta Crystallogr Sect F Struct Biol Cryst Commun* **65**, 878 880.

25 Sjöberg B-M (1997) Ribonucleotide reductases a group of enzymes with different metallosites and a similar reaction mechanism. *Struct & Bonding* **88**, 139 173.

26 Jander G, Blasius E, Strähle J & Schweda E (2002) *Lehrbuch der analytischen und präparativen anorganischen Chemie*. Hirzel, Stuttgart.

27 Abbouni B, Oehlmann W, Stolle P, Pierik AJ & Auling G (2009) Electron paramagnetic resonance (EPR) spectroscopy of the stable-free radical in the native metallocofactor of the manganese-ribonucleotide reductase (Mn-RNR) of *Corynebacterium glutamicum*. *Free Radic Res* **43**, 943 950.

28 Cox N, Ogata H, Stolle P, Reijerse E, Auling G & Lubitz W (2010) A Tyrosyl Dimanganese Coupled Spin System is the Native Metalloradical Cofactor of the R2F Subunit of the Ribonucleotide Reductase of *Corynebacterium ammoniagenes*. *J Am Chem Soc* **132**, 11197 11213.

29 Nordlund P & Reichard P (2006) Ribonucleotide reductases. *Annu Rev Biochem* **75**, 681 706.

30 Cotruvo JA & Stubbe J (2010) An active dimanganese(III)-tyrosyl radical cofactor in *Escherichia coli* class Ib ribonucleotide reductase. *Biochemistry* **49**(6), 1297 1309.

31 Kennedy M, Yu L, Lima MJ, Ascenso CS, Czaja C, Moura I, Moura JJG & Rusnak F (1998) Metal binding to the tetrathiolate motif of desulforedoxin and related polypeptides. *J Biol Inorg Chem* **3**, 643 649.

32 Hidalgo A, Betancor L, Moreno R, Zafra O, Cava F, Fernandez-Lafuente R, Guisan JM & Berenguer J (2004) *Thermus thermophilus* as a cell factory for the production of a thermophilic Mn-dependent catalase which fails to be synthesized in an active form in *Escherichia coli*. *Appl Environ Microbiol* **70**, 3839 3844.

33 Mulrooney SB & Hausinger RP (2003) Metal ion dependence of recombinant *Escherichia coli* allantoinase. *J Bacteriol* **185**, 126 134.

34 Paik JE & Lee BR (2003) Isolation of transcription initiation signals from *Corynebacterium ammoniagenes* and comparison of their gene expression levels in *C. ammoniagenes* and *Escherichia coli*. *Biotechnol Lett* **25**, 1311 1316.
35 Torrents E, Roca I & Gibert I (2003) *Corynebacterium ammoniagenes* class Ib ribonucleotide reductase: transcriptional regulation of an atypical genomic organization in the *nrd* cluster. *Microbiology* **149**, 1011 1020.
36 Larsson A, Climent I, Nordlund P, Sahlin M & Sjöberg BM (1996) Structural and functional characterization of two mutated R2 proteins of *Escherichia coli* ribonucleotide reductase. *Eur J Biochem* **237**, 58 63.
37 Jordan A, Pontis E, Atta M, Krook M, Gibert I, Barbe J & Reichard P (1994) A second class I ribonucleotide reductase in *Enterobacteriaceae*: characterization of the *Salmonella typhimurium* enzyme. *Proc Natl Acad Sci USA* **91**, 12892 12896.
38 Lee JW & Helmann JD (2007) Functional specialization within the Fur family of metalloregulators. *Biometals* **20**, 485 499.
39 Dann CE, Wakeman CA, Sieling CL, Baker SC, Irnov I & Winkler WC (2007) Structure and mechanism of a metal-sensing regulatory RNA. *Cell* **130**, 878 892.
40 Plönzig J & Auling G (1987) Manganese deficiency impairs ribonucleotide reduction but not replication in *Arthrobacter* species. *Arch Microbiol* **146**, 396 401.
41 Pierik AJ, Hagen WR, Redeker JS, Wolbert RB, Boersma M, Verhagen MF, Grande HJ, Veeger C, Mutsaers PH, Sands RH *et al.* (1992) Redox properties of the iron-sulfur clusters in activated Fe-hydrogenase from *Desulfovibrio vulgaris* (Hildenborough). *Eur J Biochem* **209**, 63 72.
42 Miller JH (1972) *Experiments in Molecular Genetics*. Cold Spring Harbour Laboratory Press, New York.
43 Barckhausen O (2004) Nachweis eines mononuclearen Mangan (II)-Zentrums in der Ribonucleotid-Reduktase aus *Corynebacterium ammoniagenes* ATCC 6872 nach Überexpression des den Metallocofaktor codierenden *nrdF*-Gens im Originalstamm. Universität Hannover.
44 Thompson JD, Gibson TJ, Plewniak F, Jeanmougin F & Higgins DG (1997) The CLUSTAL_X windows interface: flexible strategies for multiple sequence alignment aided by quality analysis tools. *Nucleic Acids Res* **25**, 4876 4882.
45 Sambrook J, Fritsch EF & Maniatis T (1989) *Molecular Cloning: A Laboratory Manual*, Vol. 2. Cold Spring Harbor Laboratory Press, US.
46 Haynes JA & Britz ML (1989) Electrotransformation of *Brevibacterium lactofermentum* and *Corynebacterium glutamicum*: growth in tween 80 increases transformation frequencies. *FEMS Microbiol Lett* **61**, 329 333.
47 Bradford MM (1976) A rapid and sensitive method for the quantitation of microgram quantities of protein utilizing the principle of protein-dye binding. *Anal Biochem* **72**, 248 254.
48 Laemmli UK (1970) Cleavage of structural proteins during the assembly of the head of bacteriophage T4. *Nature* **227**, 680 685.
49 Towbin H, Staehelin T & Gordon J (1979) Electrophoretic transfer of proteins from polyacrylamide gels to nitrocellulose sheets: procedure and some applications. *Proc Natl Acad Sci USA* **76**, 4350 4354.
50 Kinter M & Sherman NE (2000) *Protein Sequencing and Identification Using Tandem Mass Spectrometry*. Chichester, England.
51 Pal BC, Regan JD & Hamilton FD (1975) Separation of bases, ribonucleosides and deoxyribonucleosides by anion-exclusion and partition chromatography on cation-exchange resin: application to the assay of ribonucleotide reductase, deaminase and nucleosidase. *Anal Biochem* **67**, 625 633.
52 Stoer J (2005) *Stoer, Josef, Bd.1: Numerische Mathematik*. Springer, Berlin.
53 Heffeter P, Popovic-Bijelic A, Saiko P, Dornetshuber R, Jungwirth U, Voevodskaya N, Biglino D, Jakupec MA, Elbling L, Micksche M *et al.* (2009) Ribonucleotide Reductase as One Important Target of Tris(1,10-phenanthroline)lanthanum(III) Trithiocyanate (KP772). *Curr Cancer Drug Targets* **9**, 595 607.
54 Allard P, Barra AL, Andersson KK, Schmidt PP, Atta M & Gräslund A (1996) Characterization of a new tyrosyl free radical in *Salmonella typhimurium* ribonucleotide reductase with EPR at 9.45 and 245 GHz. *J Am Chem Soc* **118**, 895 896.

Supporting information

The following supplementary material is available:
Fig. S1. Disintegration of the coupled spin system by the elimination of the radical using HU.

This supplementary material can be found in the online version of this article.

Please note: As a service to our authors and readers, this journal provides supporting information supplied by the authors. Such materials are peer-reviewed and may be re-organized for online delivery, but are not copy-edited or typeset. Technical support issues arising from supporting information (other than missing files) should be addressed to the authors.

7.3 Publikation II: Crystallization and preliminary X-ray Analysis of the Small Subunit (R2F) of Native Ribonucleotide Reductase from *Corynebacterium ammoniagenes*

Eigenanteil:

Durch die optimierte Chromatographie konnten nahezu beliebige Mengen R2F von *C. ammoniagenes* für Kristallisationsversuche geliefert werden. In gezielten Vorarbeiten wurden die Kristallisationsbedingungen so eingeengt, dass hier in kürzester Zeit (2 Wochen) Kristalle mit hoher Auflösung (1.36 Å) erhalten wurden.

Acta Crystallographica Section F
Structural Biology and Crystallization Communications
ISSN 1744-3091
Editors: **H. M. Einspahr and M. S. Weiss**

Crystallization and preliminary X-ray analysis of the small subunit (R2F) of native ribonucleotide reductase from *Corynebacterium ammoniagenes*

Hideaki Ogata, Patrick Stolle, Matthias Stehr, Georg Auling and Wolfgang Lubitz

Acta Cryst. (2009). F**65**, 878–880

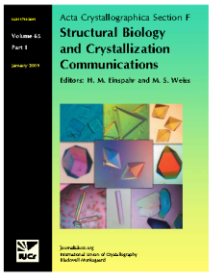

crystallization communications

Acta Crystallographica Section F
Structural Biology and Crystallization Communications
ISSN 1744-3091

Crystallization and preliminary X-ray analysis of the small subunit (R2F) of native ribonucleotide reductase from *Corynebacterium ammoniagenes*

Hideaki Ogata,[a] Patrick Stolle,[b] Matthias Stehr,[b] Georg Auling[b] and Wolfgang Lubitz[a]*

[a]Max-Planck-Institut für Bioanorganische Chemie, Stiftstrasse 34-36, D-45470 Mülheim an der Ruhr, Germany, and [b]Institut für Mikrobiologie, Leibniz Universität Hannover, Schneiderberg 50, D-30167 Hannover, Germany

Correspondence e-mail: lubitz@mpi-muelheim.mpg.de

Received 22 June 2009
Accepted 22 July 2009

Ribonucleotide reduction, the unique step in DNA-precursor biosynthesis, involves radical-dependent redox chemistry and diverse metallo-cofactors. The metallo-cofactor (R2F) encoded by the *nrdF* (*n*ucleotide *red*uction) gene in *Corynebacterium ammoniagenes* ATCC 6872 was isolated after homologous expression and a new crystal form of ribonucleotide reductase R2F was obtained. R2F was crystallized at 277 K using the vapour-diffusion method with PEG as the precipitating agent. A data set was collected to 1.36 Å resolution from a single crystal at 100 K using synchrotron radiation. The crystal belonged to space group *C*2, with unit-cell parameters a = 96.21, b = 87.68, c = 83.25 Å, β = 99.29°. The crystal contained two molecules per asymmetric unit, with a Matthews coefficient (V_M) of 2.69 $Å^3$ Da^{-1}; the solvent content was estimated to be 54.3%. X-ray fluorescence spectroscopy and MAD diffraction data indicated the presence of manganese in the molecule and the absence of iron.

1. Introduction

DNA synthesis requires a continuous supply of deoxyribonucleotides. These are provided by ribonucleotide reductase (RNR), which catalyzes the reduction of ribonucleotides to 2′-deoxyribonucleotides (Follmann, 2004). Three classes of RNR (EC 1.17.4) have been described, which differ in their cofactor or metal requirements (Eklund *et al.*, 2001). While the redox chemistry in class I appears to be heterogeneous, class II enzymes use cobalamin-dependent radical generation (Licht *et al.*, 1996) and a stable glycyl radical is formed by class III enzymes with the help of an iron–sulfur protein and *S*-adenosylmethionine (Logan *et al.*, 1999). Based on the discovery of a new pattern of allosteric regulation (Eliasson *et al.*, 1996) and differences in metal-site structure and radical identity (Högbom *et al.*, 2004), class I has been further divided into class Ia enzymes, with the *Escherichia coli* prototype encoded by *nrdAB* genes, class Ib enzymes, with the *Salmonella typhimurium* prototype encoded by *nrdEF* genes, and class Ic, which consists of *Chlamydia trachomatis* RNR and related enzymes.

The nature of the Mn-RNR from the Gram-positive bacterium *Corynebacterium ammoniagenes* ATCC 6872 (Willing *et al.*, 1988; Griepenburg *et al.*, 1998) as a distinct class IV enzyme (Follmann, 2004) has been disputed by its allocation to class Ib from heterologous expression in *E. coli* (Fieschi *et al.*, 1998; Huque *et al.*, 2000). The *C. ammoniagenes* Mn-RNR consists of a monomeric catalytic R1E subunit (81 kDa) and a dimeric metallo-cofactor (R2F; 38 kDa) which contains manganese and a tyrosyl radical (Griepenburg *et al.*, 1996).

To date, several crystal structures of *E. coli* and mouse R2 or *Mycobacterium tuberculosis* and *C. ammoniagenes* R2F expressed in *E. coli* have been studied in various oxidation states and forms obtained by site-directed mutagenesis or by metal substitution (Nordlund *et al.*, 1990; Logan *et al.*, 1996; Voegtli *et al.*, 2000; Högbom

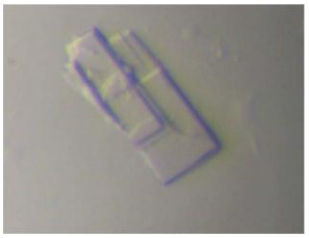

et al., 2002, 2003; Uppsten *et al.*, 2004; Strand *et al.*, 2004; Lendzian, 2005). Recently, the structure of the Mn/Fe metallo-cofactor of the chlamydial RNR has been studied by extended X-ray absorption fine-structure spectroscopy (Younker *et al.*, 2008).

In order to determine the metal composition and the coordination of its metal centre, we purified the metallo-cofactor of the native Mn-RNR from *C. ammoniagenes*. The R2F subunit obtained from homologous expression from its original source, *C. ammoniagenes* ATCC 6872 (Schimpff-Weiland *et al.*, 1981; Willing *et al.*, 1988), showed a high RNR activity in a biochemical complementation assay with the large catalytic R1E subunit (Stolle *et al.*, in preparation). Here, we report the crystallization and preliminary X-ray analysis of *C. ammoniagenes* R2F. X-ray fluorescence spectroscopy (XFS) and MAD diffraction data indicated the presence of manganese in the molecule.

2. Materials and methods

2.1. Purification

The *nrdF* gene of *C. ammoniagenes* strain ATCC 6872 was homologously expressed using the vector pOCA2 and the R2F protein was prepared as described elsewhere (Stolle *et al.*, in preparation). *C. ammoniagenes* pOCA2 was grown aerobically in LB medium in the presence of chloramphenicol (15 µg ml^{-1}) in a 10 l bioreactor (Biostat V, B-Braun) at 303 K with aeration at 8 l min^{-1} and agitation at 350 rev min^{-1} until an OD_{600} of 6 was reached. After a 4 h incubation in the presence of 1 m*M* IPTG and 25 µ*M* Mn^{2+}, the biomass was harvested and resuspended in 85 m*M* potassium phosphate buffer containing 2 m*M* DTT pH 6.6 as a standard buffer supplemented with 10 m*M* KCl. The homogenate resulting from disruption in a French pressure-cell press was precipitated with ammonium sulfate (472 mg ml^{-1}), dissolved in the standard buffer as above and desalted on a HiTrap desalting column (GE Healthcare). A 20 ml UNOsphere Q anion-exchange column (GE Healthcare) was used for stepwise gradient elution at 350 m*M* KCl in standard buffer with 2 m*M* magnesium acetate and the eluate was applied onto a Superdex 200 column (GE Healthcare) using the standard buffer. The resulting 30–45 kDa eluate was dialyzed and applied onto a final MonoQ HR 5-5 anion-exchange chromatography column (GE Healthcare) and eluted at 490 m*M* KCl, 50 m*M* Tris–HCl, 2 m*M* DTT, 15% glycerol pH 7.5. The metallo-cofactor was assessed for purity by SDS–PAGE and confirmed by Western blotting using an anti-R2F antibody. The protein was quantified using the Bradford protein assay (Roth). Amicon Ultra-4 devices (10 kDa molecular-weight cutoff, Millipore) were used for buffer exchange and concentration prior to crystallization. The native R2F protein, purified to homogeneity, was stored in standard buffer with 15%(*v*/*v*) glycerol in the gaseous phase of liquid nitrogen.

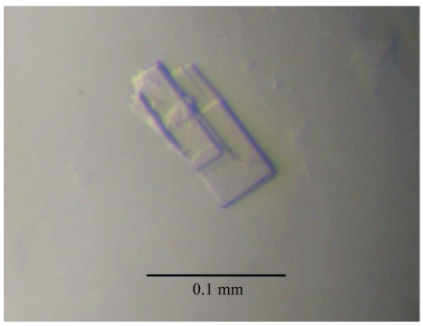

Figure 1
Crystal of ribonucleotide reductase R2F from *C. ammoniagenes*.

Table 1
X-ray data-collection statistics.

Values in parentheses are for the highest resolution shell.

	Native	Peak	Remote
Wavelength (Å)	1.00000	1.89000	1.89900
Space group	*C*2	*C*2	*C*2
Unit-cell parameters			
a (Å)	96.21	95.97	96.08
b (Å)	87.68	87.55	87.64
c (Å)	83.25	83.29	83.32
β (°)	99.29	99.36	99.36
Resolution (Å)	31.17–1.36 (1.41–1.36)	33.01–1.84 (1.91–1.84)	33.03–1.85 (1.92–1.85)
No. of observed reflections	502993	206100	204123
No. of unique reflections	140012	58827	58039
R_{merge}†	0.073 (0.477)	0.077 (0.341)	0.073 (0.382)
Completeness (%)	96.1 (72.7)	99.7 (100.0)	99.8 (99.8)
$\langle I/\sigma(I)\rangle$	13.4 (2.1)	28.4 (4.1)	13.6 (3.7)
Redundancy	3.6	3.5	3.5

† $R_{merge} = \sum_{hkl}\sum_i |I_i(hkl) - \langle I(hkl)\rangle| / \sum_{hkl}\sum_i I_i(hkl)$, where $I_i(hkl)$ is the intensity of the *i*th observation and $\langle I(hkl)\rangle$ is the mean intensity of the reflections.

2.2. Crystallization

Crystallization of the native RNR metallo-cofactor from *C. ammoniagenes* was carried out using the sitting-drop vapour-diffusion method at 277 K under aerobic conditions. The protein droplets were prepared by mixing 10 µl RNR solution and 10 µl reservoir buffer solution and were set up in a Cryschem plate (Hampton Research, California, USA) with 1 ml reservoir solution. Crystals were obtained after three weeks. Crystals suitable for diffraction experiments were obtained under the following conditions: 0.1 *M* sodium citrate, 27.5% PEG 4000, 0.05 *M* ammonium acetate pH 6.0 and 0.1 *M* ammonium acetate pH 7.0 with 0.05 *M* Tris–HCl pH 7.5 buffer. The crystal dimensions were typically 0.1 × 0.05 × 0.01 mm (Fig. 1).

2.3. Data collection and analysis

In order to collect the data at cryogenic temperature, the crystal was frozen in liquid nitrogen and mounted on the goniostat under a nitrogen-gas stream at 100 K. All data were collected on beamline BL41XU at SPring-8 (Hyogo, Japan). An MX225HE detector (MAR Research, Germany) was used. A complete native data set was collected to 1.36 Å resolution at an X-ray wavelength of 1.00000 Å. For the native data set, 180 frames of 1 s exposure time and 1.0° oscillation were collected. The distance between the crystal and the detector was maintained at 190 mm. In addition, two-wavelength Mn-MAD data sets were collected to 1.84 and 1.85 Å resolution, respectively. The wavelength of the X-rays was chosen as 1.89000 Å (peak) and 1.89900 Å (remote), respectively. For the Mn-MAD data set, 180 frames of 1 s exposure time each and 1.0° oscillation were collected. The distance between the crystal and the detector was maintained at 85 mm. Diffraction images were indexed, integrated and scaled using the program *HKL*-2000 (Otwinowski & Minor, 1997). The molecular replacement and the initial refinement were carried out using the programs *MOLREP* (Vagin & Isupov, 2001) and *REFMAC* (Vagin *et al.*, 2004), respectively, from the *CCP*4 program package (Collaborative Computational Project, Number 4, 1994). The conditions of the data collection and the results obtained are

summarized in Table 1. XFS experiments for the determination of the metal components were carried out on beamline BL14.2 at BESSY II (Berlin, Germany).

3. Results and discussion

The new crystal form of RNR R2F from *C. ammoniagenes* was obtained at 277 K using the sitting-drop vapour-diffusion method with PEG as a precipitating agent. The crystals diffracted to 1.36 Å resolution and belonged to space group *C*2, with unit-cell parameters $a = 96.21$, $b = 87.6$, $c = 83.25$ Å, $\beta = 99.29^{\circ}$. The calculated Matthews coefficient (V_M) of 2.69 $Å^3$ Da^{-1} with a solvent content of 54.3% indicates the presence of two molecules in the asymmetric unit.

XFS experiments were carried out in order to determine the metal components of the RNR R2F subunit. No fluorescence was observed near the energy range of the metals Fe, Co, Ni and Cu (data not shown). However, fluorescence corresponding to Mn was observed. Furthermore, the Mn-MAD method was applied to a crystal of RNR R2F at X-ray wavelengths of 1.89000 and 1.89900 Å. The anomalous difference Patterson map showed peaks corresponding to the Mn atoms. The results showed that Mn is the metal component of *C. ammoniagenes* RNR R2F.

Initial phases were calculated from the Mn-MAD data set using the *CCP*4 program suite. The phase calculation confirmed the presence of two molecules in the asymmetric unit. Subsequently, the molecular-replacement method was applied using the program *MOLREP*. The data for the oxidized state of the Fe-containing RNR R2F from *C. ammoniagenes* (PDB code 1kgp) were used as coordinates for the search model. After the calculation of the electron-density map using the molecular-replacement solution, a homodimer in the asymmetric unit was observed. The electron-density map shows the Mn site to be near to the tyrosyl radical Tyr115. Model building and refinement are now in progress.

We thank the staff of beamline BL41XU at SPring-8 (Hyogo, Japan) and beamline BL14.2 at BESSY II (Berlin, Germany) for their assistance during data collection. This work was supported by the Max Planck Society.

References

Collaborative Computational Project, Number 4 (1994). *Acta Cryst.* D**50**, 760–763.
Eklund, H., Uhlin, U., Färnegårdh, M., Logan, D. T. & Nordlund, P. (2001). *Prog. Biophys. Mol. Biol.* **77**, 177–268.
Eliasson, R., Pontis, E., Jordan, A. & Reichard, P. (1996). *J. Biol. Chem.* **271**, 26582–26587.
Fieschi, F., Torrents, E., Toulokhonova, L., Jordan, A., Hellman, U., Barbe, J., Gibert, I., Karlsson, M. & Sjöberg, B. M. (1998). *J. Biol. Chem.* **273**, 4329–4337.
Follmann, H. (2004). *Chem. Soc. Rev.* **33**, 225–233.
Griepenburg, U., Blasczyk, K., Kappl, R., Hüttermann, J. & Auling, G. (1998). *Biochemistry*, **37**, 7992–7996.
Griepenburg, U., Lassmann, G. & Auling, G. (1996). *Free Radic. Res.* **24**, 473–481.
Högbom, M., Galander, M., Andersson, M., Kolberg, M., Hofbauer, W., Lassmann, G., Nordlund, P. & Lendzian, F. (2003). *Proc. Natl Acad. Sci. USA*, **100**, 3209–3214.
Högbom, M., Huque, Y., Sjöberg, B. M. & Nordlund, P. (2002). *Biochemistry*, **41**, 1381–1389.
Högbom, M., Stenmark, P., Voevodskaya, N., McClarty, G., Gräslund, A. & Nordlund, P. (2004). *Science*, **305**, 245–248.
Huque, Y., Fieschi, F., Torrents, E., Gibert, I., Eliasson, R., Reichard, P., Sahlin, M. & Sjoberg, B. M. (2000). *J. Biol. Chem.* **275**, 25365–25371.
Lendzian, F. (2005). *Biochim. Biophys. Acta*, **1707**, 67–90.
Licht, S., Gerfen, G. J. & Stubbe, J. (1996). *Science*, **271**, 477–481.
Logan, D. T., Andersson, J., Sjöberg, B. M. & Nordlund, P. (1999). *Science*, **283**, 1499–1504.
Logan, D. T., Su, X.-D., Åberg, A., Regnström, K., Hajdu, J., Eklund, H. & Nordlund, P. (1996). *Structure*, **4**, 1053–1064.
Nordlund, P., Sjöberg, B. M. & Eklund, H. (1990). *Nature (London)*, **345**, 593–598.
Otwinowski, Z. & Minor, W. (1997). *Methods Enzymol.* **276**, 307–326.
Schimpff-Weiland, G., Follmann, H. & Auling, G. (1981). *Biochem. Biophys. Res. Commun.* **102**, 1276–1282.
Strand, K. R., Karlsen, S., Kolberg, M., Rohr, A. K., Görbitz, C. H. & Andersson, K. K. (2004). *J. Biol. Chem.* **279**, 46794–46801.
Uppsten, M., Davis, J., Rubin, H. & Uhlin, U. (2004). *FEBS Lett.* **569**, 117–122.
Vagin, A. A. & Isupov, M. N. (2001). *Acta Cryst.* D**57**, 1451–1456.
Vagin, A. A., Steiner, R. A., Lebedev, A. A., Potterton, L., McNicholas, S., Long, F. & Murshudov, G. N. (2004). *Acta Cryst.* D**60**, 2184–2195.
Voegtli, W. C., Khidekel, N., Baldwin, J., Ley, B. A., Bollinger, J. M. Jr & Rosenzweig, A. C. (2000). *J. Am. Chem. Soc.* **122**, 3255–3261.
Willing, A., Follmann, H. & Auling, G. (1988). *Eur. J. Biochem.* **170**, 603–611.
Younker, J. M., Krest, C. M., Jiang, W., Krebs, C., Bollinger, J. M. Jr & Green, M. T. (2008). *J. Am. Chem. Soc.* **130**, 15022–15027.

7.4 Publikation III: A Tyrosyl-Dimanganese Coupled Spin System is the Native Metalloradical Cofactor of the R2F Subunit of the Ribonucleotide Reductase of *Corynebacterium ammoniagenes*

Eigenanteil:

Die spektroskopische Auflösung des ungewöhnlichen Tyrosylradikals mit „multi-frequency"-EPR Spektroskopie benötigt gerade im Hochfeld (122 und 244 GHz) sehr hohe Spinkonzentrationen, um ein interpretierbares Signal messen zu können. Bei Aufnahme der vorliegenden Dissertation war dies wegen der geringen Halbwertszeit des aktiven Metallocofaktors unter den vorgefundenen Bedingungen nicht gewährleistet. Mit verschiedenen Maßnahmen wurde die Stabilität des Metalloradikalcofaktors drastisch erhöht, so dass die Ribonucleotid-Reduktase aus *C. ammoniagenes* erstmals für langwierige physikalische Messverfahren in externen Forschungszentren (MPI für Bioanorganische Chemie, Mülheim; HZI für Materialien und Energie, BESSY II, Berlin; EMBL Outstation, DESY, Hamburg; Spring-8, Hyogo, Japan) zur Verfügung gestellt werden konnte. Auf diese Weise wurde mit einer hochaktiven biochemischen Präparation über Strukturanalyse und Multifrequenz-EPR ein neuartiges Tyrosyl-$Mn^{III}Mn^{III}$ gekoppelten Spinsystems beschrieben.

Es war attraktiv, eine Modellvorstellung zur Entstehung des neuartigen Tyrosylradikal-Mn_2 gekoppelten Spinsystems der RNR von *C. ammoniagenes* zu entwickeln. Dafür wurden entscheidende Hinweise in ausführlichen Reaktivierungsversuchen nach gezielter Reduktion des Tyrosylradikals erarbeitet. Diese deuten auf die Beteiligung von H_2O_2 bei der Oxidation des Metallclusters für die Generation des Tyrosylradikals hin (Fig. 13).

J|A|C|S
ARTICLES

Published on Web 07/22/2010

A Tyrosyl−Dimanganese Coupled Spin System is the Native Metalloradical Cofactor of the R2F Subunit of the Ribonucleotide Reductase of *Corynebacterium ammoniagenes*

Nicholas Cox,*,† Hideaki Ogata,† Patrick Stolle,‡ Edward Reijerse,† Georg Auling,‡ and Wolfgang Lubitz*,†

Max-Planck-Institut für Bioanorganische Chemie, Stiftstrasse 34-36, D-45470 Mülheim (Ruhr), Germany, and Institut für Mikrobiologie, Leibniz Universität Hannover, Schneiderberg 50, D-30167 Hannover, Germany

Received April 30, 2010; E-mail: cox@mpi-muelheim.mpg.de; lubitz@mpi-muelheim.mpg.de

Abstract: The X-ray crystallographic structure of the native R2F subunit of the ribonucleotide reductase (RNR) of *Corynebacterium ammoniagenes* ATCC 6872 is reported, with a resolution of 1.36 Å. The metal site contains an oxo/hydroxo-bridged manganese dimer, located near a tyrosine residue (Y115). The coordination of the manganese dimer and its distance to a nearby tyrosine residue resemble the di-iron metalloradical cofactor of class I RNR from *Escherichia coli*. Multifrequency EPR measurements of the highly active *C. ammoniagenes* R2F subunit show that the metal site contains a ferromagnetically exchange-coupled $Mn^{III}Mn^{III}$ dimer weakly coupled to a tyrosyl radical. A mechanism for the metalloradical cofactor ($Mn^{III}Mn^{III}Y^{\bullet}$) generation is proposed. H_2O_2 (HO_2^-) instead of O_2 is hypothesized as physiological oxidant for the Mn dimer which in turn oxidizes the tyrosine Y115. Changes in the ligand sphere of both manganese ions during metalloradical generation direct the complex formation of this cofactor, disfavoring alternate reaction pathways such as H_2O_2 dismutation, as observed for manganese catalase, a structural analogue of the R2F metal site. The presented results demonstrate the importance of manganese for radical formation in this RNR and confirm the assignment of this enzyme to class Ib.

1. Introduction

Deoxyribonucleic acid (DNA)—nature's universal information storage medium—is synthesized from deoxyribonucleotide monomers, which are provided by a single enzyme, ribonucleotide reductase (RNR), in all organisms.[1,2] Ribonucleotide substrate conversion occurs via a radical reaction mechanism that is highly conserved.[3] The currently accepted reaction pathway is initiated by a distant radical species and involves the sequential activation of a cysteine or a glycine to facilitate deoxygenation of the ribonucleotide via hydrogen abstraction and water release.[1,4]

Class I RNR consists of two homodimeric proteins, a larger subunit R1 that contains the catalytic site and the binding site for allosteric effectors and a smaller subunit R2 that harbors the metalloradical cofactor, a ferric di-iron cluster that stabilizes a free tyrosyl radical,[2,5,6] the distant radical species that initiates cysteine activation i.e. enzymatic function. Class I is further divided into: class Ia, encoded by the *nrdAB* genes and class Ib, encoded by *nrdE* (R1E) and *nrdF* (R2F). A third subclass, class Ic was established for the tyrosyl radical lacking *Chlamydia trachomatis* RNR.[7−10] Both class Ia and Ib are expressed in *E. coli*. In *E. coli*, class Ib RNR is up-regulated under stress conditions including Fe starvation and oxidative stress;[11−13] the exogenous addition of H_2O_2 increases the expression of class Ib RNR.

The native RNR of the Gram-positive bacterium *Corynebacterium ammoniagenes* shares many of the characteristics of class Ib RNRs: oxygen sensitivity, genetic encoding, behavior toward reductant—in particular NrdH-redoxins, which are characterized by a glutaredoxin-like amino acid sequence but show a thioredoxin-like activity profile.[14−17] In addition, the R2F subunit of RNR from *C. ammoniagenes* has been shown to be

† Max-Planck-Institut für Bioanorganische Chemie.
‡ Institut für Mikrobiologie, Leibniz Universität Hannover.

(1) Follmann, H. *Chem. Soc. Rev.* **2004**, *33*, 225–233.
(2) Sjöberg, B. In *Metal Sites in Proteins and Models*; Allen, H., Hill, O., Sadler, P. J., Thomson, A. J., Eds.; Structure and Bonding, Vol. Springer-Verlag: Berlin, 1997; pp 139−173.
(3) Reichard, P. *Science* **1993**, *260*, 1773–1777.
(4) Stubbe, J.; Nocera, D. G.; Yee, C. S.; Chang, M. C. *Chem Rev* **2003**, *103*, 2167–201.
(5) Nordlund, P.; Sjöberg, B.; Eklund, H. *Nature* **1990**, *345*, 593–598.
(6) Uhlin, U.; Eklund, H. *Nature* **1994**, *370*, 533–539.
(7) Jiang, W.; Yun, D.; Saleh, L.; Barr, E. W.; Xing, G.; Hoffart, L. M.; Maslak, M.-A.; Krebs, C.; Bollinger, J. M., Jr. *Science* **2007**, *316*, 1188–1191.
(8) Voevodskaya, N.; Lendzian, F.; Ehrenberg, A.; Gräslund, A. *FEBS Lett.* **2007**, *581*, 3351–3355.
(9) Voevodskaya, N.; Narvaez, A.-J.; Domkin, V.; Torrents, E.; Thelander, L.; Gräslund, A. *Proc. Natl. Acad. Sci. U.S.A.* **2006**, *103*, 9850–9854.
(10) Högbom, M.; Stenmark, P.; Voevodskaya, N.; McClarty, G.; Gräslund, A.; Nordlund, P. *Science* **2004**, *305*, 245–248.
(11) McHugh, J. P.; Rodriguez-Quinones, F.; Abdul-Tehrani, H.; Svistunenko, D. A.; Poole, R. K.; Cooper, C. E.; Andrews, S. C. *J. Biol. Chem.* **2003**, *278*, 29478–29486.
(12) Monje-Casas, F.; Jurado, J.; Prieto-Álamo, M.-J.; Holmgren, A.; Pueyo, C. *J. Biol. Chem.* **2001**, *276*, 18031–18037.
(13) Vassinova, N.; Kozyrev, D. *Microbiology* **2000**, *146*, 3171–3182.

10.1021/ja1036995

structurally similar to class Ib RNR sourced from *Salmonella typhimurium*, which has thus far been described as a di-iron enzyme.[18,19] However, unlike class I RNRs *C. ammoniagenes* appears to require manganese instead of iron for enzymatic function.[14,20]

The precise function of cellular manganese in *C. ammoniagenes* remains an open question. Manganese deprivation[21] of *C. ammoniagenes* leads to a reduced DNA content, suggesting the native RNR uses manganese instead of iron for metalloradical cofactor assembly.[14,22,23] Studies of Griepenburg et al.[24,25] supported the notion that the R2F subunit did indeed display properties divergent from that of class Ia, RNR. However, this contrasted with the first crystal structure of the R2F subunit, reported by Högbom et al.[26] Here the cloned *nrdF* gene of *C. ammoniagenes* was heterologously expressed in *E. coli*, and the isolated apo-R2F subunit was subsequently reactivated with Fe^{II} ascorbate *in vitro*. When prepared under aerobic conditions, the R2F subunit contained a μ-oxo-bridged $Fe^{III}Fe^{III}$ metallocofactor analogous to that observed for *E. coli* class Ia RNR. This led these authors to propose a di-iron metalloradical cofactor.[15,27]

The crystallographic results described above are in conflict with experiments performed in the native system. Homologous expression of R2F sourced from *C. ammoniagenes* ATCC 6872, the strain from which the enzyme was originally isolated,[14] does not show any significant iron incorporation into the enzyme. Similarly, iron-substituted RNR displays a significantly lower activity when compared to the native enzyme, which has turnover rates comparable to that of the RNR of *E. coli*.[28] These results suggest that in vitro metal reconstitution as described above may lead to incorrect metal incorporation into this metalloprotein.

Recently, a highly active Mn-RNR was obtained as a native protein from a wild type strain of *C. glutamicum* with a distinct tyrosyl radical.[29] The genome of this amino acid producer harbors only *nrdEF* genes,[30] and its DNA content is reduced under Mn deprivation (unpublished results). Similarly, ribonucleotide reduction, but not DNA replication, is impaired by manganese deprivation in related bacteria of the genus *Arthrobacter*.[31]

The role of Mn as an integral component of the native metalloradical cofactor of all class Ib RNRs has recently been raised by Cotruvo and Stubbe.[32] These authors have shown that the usually inactive class Ib enzyme of *E. coli* can be activated by Mn using apo-R2F and an additional flavodoxin (NrdI) encoded by the *nrdI* gene. This additional protein may be common to all class Ib enzymes.[32] They propose that the role of the NrdI in metalloradical cofactor biosynthesis is to provide oxidizing equivalents (H_2O_2, HO_2^-, etc.), derived from O_2,[33] to the reduced Mn complex. This would then suggest that cofactor assembly in part resembles the Mn catalase H_2O_2 dismutation reaction pathway.[34−36] They also note that the same protein can assemble an Fe metalloradical cofactor albeit with lower enzyme activity. In this light, it is conceivable that Mn, not Fe, may be the native metal used *in vivo* by all class Ib RNRs.

Here we present new spectroscopic and crystallographic data on native-type R2F from *C. ammoniagenes* ATCC 6872. These measurements show conclusively that the metalloradical cofactor contains a μ-oxo/hydroxo-bridged manganese dimer, with a structure very similar to that of the di-iron complex of *E. coli* R2 in its oxidized, active form. Spectral simulations of the metalloradical cofactors' EPR signal observed at 9, 34, and 244 GHz suggest that the two manganese centers are ferromagnetically exchange-coupled, and interact weakly with the nearby tyrosyl radical. These findings underline the important role of the manganese for the radical formation in this unusual RNR and support the current assignment of RNR derived from *C. ammoniagenes* to class Ib.

2. Materials and Methods

2.1. Purification of the Native R2F Subunit. *C. ammoniagenes* pOCA2 was grown aerobically at 27 °C in LB medium with chloramphenicol (15 μg/mL) in a 10-L New Brunswick bioreactor (aeration 8 L/min; agitation 350 rpm). The *nrdF* gene was induced by addition of 0.6 mM isopropyl-β-D-thiogalactopyranoside (IPTG) and 185 μM $MnCl_2$ or $Fe(NH_4)_2$-citrate in the midlogarithmic growth phase at an OD_{600} of 7. After 4 h, maximal R2F biosynthesis was reached, as observed by SDS-PAGE and Western blotting. The culture was rapidly cooled down to 4 °C and was kept at this temperature during all further operations. Sixty grams of cells (wet weight) were harvested by centrifugation and resuspended in a buffer containing 85 mM phosphate, 100 mM KCl, 2 mM dithiothretiol (DTT), 0.1% Tween 80 (pH 6.6). The cells were disrupted by three passages in a French Press at 1500 psi. R2F precipitated in the range of 40−60% ammonium sulfate saturation. Salts were removed using HiTrap desalting columns and standard buffer (85 mM phosphate buffer, pH 6.6, 2 mM DTT) prior to enrichment by ion-exchange chromatography (IEC) using a three-step gradient and a Unosphere Q column. The R2F subunit eluted at 350 mM KCl (standard buffer including 1 M KCl) and was submitted to size exclusion chromatography (SEC) using Superdex

(14) Willing, A.; Follmann, H.; Auling, G. *Eur. J. Biochem.* **1988**, *175*, 167–173.
(15) Fieschi, F.; Torrents, E.; Toulokhonova, L.; Jordan, A.; Hellman, U.; Barbe, J.; Gibert, I.; Karlsson, M.; Sjöberg, B.-M. *J. Biol. Chem.* **1998**, *273*, 4329–4337.
(16) Oehlmann, W.; Griepenburg, U.; Auling, G. *Biotechnol. Lett.* **1998**, *20*, 483–488.
(17) Stehr, M.; Lindqvist, Y. *Proteins* **2004**, *55*, 613–619.
(18) Eriksson, M.; Jordan, A.; Eklund, H. *Biochemistry* **1998**, *37*, 13359–13369.
(19) Jordan, A.; Pontis, E.; Atta, M.; Krook, M.; Gibert, I.; Barbe, J.; Reichard, P. *Proc. Natl. Acad. Sci. U.S.A.* **1994**, *91*, 12892–12896.
(20) Auling, G.; Follmann, H. In *Metal Ions in Biological Systems*; Sigel, H., Sigel, A., Eds.; Marcel Dekker Inc: New York, 1994; Vol. 30, pp 132−161.
(21) Oka, T.; Udagawa, K.; Kinoshita, S. *J. Bacteriol.* **1968**, *96*, 1760–1767.
(22) Auling, G.; Thaler, M.; Diekmann, H. *Arch. Microbiol.* **1980**, *127*, 105–114.
(23) Schimpff-Weiland, G.; Follmann, H.; Auling, G. *Biochem. Biophys. Res. Commun.* **1981**, *102*, 1276–1282.
(24) Griepenburg, U.; Lassmann, G.; Auling, G. *Free Radical Res.* **1996**, *24*, 473–481.
(25) Griepenburg, U.; Blasczyk, K.; Kappl, R.; Hüttermann, J.; Auling, G. *Biochemistry* **1998**, *37*, 7992–6.
(26) Högbom, M.; Huque, Y.; Sjöberg, B.-M.; Nordlund, P. *Biochemistry* **2002**, *41*, 1381–1389.
(27) Huque, Y.; Fieschi, F.; Torrents, E.; Gibert, I.; Eliasson, R.; Reichard, P.; Sahlin, M.; Sjöberg, B. M. *J. Biol. Chem.* **2000**, *275*, 25365–25371.
(28) Stolle, P.; Barckhausen, O.; Oehlmann, W.; Knobbe, N.; Vogt, C.; Pierik, A.; Schmidt, P.; Reijerse, E.; Lubitz, W.; Auling, G. *FEBS Journal.* **2010**, submitted.
(29) Abbouni, B.; Oehlmann, W.; Stolle, P.; Pierik, A. J.; Auling, G. *Free Radical Res.* **2009**, 1–8.
(30) Kalinowski, J.; et al. *J. Biotechnol.* **2003**, *104*, 5−25.
(31) Plönzig, J.; Auling, G. *Arch. Microbiol.* **1987**, *146*, 396–401.
(32) Cotruvo, J. A.; Stubbe, J. *Biochemistry* **2010**, *49*, 1297–1309.
(33) Massey, V. *J. Biol. Chem.* **1994**, *269*, 22459–22462.
(34) Dismukes, G. C. *Chem. Rev.* **1996**, *96*, 2909–2926.
(35) Boelrijk, A. E. M.; Dismukes, G. C. *Inorg. Chem.* **2000**, *39*, 3020–3028.
(36) Barynin, V. V.; Whittaker, M. M.; Antonyuk, S. V.; Lamzin, S. V.; Harrison, P. M.; Artymiuk, A. J.; Whittaker, J. M. *Structure* **2001**, *9*, 725–738.

Table 1. X-ray Data Collection Statistics and Refinement Statistics[a]

	native	Mn_{peak}
Data Collection		
X-ray source	BL41XU at SPring-8	BL41XU at SPring-8
wavelength (Å)	1.00000	1.89000
space group	*C*2	*C*2
unit-cell parameters		
a, *b*, *c* (Å)	96.21, 87.68, 83.25	95.97, 87.55, 83.29
α, β, γ (deg)	90.00, 99.29, 90.00	90.00, 99.36, 90.00
resolution (Å)	31.17−1.36 (1.41−1.36)	33.01−1.84 (1.91−1.84)
no. of observed reflections	502993	206100
no. of unique reflections	140012	58827
R_{merge}	0.073 (0.477)	0.077 (0.341)
completeness (%)	96.1 (72.7)	99.7 (100.0)
$\langle I/\sigma(I)\rangle$	13.4 (2.1)	28.4 (4.1)
redundancies	3.6	3.5
Refinement		
no. of reflections used in refinement	132961	
resolution used in refinement	20.0−1.36	
R	0.164	
R_{free}	0.210	
rms deviation		
bonds (Å)	0.010	
angles (deg)	0.026	
no. of protein atoms	4838	
no. of water molecules	606	

[a] Values in parentheses are for the highest resolution shell.

200. R2F was solely recovered in the 32−45 kDa fractions as assessed by SDS-PAGE and Western blot with anti-R2F antibody. The R2F-positive fractions were adsorbed to a Mono Q HR 5/5 column, eluted in the range of 520−535 mM KCl using a linear gradient and concentrated using Amicon Ultra-4 centrifugal devices (cut off 10 kDa). Further details of the molecular biological and biochemical protocol are described elsewhere, by Stolle et al.[28] Metal quantification was performed using: (i) graphite furnace atomic absorption spectroscopy (GF-AAS), (ii) inductively coupled plasma mass spectrometry (ICPMS), and (iii) by oxidation of the bound Mn to MnO_4^-.[28] The enzyme activity was determined according to ref 37.

2.2. Crystallographic Analysis of the R2F Protein. The purified R2F protein solution was concentrated to 10 mg·mL^{-1}. Crystallization was carried out using the sitting-drop vapor diffusion method at 277 K under aerobic condition. Crystals suited for diffraction experiments required a buffering medium that included: 0.1 M sodium citrate, 27.5% PEG4000, 0.05 M ammonium acetate pH 6.0, and 0.1 M ammonium acetate pH 7.0, with 0.05 M Tris/HCl pH 7.5. All data sets were collected at 100 K using the BL41XU beamline at SPring-8 (Hyogo, Japan). The detector used was a MX225HE (MAR research, Germany). The data sets were indexed, integrated, and scaled using the program HKL2000.[38] The molecular replacement and the initial refinement of the structure were carried out using the program CCP4 and REFMAC, respectively.[39] As coordinates for the search model, the data from R2F from *C. ammoniagenes* (PDB ID 1kgp) was used. Model building and final refinement were performed using WINCOOT and SHELX-97.[40,41] The experimental conditions are summarized in Table 1. XRF experiments for determination of the metal composition of R2F were carried out using the BL14.2 beamline at BESSY II (Berlin, Germany). A preliminary report was published in ref 42.

2.3. Multifrequency EPR Measurements. X-band spectra (9.4 GHz) were recorded with a Bruker Elexsys E500 spectrometer equipped with an Oxford Instruments ESR-910 helium flow cryostat. The samples were contained in quartz tubes of 4 mm outer diameter. Q-band spectra (34.0 GHz) were recorded with a Bruker ESP300E EPR spectrometer equipped with an Oxford instruments CF935 helium flow cryostat and a standard Bruker ER5106QT resonator. Q-band samples were contained in 3 mm quartz tubes. High-field EPR measurements at 244 GHz were recorded using a home-built quasi-optical EPR spectrometer described in ref 43. The CW EPR spectra were recorded at 5 K in a nonresonant Teflon sample holder containing 20 μL of 1 mM protein solution. Approximately 5 mW microwave power was available at 244 GHz leading to partial saturation of the radical signal such that a "passage" (absorption-like) line shape was obtained. The recorded spectra were pseudomodulated to obtain the derivative mode line shape presented in Figure 11. The magnetic field axis was calibrated using a Mn(II)/MgO standard.[44]

EPR signals observed at 9, 34, and 244 GHz were simultaneously fit assuming a three-spin model (see Theory). The calculations assumed that all tensors were colinear. Spectral simulations were performed numerically using Scilab-4.4.1, an open source vector-based linear algebra package (www.scilab.org) and the easyspin package[45] in MATLAB.

3. Theory

3.1. The Spin Hamiltonian Formalism 1: A General Model. Here we consider an exchange coupled Mn dimer (Mn_A−Mn_B) weakly coupled to an organic radical R with $S = {}^1/_2$. The precise oxidation states of the two Mn are unknown but are limited to three states: Mn^{II} ($S = {}^5/_2$), Mn^{III} ($S = 2$) or Mn^{IV} ($S = {}^3/_2$). As a consequence, there are five different oxidation state combinations the Mn dimer can take: $Mn^{II}Mn^{II}$, $Mn^{II}Mn^{III}$, $Mn^{III}Mn^{III}$, $Mn^{III}Mn^{IV}$, $Mn^{IV}Mn^{IV}$.

A basis set that describes the Mn-dimer−radical (R', $S_R = {}^1/_2$) spin manifold can be built from the product of the eigenstates of the three interacting spins:

$$|S_A S_B S_R m_A m_B m_R\rangle \tag{1}$$

Here S_A, S_B and S_R refer to the electronic spin state of Mn_A, Mn_B and S_R; m_A, m_B and m_R refer to the magnetic sublevels of each spin. m_X takes values S_X, S_X−1, ..., 1−S_X, S_X (where X = A, B, R). S_A and S_B can take values 1, ${}^3/_2$, and 2, depending on the oxidation state of the Mn dimer. S_R is always ${}^1/_2$. Thus, the model describing a $Mn^{II}Mn^{II}$ dimer interacting with a radical requires 72 basis vectors, the $Mn^{III}Mn^{III}$−R' model requires 50 basis vectors and the $Mn^{IV}Mn^{IV}$−R' model requires only 32 basis vectors.

The spin Hamiltonian appropriate to describe our system can be written as

(37) Willing, A.; Follmann, H.; Auling, G. *Eur. J. Biochem.* **1988**, *170*, 603–611.
(38) Otwinowski, Z.; Minor, W. *Methods Enzymol.* **1997**, *276*, 307–326.
(39) Collaborative Computational Project, N. *Acta Crystallogr., Sect. D* **1994**, 50.
(40) Emsley, P.; Cowtan, K. *Acta Crystallogr., Sect. D* **2004**, 60.
(41) Sheldrick, G. M. *Acta Crystallogr., Sect. A* **2008**, 64.
(42) Ogata, H.; Stolle, P.; Stehr, M.; Auling, G.; Lubitz, W. *Acta Crystallogr., Sect. F* **2009**, *65*, 878–880.
(43) Reijerse, E.; Schmidt, P.; Klihm, G.; Lubitz, W. *Appl. Magn. Reson.* **2007**, *31*, 611–626.
(44) Burghaus, O.; Rohrer, M.; Goetzinger, T.; Plato, M.; Moebius, K. *Meas. Sci. Technol.* **1992**, *3*, 765–774.
(45) Stoll, S.; Schweiger, A. *J. Magn. Reson.* **2006**, *178*, 42–55.

$$H = \sum_{i=A,B} (D_i[(S_{iZ}^2 - {}^1/_3 S_i(S_i+1) + {}^{E_i}/_{D_i}(S_{iX}^2 - SX_{iY}^2)] + \beta B \cdot g_{Mn_i} \cdot S_i - S_i \cdot J_{Int_i} \cdot S_R) - S_A \cdot J \cdot S_B + \beta B \cdot g_R \cdot S_R \quad (2)$$

Here all nuclear hyperfine and quadrupole terms of magnetic nuclei (e.g., ^{55}Mn) have been excluded since they are small and only contribute to the fitted line width. The spin Hamiltonian includes three coupling tensors that describe the interaction between the two Mn and the interaction between each Mn and the tyrosyl radical; three Zeeman tensors (**g**), one for each spin center; and two fine structure tensors, one for each Mn.

3.2. The Coupling Tensors $S_A \cdot J \cdot S_B$ and $S_i \cdot J_{int} \cdot S_R$. The coupling tensors $S_A \cdot J \cdot S_B$ and $S_i \cdot J_{int} \cdot S_R$ (where i = A, B) include all isotropic and anisotropic interactions between the two spins. The first tensor, the Mn−Mn interaction is expected to be large and dominated by the exchange coupling term. In most systems it is sufficient to treat this interaction as isotropic i.e. $JS_1 \cdot S_2$. In contrast, the two Mn−radical interactions are expected to be small. Here both exchange (through bond) and dipolar (through space) mechanisms contribute to the interaction. The Mn−radical interaction tensor can be decomposed into two parts (J_{iso}, J_{aniso})

$$S_i \cdot J_{int} \cdot S_R = J_{iso} S_i \cdot S_R + S_i \cdot J_{aniso} \cdot S_R \quad (3)$$

In general the anisotropic term has both exchange and dipolar contributions. However, it is usually sufficient to ignore the exchange component of this term and assume the anisotropic interaction is dominantly derived from the through space dipolar interaction between the two spins:

$$S_i \cdot J_{aniso} \cdot S_R \approx S_i \cdot d_{dip} \cdot S_R \quad (4a)$$

$$S_i \cdot d_{dip} \cdot S_R = g_i g_R \beta^2 [S_{iX} \;\; S_{iY} \;\; S_{iZ}] \cdot \begin{bmatrix} -\frac{2}{r^3} & 0 & 0 \\ 0 & \frac{1}{r^3} & 0 \\ 0 & 0 & \frac{1}{r^3} \end{bmatrix} \cdot \begin{bmatrix} S_{RX} \\ S_{RY} \\ S_{RZ} \end{bmatrix} \quad (4b)$$

Here r represents the distance between the two spin centers. The traceless dipole−dipole tensor (d_{dip}) as shown above is written such that the interspin vector is aligned along the X axis. Canonical rotation realigns the interspin vector along Y or Z. A nondiagonal dipole−dipole tensor is observed for an arbitrary interspin vector orientation.

For all the simulations presented in the manuscript the full coupling tensor J_{int} with components (J_{intX}, J_{intY}, J_{intZ}) was used. The isotropic component of the coupling tensor was not treated as a separate variable, nor was the coupling tensor assumed to be axially symmetric.

3.3. Split-Radical Signals. A 'Split-Radical' signal, as seen in EPR, is observed when a radical is weakly coupled to another paramagnetic center. The interaction has to be of the order of the radical's line width i.e. ~100 MHz. The split radical signal can be considered, to zeroth order, as an isolated radical that is perturbed by its interaction with a nearby paramagnetic center. An important subset of split radical signals is that where the radical interacts with a metal center. Metal centers typically have large inhomogeneous linewidths associated with **g** and hyperfine

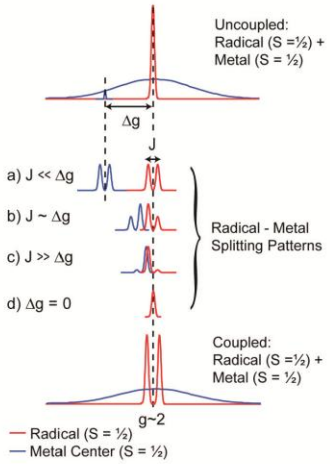

Figure 1. A pictorial representation of a S = ½ radical weakly interacting with a S = ½ metal ion. The top trace shows the uncoupled radical-metal signal. Metals characteristically have large inhomogeneous EPR linewidths due to large g and hyperfine anisotropy as compared to organic radicals. As represented in figure 1, unresolved g and hyperfine anisotropy broaden the EPR lineshape of the metal significantly, resulting in a structureless signal centered at g~2. The radical-metal interaction depends on which component of the metal's inhomogeneous line the radical interacts with. For most orientations (specific sites within the metal signal envelope) the coupling between the metal and the radical is small relative to the difference in g-value ($J \ll \Delta g$). In this case, the radical and metal signals split about their uncoupled g-positions, with each peak approximately having the same intensity (a). As the Δg decreases relative to J, a more complicated coupled signal pattern emerges (b and c). The intensity of the four peaks is redistributed such that the outer peaks' (satellites) intensity decreases relative to the center peaks. The powder spectrum observed is the sum of all these interaction types. For a sufficiently broad metal signal, the weak coupling limit ($J \gg \Delta g$) dominates. Its CW EPR spectrum resolves a 'splitting' of the radical signal and a broader metal site distribution that may or may not resolve a splitting. Although a Gaussian lineshape is assumed for the EPR signal of the metal ion, the same arguments are applicable for any arbitrary lineshape.

anisotropy as compared to radical signals, which are generally not broader than 100 MHz. For most orientations–specific sites within the metal signal envelope–the coupling between the metal and the radical is small relative to the difference in g-value ($J \ll \Delta g$), i.e. we are in the weak coupling limit.[46] The sum over all orientations yields a 'splitting' of the radical signal and a broader metal site distribution that may or may not resolve a splitting. The split radical signal pattern for a radical interacting with a $S = {}^1/_2$ metal center is shown in Figure 1.

The number of 'splittings'–spectral lines of the split radical pattern centered about $g \approx 2.0$–corresponds to the number of discrete magnetic sublevels (m_S sublevels) the metal system contains. For instance, a $S = 2$ metal contains five m_S sublevels (Figure 2). When weakly coupled to a radical, the radical line splits into five spectral lines. The low- and high-field edges of the split radical signal are defined by the radical's interaction with the $|m_S| = 2$ sublevels. The radical's interaction with $|m_s| = 1$ sublevels appear toward the center of the split-pattern. The coupling of the radical to the $m_S = 0$ sublevel results in no perturbation of the radical. The line separation within the split-pattern is equal to the metal−radical coupling J, for an isotropic

(46) Carrington, A.; McLachlan, A. D. *Introduction to Magnetic Resonance*, 1st ed.; Harper and Row: New York, 1967.

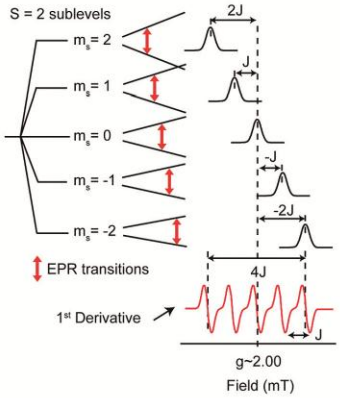

Figure 2. 'Split-radical' pattern observed in CW EPR for a $S = {}^1/_2$ radical coupled to a metal center of $S = 2$. Five transitions are observed, corresponding to the interaction of the radical with each of the electronic sublevels of the metal. The low- and high-field lines are defined by the radical's interaction with the $|m_s| = 2$ sublevels. The first derivative EPR spectrum resolves five features: four lines are observed about an unperturbed central line. The central line is derived from the interaction of the radical with the $m_s = 0$ sublevel of the metal center. The separation of the lines in the first derivative spectrum (red) is equal to J.[46]

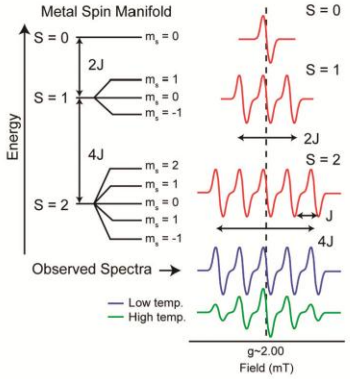

Figure 3. 'Split-radical' pattern observed in CW EPR for a $S = {}^1/_2$ radical coupled to a metal spin manifold with ground state $S = 2$. At low temperatures, only the ground state of the spin manifold is populated and the EPR spectrum shows only the radical interacting with an $S = 2$ spin. As the temperatures is increased, higher spin states of the metal spin manifold are populated, namely $S_T = 1$ and $S_T = 0$. The ground state in a ferromagnetically coupled dimer will always have the highest effective spin (S_T) as compared to all the other spin manifold states and thus its interaction with a radical will yield the broadest contribution to the observed EPR signal.

metal–radical interaction and thus the total spectral breadth of this signal is $4J$ (Figure 2). This represents a general result for all split-radical signals. The observation that the coupling of a radical to the $m_S = 0$ sublevel of the metal spin manifold does not affect the position and shape of its signal provides one way to discriminate between different metal–radical interactions. The interaction of a radical with a half-integer spin metal (i.e., Mn^{IV}, $S = {}^3/_2$) should not contain an unperturbed central line at $g \approx 2$, whereas its interaction with an integer spin metal (i.e., Mn^{III}, $S = 2$) should.

The spin manifold of a coupled spin system can contain more than one contribution. Higher spin states can also add to the observed split-radical signal pattern. This is shown in Figure 3 for a ferromagnetically coupled $S_T = 2$ spin manifold. At low temperatures, only the ground state of the spin manifold is populated and the EPR spectrum shows only the radical interacting with an $S = 2$ spin. As the temperature is increased, the spectrum may also contain contributions from higher spins states, in this instance $S_T = 1$ and $S_T = 0$. These add intensity to the center of the pattern. The ground state in a ferromagnetically coupled dimer will always have the highest effective spin (S_T) as compared to all the other spin manifold states and thus its interaction with a radical will yield the broadest contribution to the observed EPR signal.[47] The opposite is observed for an antiferromagnetically coupled dimer. Here the ground state contribution to the EPR spectrum will be the narrowest component. The magnitude of the exchange coupling within the metal spin system dominantly determines the ladder spacing of the manifold and as a consequence, the temperature dependence of the split radical signal. In the case of a Mn dimer, the exchange coupling (J) between the two metal centers has to be of the order of the microwave quantum for the split-radical signal to show any significant temperature dependence at cryogenic temperatures (5–30 K).

(47) The splitting to first order is expected to scale with S_T, splitting $= 2J_{int}S_TS_R = 2J_{int}{}^1/_2S_T = J_{int}S_T$. As the ground spin multiplet has the largest total spin, it defines the edges of the signal envelope.

The energy levels of the metal/metal system, as shown in Figures 2 and 3, assume that the Zeeman term is the dominant term in the spin Hamiltonian. In this case the eigenstates of the metal can be assumed to be the unperturbed basis set to a good approximation, i.e. for $S = 2$, the eigenstates for a single metal are: $|2,2\rangle$, $|2,1\rangle$,$|2,0\rangle$, $|2,-1\rangle$,$|2,-2\rangle$. Mn^{III} and Mn^{IV} typically have zero-field splittings of $\sim 1\ cm^{-1}$. This is of the order of the microwave quanta (Zeeman term) at X ($\sim 0.3\ cm^{-1}$)- and Q ($\sim 0.9\ cm^{-1}$)-bands. Here the eigenstates of the system are mixed, such that the ladder of states as presented in Figure 2 is no longer valid. However, in this case the same key observations still apply, namely (i) the number of lines in the split signal pattern is still dependent on the number of energy levels the metal/metal system contains, and (ii) the spectral breadth of the split radical signal is defined by the metal–radical coupling interaction. The effect of the on site zero-field splitting of the metal is to redistribute signal intensity within the split-radical pattern. This effect can also lead to a norrowing of the spilt-radical pattern.

3.4. The Spin Hamiltonian Formalism 2: A Simplified Model. It is observed that the split radical signal is derived from only one component of the total spin manifold (Figure 1) and as such is only sensitive to specific elements of the above spin Hamiltonian, in particular those that involve the spin operator S_R. These include the Mn–radical exchange terms and at high field, the intrinsic **g**-tensor of the radical. Terms that only include the S_A and S_B operators are less well defined. For instance the Mn g-anisotropy is shown to have little effect on the split radical signal and can be approximated by a single isotropic value. This allows us to use a simpler Hamiltonian outlined below to ensure the derived solution is unique.

$$H = \sum_{i=A,B} (D_i[(S_{iZ}^2 - {}^1/_3S_i(S_i+1) + {}^{E_i}/_{D_i}(S_{iX}^2 - S_{iY}^2)] + g_{Mn}\beta B \cdot S_i - S_i \cdot J_{Int} \cdot S_R) - JS_A \cdot S_B + \beta B \cdot g_R \cdot S_R \quad (5)$$

Here both g_{Mn} and $\mathbf{J_{int}}$ are assumed to be the same for both Mn centers to limit the size of the parameter set.

4. Results

4.1. Biochemical Assay.

4.1.1. Characterization of the Native-Type R2F from *C. ammoniagenes*. To improve R2F synthesis yields, a second, cloned *nrdF* gene from *C. ammoniagenes* ATCC 6872[16] was introduced into the same strain (*C. ammoniagenes* ATCC 6872) under control of the IPTG-inducible *tac*-promotor,[28] in addition to its intrinsic gene. This approach required the growth medium to be supplemented with Mn. Nonphysiological levels of all metals, including Mn, were avoided. The typical Mn concentration used to generate Mn-R2F (native-type R2F) was 185 μM $MnCl_2$. The addition of equimolar amounts of Mn^{2+} and Fe^{2+} did not change the level of metalloradical assembly or radical generation in R2F (see below). In addition, if the growth media was only supplemented with Fe^{2+}, no Fe^{2+} was incorporated to a significant extent into R2F and no tyrosyl radical, as measured by its UV/vis absorbance at 408 nm, was observed. Thus, *C. ammoniagenes* restricts the incorporation of Fe into R2F *in vivo* even in the absence of Mn and it is the availability of Mn that is the limiting factor that determines the amount of functional metalloradical cofactor obtained.

The R2F preparation used for the crystal structure and multifrequency EPR measurements detailed below, typically displayed an activity of 69 $\mu mol \cdot mg^{-1} \cdot min^{-1}$. This value exceeds the measured activity of all other RNRs by at least 10-fold, with the exception of *C. glutamicum* (see Supporting Information, Table S1). In addition this value is a thousand-fold higher than that obtained from *C. ammoniagenes* R2F expressed in *E. coli* and reconstituted with Fe (48 $nmol \cdot mg^{-1} \cdot min^{-1}$).[26] In this earlier study the *C. ammoniagenes nrdF* gene was heterologously expressed in *E. coli* and the purified apo-R2F protein was reactivated with Fe^{II}-ascorbate *in vitro*.

The number of Mn per R2F monomer was determined to be 0.74 ± 0.04 by graphite furnace atomic absorption spectroscopy (GF-AAS) and inductively coupled plasma mass spectrometry (ICPMS), see ref 28. By comparison, the number of Fe per monomer was determined to be 0.03 ± 0.04. Thus, the metal cofactor contains at least 1 Mn per R2F monomer and ~0 Fe per R2F monomer. The radical content was estimated to be 0.18 $Y^{\bullet}$ per R2F monomer, from its UV/vis absorption at 408 nm. As the radical content is significantly smaller than 1, only a fraction of centers (20%) contain a fully assembled metalloradical cofactor.

The addition of hydroxyurea (HU), a radical scavenger, to the holoenzyme quenches the tyrosyl radical, inhibiting enzymatic function, see ref 25. Removal of HU, under aerobic conditions, results in the recovery of the holoenzyme's catalytic function.[37] Typically up to 75% of the original activity is observed after removal of the radical scavenger.[37] Quenching of the tyrosyl radical, as measured by its UV/vis absorption at 408 nm, was also observed in this study, upon addition of HU to the purified R2F subunit. Here a tyrosyl radical signal was recovered after HU had been removed via ultrafiltration by the concomitant addition of 10 μM H_2O_2 and 2.5 μM methylviologen (as a mediator). The tyrosyl radical showed rapid and complete recovery within 60 s of H_2O_2 addition. It was noted that the final concentration of the tyrosyl radical signal typically exceeded its initial concentration by 30%. It is unclear whether this additional increase reflects the amount of radical lost during our purification procedure or is derived from newly assembled centers that either contained no Mn cofactor (apo-R2F), or a partially assembled Mn cofactor. Regardless, treatment of the inactivated R2F with H_2O_2 leads to assembly of a functional metalloradical cofactor.

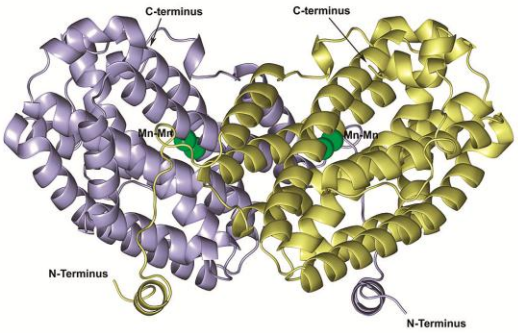

Figure 4. Overall structure of the all helix bundle R2F subunit obtained from *C. ammoniagenes*. The yellow and blue ribbons show the protein backbone of the two monomer units of the dimer. The two Mn atoms in each monomer are shown as green spheres.

A recent report of Cotruvo and Stubbe suggested the involvement of an additional flavodoxin, NrdI in class Ib metallocofactor assembly.[32] In *C. ammoniagenes* the *nrdI* gene is located in the *nrd* operon in front of *nrdE*.[48] In the R2F preparations used for this study we could not identify an equivalent small protein (*C. ammoniagenes*-NrdI acc. no., PDB O69272) as detected by ESI-QTOF mass spectrometry. Attempts to identify this protein in *C. ammoniagenes* form part of ongoing experiments.

4.2. Crystal Structure.

4.2.1. Structure Determination and Overall Structure. Crystals of the R2F subunit of RNR obtained from *C. ammoniagenes* diffracted to 1.36 Å resolution and belonged to the space group *C*2 with unit-cell parameters $a = 96.21$ Å, $b = 87.63$ Å, $c = 83.25$ Å, $\beta = 99.29°$.[42] Figure 4 shows the structure of R2F from *C. ammoniagenes*. The homodimeric protein contains only helical bundles. The overall structure is very similar to the R2F structure reported earlier by Högbom et al.[26] obtained from heterologous expression in *E. coli*.

4.2.2. The Metalloradical Cofactor. X-ray fluorescence spectroscopy (XRF) was carried out in order to determine the metal components of the R2F subunit. Spectra for each metal fluorescence energy range are shown in the Supporting Information (Figure S1). No fluorescence was observed for zinc, copper, cobalt, iron, or nickel (see Figure S1A–C, Supporting Information). However, a manganese signal was observed (see Supporting Information Figure S1D). The results indicate that manganese alone is the native metal of the R2F subunit. The single-wavelength anomalous dispersion (SAD) method was applied to the manganese signal and peak data were collected at an X-ray wavelength of 1.89000 Å (see Table 1). The anomalous difference map revealed four manganese peaks. As the R2F dimer has a noncrystallographic symmetry between the two R2F monomers, the four peaks in the difference map indicate the presence of 2 Mn per R2F monomer. The anomalous difference map for one R2F monomer subunit is shown in Figure

(48) Torrents, E.; Roca, I.; Gibert, I. *Microbiology* **2003**, *149*, 1011–1020.
(49) Almost no electron density was observed at position Oε2 of residue E168. Another set of diffraction data of Mn-R2F solved at 1.65 Å resolution also showed only a weak electron density at this position (data not shown).

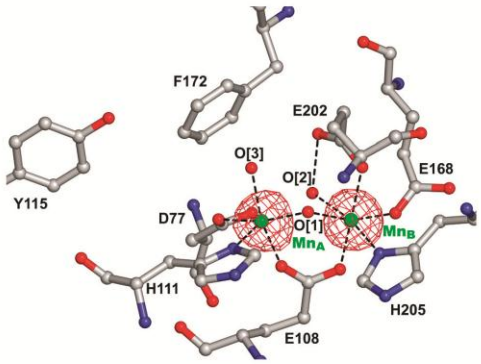

Figure 5. Single-wavelength anomalous dispersion (SAD) of the R2F subunit of *C. ammoniagenes* (monomer). The manganese signal was recoded at 1.89000 Å (see Table 1). The anomalous difference map revealed four manganese peaks, two for each monomer subunit. The difference map (red meshed surface) has been overlaid on the proposed coordination sphere as determined from fitting the electron density map.

5 (red meshed surface). It has been overlaid onto the proposed coordination sphere as determined from the fitting of the electron density map (see Figure 6A). The value of 2 Mn per R2F falls within the allowed range as determined by the chemical analysis (see 4.1). As the metal site uniformly contains two Mn, it is suggested that only the fully assembled R2F protein fraction readily crystallizes. Apo-R2F protein and R2F which contain only 1 Mn center are assumed to crystallize more slowly or not at all.

The electron density map of the metalloradical cofactor of R2F is shown in Figure 6A and the corresponding bond distances in Figure 6B. The metal site contains two Mn centers, Mn_A (proximal to the tyrosine Y115) and Mn_B (distal to the Y115). The Mn−Mn separation is 3.3 Å. Both Mn are coordinated by a histidine residue (H111 for Mn_A and H205 for Mn_B) and bridged by a glutamic acid (E108). Two additional glutamic acids (E202 and E168[49]) coordinate Mn_B; only an aspartate residue (D77) was identified as a coordinating residue to Mn_A. A bridging oxo/hydroxo (O[1]), with Mn−O−Mn bond angle of ∼120° was observed between Mn_A and Mn_B, analogous to the di-iron metallocofactor of class Ia RNRs. A second asymmetric bridging oxygen (O[2]) was also observed. The Mn_A−O[2] bond length (∼2.7 Å) is too long for the O[2] to be considered a real bridging oxo/hydroxo ligand. Instead, it may form part of an extended hydrogen-bonding network about the Mn−Mn core, which possibly includes the aspartate (D77) ligand of Mn_A, 2.7 Å away. A third, terminal hydroxo/water (O[3]) was identified as a ligand to Mn_A. An additional water molecule was not observed between the tyrosine residue Y115 and the hydroxo/water molecule (O[3]) bound to Mn_A. The distance between the center of the tyrosine residue (Y115) and the center of the Mn dimer is approximately 9.8 Å. The hydroxo/water ligation of Mn_A (O[3] in Figure 6B) is 5.6 Å from the tyrosine (Y115) and the edge-to-edge distance of the Mn_A to Y155 is 6.8 Å. It is also noted that the tyrosyl radical has probably significantly decayed during the crystallization process.

The Mn metalloradical cofactor (Mn-R2F) described here is significantly different from earlier inactive structures described in the literature. Both Högbom et al.[26] (PDB ID 1kgp) and Atta et al.[50] have reported crystal structures of the Mn-R2F/Mn-R2 subunit that contained a $Mn^{II}Mn^{II}$ dimer (Figure 6C). Both structures were obtained from apo-R2F/R2 protein that was subsequently reloaded with Mn^{II} *in vitro*. These structures more closely resembled the reduced protein obtained for the diferrous metallocofactor (Fe-R2F) as described below, which was assigned to a resting form of the enzyme.

The diferric metalloradical cofactor (Fe-R2F), previously reported by Högbom et al., was obtained from heterologous expression in *E. coli* and reactivation of the protein by treatment with Fe^{II}-ascorbate *in vitro*.[26] The crystal structure of the Fe-R2F subunit obtained using this preparatory approach showed that two iron centers had been incorporated into the metal binding site and UV/vis measurements confirmed that the R2F subunit contained a tyrosyl radical (0.26 per R2F protein subunit). The Fe-R2F was shown to exist in two stable forms. In its reduced form (PDB ID 1kgo), prior to its activation with O_2, the metal cluster contained two ferrous centers that are separated by ∼4 Å and bridged by two glutamic acids. In its active oxidized form (PDB ID 1kgn), the met state, the cluster contained two ferric centers with a center-to-center separation of ∼3.5 Å and, in addition to a carboxylate bridge, an oxo bridge derived from O_2 (Figure 6D). Figure 7 compares the structures of the metalloradical cofactor of R2F containing either a dimanganese or di-iron R2F (met state) from *C. ammoniagenes*. The overall architecture of the Fe containing dimeric unit is highly similar to the Mn metalloradical cofactor seen in the present work. Only small changes between the two structures are observed: (i) the ring plane of the Phe172 is rotated in the Mn-R2F, displacing a water molecule that is present in the corresponding Fe-R2F and; (ii) the carboxylate of Asp77 has changed its orientation relative to the Mn site, with both oxygens now providing a ligand and/or hydrogen bond to the metallocofactor (see above). The absence of a water molecule between Y115 and the Mn dimer in the Mn-R2F (in addition to O[3]) indicates that the hydrogen bonding networks about the Y115 are different in the Mn-R2F and Fe-R2F proteins.

4.3. Multifrequency EPR Measurements.

4.3.1. Frozen Solution CW X-Band Measurements at 80 K: Detection of a Tyrosyl Radical. A radical signal (at g ∼ 2.004) was observed at $T = 80$ K in Mn-R2F sourced from *C. ammoniagenes* that is similar to a tyrosyl radical (Figure 8, trace A). The signal's hyperfine structure is typical of tyrosyl radical signals observed in RNR class Ib as shown in Figure 8, trace C. Trace C represents a simulated spectrum of a tyrosyl radical using the hyperfine parameters observed for *Salmonella typhimurium*.[51] The simulation can, however, not explain the broadened line shape of the signal. The overall signal profile matches a Lorentzian line shape as shown in Figure 8, trace B. It was also observed that the maximum available microwave power of 200 mW did not saturate the radical at 80 K. These two observations suggest that the tyrosyl radical is not isolated but instead interacts with another paramagnetic species.

4.3.2. Frozen Solution CW X-Band Measurements at 5−30 K: Manifestation of a 'Split-Tyrosyl Radical' Signal. At cryogenic temperatures (<30 K) the appearance of the X-band EPR signal of the tyrosyl radical changes dramatically. A broader signal was observed with spectral features that extend over a field range of ∼40 mT (Figure 9, black traces). The total

(50) Atta, M.; Nordlund, P.; Aberg, A.; Eklund, H.; Fontecave, M. *J. Biol. Chem.* **1992**, *267*, 20682–20688.

(51) Allard, P.; Barra, A. L.; Andersson, K. K.; Schmidt, P. P.; Atta, M.; Gräslund, A. *J. Am. Chem. Soc.* **1996**, *118*, 895–896.

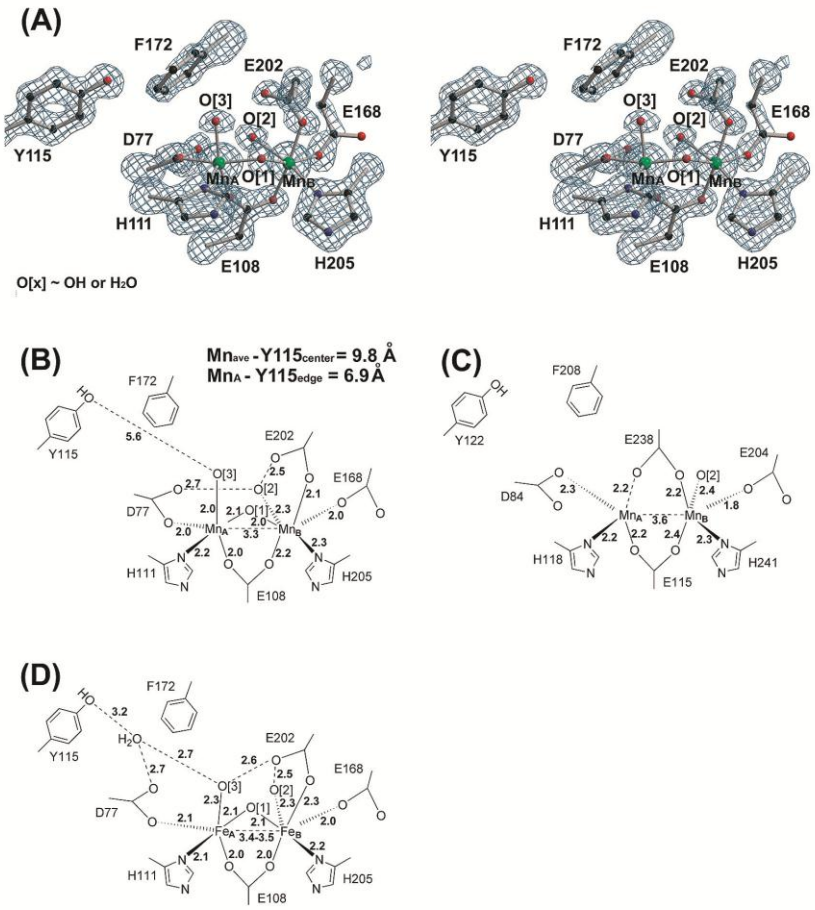

Figure 6. (A) Stereoview of the electron density map of the metalloradical cofactor with surrounding amino acid residues of the R2F subunit obtained from *C. ammoniagenes*. (B) The structure and the coordination distance (Å) of the native-type Mn-R2F from *C. ammoniagenes*. (C) The Mn-substituted form of the R2 protein obtained from *E. coli*.[50] (D) Fe-R2F subunit (in the oxidized form) of *C. ammoniagenes*.[26]

spectral breadth of the signal is significantly larger than that expected for an isolated tyrosyl radical. In addition, the new signal is highly structured at <20 K; at least five features were observed, centered at $g \approx 2.00$ (Figure 9A–C). The temperature dependence of all signals within the 310–370 mT magnetic field range obeys Curie's law (between 5 and 80 K). This suggests that both the signals at low (5 K) and high (80 K) temperatures arise from the same spin manifold. Similar broadened split-tyrosyl radical signals were recently observed at X-band for the metalloradical cofactor of R2F sourced from *E. coli* (class Ib), reactivated *in vitro* with Mn.[32] However, no theoretical rationale for the metalloradical cofactor signal was presented.

4.3.3. Frozen Solution CW Q-Band Measurements at 10–40 K: An Analogous 'Split-Tyrosyl Radical' Signal As Seen at X-Band. A 'split-tyrosyl radical' was also seen at cryogenic temperatures (<40 K) at Q-band. It displays the same basic characteristics as seen at X-band, namely: (i) it is centered about g~2; its total spectral breadth is approximately 40 mT; and it resolves a peak splitting of 4–6 mT. The temperature dependence at Q-band was also nominally the same. The wings of the signal were most readily resolved at 10 K, with their intensity decreasing relative to the central line as the temperature increased. The Q-band spectrum resolves more peak splittings than seen at X-band. These new features are unlikely to be due to an enhanced Zeeman effect as no net change in the total spectral breadth is observed. The additional splitting seen at Q-band, which manifests itself at X-band in an asymmetric line shape of several peaks (see peaks 1 and 4, Figure 9A), is a further indication of the complex spin manifold the tyrosyl radical species is interacting with.

4.3.4. Powder Pattern CW X/Q-Band Simulations: A $Mn^{III}Mn^{III}Y^{\bullet}$ or $Mn^{IV}Mn^{IV}Y^{\bullet}$ Metalloradical Cofactor. The spectral widths of the EPR signals seen at 9 and 34 GHz are consistent with the tyrosyl radical weakly interacting with the two Mn centers. These spectra can be considered, to zeroth order, as an isolated tyrosyl radical that is perturbed by its interaction with a nearby paramagnetic center. This interaction is of the order of the radical's intrinsic line width (~100 MHz/3.6 mT). The split-tyrosyl radical signal of the R2F subunit of *C. ammoniagenes* splits into 5 discrete lines at X-band, with an unperturbed central line, suggesting the tyrosyl radical must

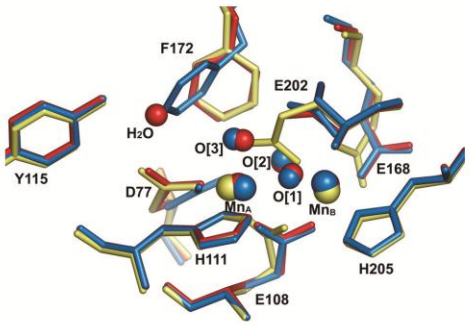

Figure 7. Comparison of the metalloradical cofactor of R2F that contains: an oxidized (active) Mn_2 cofactor (blue), a reduced (inactive) Mn_2 cofactor (yellow) or an oxidized (active) Fe_2 cofactor (red). The Mn-R2F (reduced) and Fe-R2F (oxidized) structures are taken from Högbom et al.[26] (PDB ID 1kpg, 1kgn). The ring plane of the F172 is rotated in the Mn-R2F (oxidized), displacing a water molecule as compared to the corresponding Fe-R2F. The carboxylates E202 and D77 change their orientation relative to the Mn site in the reduced and oxidized structure. E202 provides one ligand to the metallocofactor in its oxidized state (blue). In its reduced state, E202 is a bidentate ligand, bridging the two Mn (yellow). Similarly, both oxygens of D77 provide a ligand and/or hydrogen bond to the metallocofactor in its oxidized state. In its reduced state it provides only one ligand (yellow), similar to the Fe_2 cofactor (red).

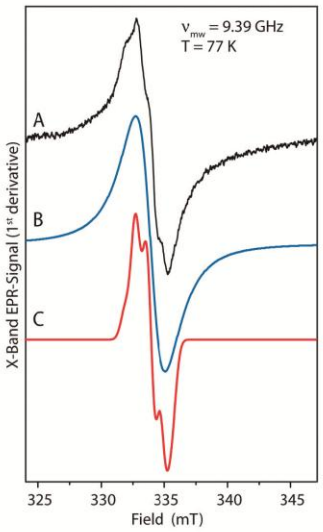

Figure 8. CW X-band EPR of the R2F subunit of *C. ammoniagenes*. (A) X-band spectrum recorded at 77 K; (B) a fitted Lorentz line shape (first derivative). A Lorentz line well reproduces the overall line shape suggesting a dominantly homogeneous line-broadening mechanism; and (C) a simulation assuming parameters typical for a class Ib RNR tyrosyl radical, (see Supporting Information Table S2). Experimental conditions: microwave frequency 9.39 GHz, microwave power 2 mW, T = 77 K, modulation amplitude 0.16 mT, modulation frequency 100 kHz, 9 scans of 84 s, time constant 82 ms.

interact with a metal center of integer spin ($S \geq 2$). A total spin of 2 ($S = 2$) corresponds to a $Mn^{V}Mn^{V}$ dimer, which is considered to be not physically realizable. The only oxidation states of the two Mn centers that are considered plausible are: Mn^{II}, Mn^{III} and Mn^{IV}. This allows for five possible Mn oxidation state configurations. It can immediately be deduced that a tyrosyl

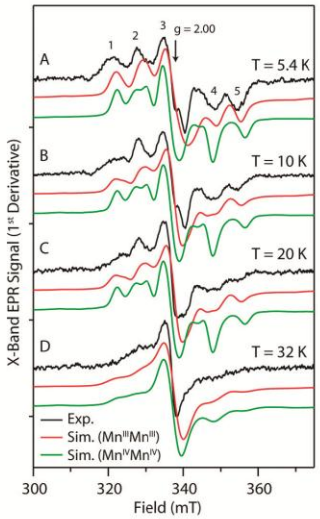

Figure 9. The temperature dependence of the CW X-band EPR spectrum of the R2F-subunit of *C. ammoniagenes* in frozen solution. Black lines: experimental data; red lines: simulations assuming the R2F subunit contain a $Mn^{III}Mn^{III}$ dimer; green lines: simulations assuming a $Mn^{IV}Mn^{IV}$ dimer. Simulation parameters are given in Table 2. Experimental conditions for A, B, C, and D: microwave frequency 9.47 GHz, microwave power 2 mW, field modulation 1.2 mT, modulation frequency 100 kHz, accumulation time 84 s, time constant 164 ms.

Table 2. Optimized Simulation Parameters Used for Simulations at 9, 34, and 244 GHz Shown in the Text for the $Mn^{III}Mn^{III}$ Dimer and $Mn^{IV}Mn^{IV}$ Dimer Simulations (see Figures 9, 10 and 11)

		fit value in MHz (cm^{-1})					
		$Mn^{III}Mn^{III}$			$Mn^{IV}Mn^{IV}$		
J		17688 (0.59)			80644 (3.48)		
Mn_A	D_A	24714 (0.82)			24809 (0.83)		
	E_A/D_A	0.10			0.10		
Mn_B	D_B	27582 (0.92)			27308 (0.91)		
	E_B/D_B	0.25			0.27		
g_{Mn}		2.026			2.025		
J_{int}		ISO	−28.9		ISO	−19.3	
		X	181.6	210.5[a]	X	219.4	238.7[a]
		Y	−130.0	−101.1[a]	Y	−183.0	−163.7[a]
		Z	−138.4	−109.5[a]	Z	−94.2	−74.9[a]
G_{tyr} (Collinear)		ISO	2.0050		ISO	2.0048	
		X	2.0046	−0.0004[a]	X	2.0052	0.0004[a]
		Y	2.0077	0.0027[a]	Y	2.0032	−0.0016[a]
		Z	2.0028	−0.0022[a]	Z	2.0060	0.0012[a]
g_{tyr} (Rotated)		iso	2.0051		iso	−[c]	
		x	2.0085	0.0034[a]	x	−	−
		y	2.0045[b]	−0.0006[a]	y	−	−
		z	2.0022[b]	−0.0029[a]	z	−	−
		α	67.2		−		
		β	30.0		−		

[a] Anisotropic component, i.e. $g_X' = g_X - g_{ISO}$; $J_X' = J_X - J_{ISO}$. [b] Fixed simulation parameters, i.e. g_y and g_z. [c] $Mn^{IV}Mn^{IV}$ simulation was unable to reproduce the experimental spectrum at high field using fitting procedure (ii), i.e. $g_y = 2.0045$, $g_z = 2.0022$.

radical coupled to the mixed valence complexes $Mn^{III}Mn^{II}$ and $Mn^{III}Mn^{IV}$ would not be able to reproduce the split pattern observed. Their spin manifolds contain only paramagnetic sublevels. As a consequence, a fitted exchange interaction between the Mn cluster and the tyrosyl radical cannot simultaneously explain both the unperturbed central line ($g \approx 2.00$) and the total width of the split signal.[52] Only the equivalent

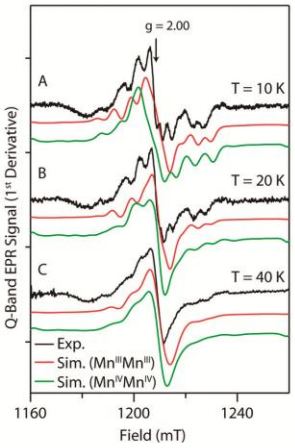

Figure 10. Temperature dependence of the CW Q-band EPR spectrum of the R2F-subunit of *C. ammoniagenes* in frozen solution. Black lines: experimental data; red lines: simulations assuming the R2F subunit contains a $Mn^{III}Mn^{III}$ dimer; green lines: simulations assuming a $Mn^{IV}Mn^{IV}$ dimer. Simulation parameters are given in Table 2. The negative feature at 1170 mT represents a baseline artifact. Experimental conditions for A, B, and C: Microwave frequency 33.94 GHz, field modulation 1.0 mT, 100kHz, 10 scans; accumulation time 84 s; time constant 82 ms.

oxidation state configurations: $Mn^{II}Mn^{II}$, $Mn^{III}Mn^{III}$ and $Mn^{IV}Mn^{IV}$ are considered feasible. It is also noted that the $Mn^{II}Mn^{II}$ oxidation state is inconsistent with crystallographic data (see Results 4.2 above) and mechanistic constraints (see Discussion). Thus, only simulations for the $Mn^{III}Mn^{III}$ and $Mn^{IV}Mn^{IV}$ configurations are presented.

Powder simulations of the 'split-tyrosyl radical' signal at X- and Q-bands are shown in Figures 9 and 10, (red trace assuming a $Mn^{III}Mn^{III}$ dimer, green trace assuming a $Mn^{IV}Mn^{IV}$ dimer). A simple rationale can be made for the 'split-tyrosyl radical' as given in the Theory section (see Figure 2). The low- and high-field edges of the split signal are derived from the tyrosyl radical's interaction with the Mn−Mn spin multiplet of highest effective spin, $S_T = 4$ for a $Mn^{III}Mn^{III}$ dimer.[53] As these features are most readily observed at low temperatures, the Mn−Mn manifold state of highest spin multiplicity must be the ground state. As a consequence the coupling between the two Mn centers must be ferromagnetic. Transitions within higher effective multiplets ($S = 3$, 2, 1, and 0) are progressively narrower (see ref 47, Theory), and add intensity to the center of the pattern (i.e., at $g \approx 2.0$). At 5 K, transitions within the ground multiplet dominate the powder spectrum. As the temperature is raised to 30 K, the relative population of higher multiplet states increases and thus the total signal at either X- or Q-bands appears to narrow; the relative intensity of the wings of the split signal decrease compared to the unperturbed central line. The superposition of the different multiplet states leads to the additional splittings seen at both X and especially Q-band. The strong temperature dependence of the 'split-tyrosyl radical' signal suggests that the energy level separations between the Mn−Mn multiplet states are small. The spin manifold ladder spacing is dominantly dependent on J, the coupling between the two Mn centers (see Figure 3).

The $Mn^{III}Mn^{III}$ model reproduces both the line shape and temperature dependence of the 'split-tyrosyl radical' signal significantly better than the $Mn^{IV}Mn^{IV}$ model at both X and Q-band frequencies. The $Mn^{IV}Mn^{IV}$ model predicts peak splittings not observed in the experimental data and the simulated line shape is approximately invariant over the 5−20 K temperature range. This disparity between the $Mn^{IV}Mn^{IV}$ model and the experimental data arises from the simulations' inability to fit the isotropic exchange J between the two Mn in the two temperature regimes. To reproduce the 'five-peak pattern' seen at 5 K at X-band (Figure 9A), J has to be of the order of several cm^{-1}. In contrast, to fit the temperature dependence (5−30 K) the exchange interaction must be small, less than 1 cm^{-1}. The fitted value of ~3.5 cm^{-1} represents a compromise between these two competing constraints. This problem is not encountered for the $Mn^{III}Mn^{III}$ simulation. It estimates the J coupling between the two Mn to be ~0.7 cm^{-1}. The small Mn−Mn exchange then readily accounts for the temperature dependence of the 'split-tyrosyl radical' signal.

The invariance of the 'split-tyrosyl radical' signal's width at X- and Q-bands frequencies is consistent with the notion that the nonfield dependent terms of the spin Hamiltonian i.e. $\mathbf{J}_{int}$, dominantly defines the total spectral breadth of the signal. The fitted exchange tensor ($\mathbf{J}_{int}$), for the $Mn^{III}Mn^{III}$ simulation, is axially symmetric and is virtually traceless suggesting the interaction between the tyrosyl radical and the two Mn centers is dominantly dipolar (i.e., $\mathbf{J}_{int} \approx \mathbf{d}_{dip}$, see Theory). The magnitudes of the tensor components are also consistent with this interpretation. The largest component of the $\mathbf{d}_{dip}$ tensor d_{dipX} (~200 MHz), assigns the inter-Mn−Tyrosyl vector (Table 2) and corresponds to an average interspin distance (r) between the tyrosyl radical and each Mn center of ~8 Å, approximately that seen in the crystal structure (see Results 4.2).

4.3.5. Frozen Solution High-Field (244 GHz) CW EPR Measurements. Cryogenic (5 K) CW EPR experiments of the tyrosyl radical of the R2F subunit were also carried out at high field (244 GHz). A 'radical-like' signal was observed with *effective* **g**-tensor components of 1.9989, 2.0040, and 2.0105 (see Figure 11, black trace). These values are unusual for a protein based radical; the intrinsic **g**-tensor values for the stable tyrosyl radical of the R2F subunit of *S. typhimurium* are 2.0022, 2.0045, and 2.0089.[51] Thus the observed tyrosyl radical seen here is approximately 3 times the spectral breadth of the tyrosyl radical observed in *S. typhimurium*. An estimate of the expected total spectral breadth of the high-field signal can be made from the low frequency X- and Q-band data. At these frequencies the total breadth of each signal was ~40 mT. It can be shown by simulation that the spectral breadth of the split-tyrosyl radical signal at these frequencies is dominantly dependent on the Mn−tyrosyl exchange interaction (see above, and Theory). At high field (244 GHz) this is no longer the case. The total breadth now includes the broadening due to the exchange interaction and the intrinsic g-anisotropy of the tyrosyl itself. An estimate of the latter contribution can be made from literature data of isolated tyrosyl radical signals, by taking the difference between the g_X and g_Z values, the edges of the tyrosyl radical spectrum, in magnetic field units i.e. $(1/g_Z - 1/g_X)\cdot\nu\cdot h/\beta$ where h, β and ν are Planck's constant, the Bohr magneton, and the microwave

(52) The exchange interaction (J_{int}) has to be both smaller than the linewidth of the unperturbed tyrosine radical to resolve the central ($g \approx 2.00$) component of the signal and significantly larger than the linewidth of the tyrosyl to resolve the total width of the split signal.

(53) A description of the Mn dimer's energy levels in terms of the 'effective spin' S_T of the different sub-manifolds of the metal is used for convenience. This description is not valid for the $Mn^{III}Mn^{III}/Mn^{IV}Mn^{IV}$ models presented here since the 'ground' spin multiplet is not well removed from the higher effective spin states.

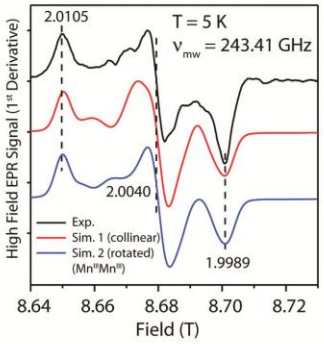

Figure 11. CW high-field EPR spectrum of the R2F-subunit of *C. ammoniagenes* in frozen solution. Black line: experiment; red line: simulation assuming the molecular **g**-tensor of the tyrosyl radical is collinear with the principal axis system of the spin Hamiltonian model (i.e., Mn_A and Mn_B, parameter set given in Table 2); blue line: simulation assuming typical tyrosyl radical **g**-tensor components and an axes rotation of the tyrosyl radical relative to the principal axis system of the spin Hamiltonian model (see Table 2). Additional simulations, where the fitted line width was varied, are shown in the Supporting Information. The data was collected using passage conditions. The absorption-like line shape obtained was pseudomodulated (2 mT amplitude) to obtain the derivative mode line shape presented. Experimental conditions: microwave frequency 243.41 GHz; microwave power: 5 mW; temperature 5 K.

frequency, respectively. At 244 GHz this relation yields an intrinsic tyrosyl radical width of ~20 mT, assuming $g_X = 2.0080$ and $g_Z = 2.0022$. The sum of the Mn−tyrosyl exchange and the *g*-anisotropy of the tyrosyl radical gives a total spectral breadth of ~60 mT, the same as seen experimentally (see Figure 11).

As the high-field (244 GHz) spectrum now contains contributions from the intrinsic *g*-anisotropy, a substantial increase in the number of spectral peaks that make up the composite line shape is expected. This is not observed; the experimental spectrum contains fewer peaks than that obtained at X-band. This effect arises from *g*-strain, a distribution in spin Hamiltonian parameters, that is enhanced at high magnetic fields. This is discussed further in the Supporting Information.

4.3.6. CW High-Field Powder EPR Simulations: Orientation of the Tyrosyl Relative to the $Mn^{III}Mn^{III}$ Dimer. The high-field spectrum can be simulated using the same spin Hamiltonian model as used for the X- and Q-band spectra, see above and the Theory section (Table 2). The parameter set employed to simulate the high-field spectrum was fixed such that the exchange and zero-field splitting parameters as determined for the X- and Q-band simulations were kept constant. Two fitting procedures were then employed: (i) the molecular frame of the tyrosyl radical was assumed to be collinear with the axis system of the spin Hamiltonian model. The high-field spectrum was then fitted by varying the **g**-tensor components of the tyrosyl radical (G_X, G_Y, G_Z); and (ii) the molecular **g**-tensor components (g_x, g_y, g_z) along g_y and g_z were fixed to values typically seen for tyrosyl radicals i.e. $g_y = 2.0045$, $g_z = 2.0022$ (see Supporting Information Table S2). The high-field spectrum was then fitted by varying the value of g_x and the orientation of the molecular frame relative to the axis system of the spin Hamiltonian model (α,β). As the spin Hamiltonian model assigns only one principal axis (*X*), which is aligned along the Mn−Tyr interspin vector, only two rotations are required to map the molecular frame to the model's axis system. The third Euler rotation is undefined in the model presented. Both of the two fitting procedures ((i) and (ii)) have the same number of free variables, i.e. 3.

The simulation ($Mn^{III}Mn^{III}$) assuming a collinear molecular frame for the tyrosyl radical (procedure (i)) is shown in Figure 11 (red trace). The obtained **g**-tensor components [G_X, G_Y, G_Z] for the $S = {}^1/_2$ radical are: $G_X = 2.0046$, $G_Y = 2.0077$, and $G_Z = 2.0028$, which are similar to those seen for tyrosyl radicals. (see Supporting Information Table S2, reproduced from[54]). The largest deviation is seen for the G_Z component. The g_z principal component, in the molecular frame of a tyrosyl radical, is along the p_z (π) orbitals of the aromatic ring of the tyrosyl radical,[55−58] perpendicular to the ring plane. It magnitude is approximately that of the free electron (2.0023). The observed difference between this value and the measured one demonstrates that the molecular **g**-tensor of the tyrosyl radical and the coordinate system of the model are not exactly collinear. A similar simulation assuming a $Mn^{IV}Mn^{IV}$ dimer gives an axial **g**-tensor [G_X, G_Y, G_Z] of $G_X = 2.0052$, $G_Y = 2.0032$, and $G_Z = 2.0060$, significantly different from that typically seen for a tyrosyl radical (not shown).

The simulation ($Mn^{III}Mn^{III}$) assuming typical tyrosyl **g**-tensor components (procedure (ii)) is shown in Figure 11 (blue trace). The obtained g_x was 2.0085 and the α and β rotations were 67° and 30°, respectively. The g_x component typically has values of 2.006−2.009 (see Supporting Information Table S2, reproduced from[54]). Unlike g_y and g_z, g_x is highly sensitive to the hydrogen bonding environment of the tyrosyl radical. A large g_x value indicates the phenolic oxygen is deprotonated.[55−58] Thus, the simulation suggests that the tyrosyl radical of *C. ammoniagenes* is deprotonated and probably only weakly hydrogen bonded.[55−58] A similar simulation, assuming a $Mn^{IV}Mn^{IV}$ dimer and typical tyrosyl g-tensor components (procedure (ii)), can not reproduce the three main turning points seen in the high-field spectrum (not shown).

As stated in the Theory and Results sections above, one of the principal axes of the spin Hamiltonian model can be deduced from the traceless (dipolar, $\mathbf{d}_{dip}$) component of the coupling tensor $\mathbf{J}_{int}$. As the largest tensor component of $\mathbf{d}_{dip}$ is d_{dipX} the X-/Q-band simulations assign the inter-Mn−tyrosyl vector along the *X*-axis of the spin-system model. The molecular g-tensor axes for a tyrosyl radical are aligned such that, g_x is along the C−O bond, g_y bisects the ring plane, perpendicular to the C−O bond and g_z is perpendicular to the ring plane. The relative orientation of the molecular axis of the tyrosyl radical (*x*,*y*,*z*) to the coordinate system used for the spin Hamiltonian model (*X*,*Y*,*Z*), as determined by fitting procedure (ii) is shown in Figure 12A in the g_x/g_y and g_x/g_z planes. The α angle corresponds to a rotation about the molecular g_z axis, i.e. it corresponds to a rotation of the tyrosyl ring plane. The β angle corresponds to a rotation about the molecular g_y axis, i.e. it corresponds to a rotation out of the ring plane of the tyrosyl.

The molecular **g**-tensor arrangement as described above compares favorably with the crystal structure. A mapping of

(54) Schünemann, V.; Lendzian, F.; Jung, C.; Contzen, J.; Barra, A.-L.; Sligar, S. G.; Trautwein, A. X. *J. Biol. Chem.* **2004**, *279*, 10919–10930.
(55) Gerfen, G. J.; Bellew, B. F.; Un, S.; Bollinger, J. M.; Stubbe, J.; Griffin, R. G.; Singel, D. J. *J. Am. Chem. Soc.* **1993**, *115*, 6420–6421.
(56) Un, S.; Gerez, C.; Elleingand, E.; Fontecave, M. *J. Am. Chem. Soc.* **2001**, *123*, 3048–3054.
(57) Faller, P.; Goussias, C.; Rutherford, A. W.; Un, S. *Proc. Natl. Acad. Sci. U.S.A.* **2003**, *100*, 8732–8735.
(58) Biglino, D.; Schmidt, P. P.; Reijerse, E. J.; Lubitz, W. *Phys. Chem. Chem. Phys.* **2006**, *8*, 58–62.

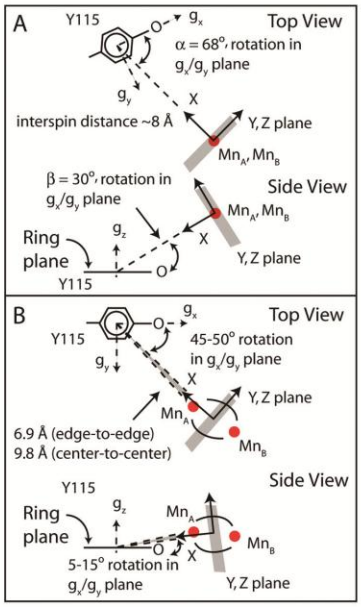

Figure 12. (Panel A) The orientation of the tyrosyl radical (Y115) relative to the Mn dimer, as determined by the multifrequency EPR simulation (assuming a $Mn^{III}Mn^{III}$ dimer). (Panel B) The orientation of the tyrosyl radical (Y115) relative to the Mn dimer as seen in the crystal structure. The coordinate system (*X*,*Y*,*Z*) of the simulation is marked along with the intrinsic g-tensor of the tyrosyl radical (*x*,*y*,*z*). The *X* direction is along the interspin vector connecting the Mn dimer to the tyrosyl radical, the *Y*, *Z* directions are not explicitly assigned, they define a plane perpendicular to *X*.

the (*X*,*Y*,*Z*) coordinate system of the spin Hamiltonian model, onto the molecular (*x*,*y*,*z*) coordinate system of the tyrosyl radical using the crystal structure is shown in Figure 12B in the g_x/g_y and g_x/g_z planes. As expected from the EPR simulations, the principal axis system of the tyrosyl radical **g**-tensor (*x*, *y*, *z*), which is assumed to be collinear with the molecular axes of Y115, is not collinear with the axis system (*X*, *Y*, *Z*) of our spin Hamiltonian model. The crystal structure predicts the ring plane of the tyrosine is rotated 45−50° and is tilted 5−15° out of the plane (about the g_y axis). The variation in the angles reported comes from the degree of uncertainty in assigning the interspin vector. The two limits given refer to the interspin vector assigned such that it connects the center of the tyrosyl ring with Mn_A or the center of the tyrosyl to the midpoint of the Mn−Mn separation. These two rotations are similar to those predicted by the EPR simulation; each differs by ~20°. It is not clear at present whether this discrepancy is reporting a real structural difference between the crystallized metalloradical cofactor and the solution sample used for EPR or arises from the many simplifications used to model the system, i.e. collinear axes of the two Mn ions, an average Mn−tyrosine exchange tensor, etc. It is noted that during the crystallization procedure, the tyrosyl radical almost completely decays. Thus, the difference in the orientation of the tyrosyl radical may report on a change in the hydrogen-bonding network upon formation of the tyrosyl radical. This would suggest that tyrosyl radical generation is coupled to proton movement. This phenomenon has been observed for other redox active tyrosines, e.g. tyrosine Z of the D1 protein of PS II.[57] Further experiments are planned on single crystals of the R2F subunit to resolve this question.

5. Discussion

The experimental results and theoretical modeling shown above demonstrate that the dominant *in vivo* form of the native metalloradical cofactor of the R2F subunit of *C. ammoniagenes* RNR contains only Mn. This is in contrast to a newly discovered class of RNR, isolated from *Chlamydia trachomatis*, which contains a Mn−Fe metallocofactor and harbors phenylalanine in the place of tyrosine[7−10] i.e. it lacks a tyrosyl radical. The metalloradical cofactor of *C. ammoniagenes* instead contains a μ-oxo-Mn−Mn complex, analogous to the diferric metallocofactor seen in the R2 subunit of class Ia RNRs. The oxidation state of the metal site and possible mechanism of radical generation of this new, active Mn-R2F subunit is discussed below.

5.1. Comparison to Split Radical Signals Found in the Literature. The metalloradical cofactor of R2F displays a coupled radical signal or 'split signal'. These types of signals have previously been observed in other biological systems with redox active tyrosine residues, in particular in PS II.[59−62] Here the isolated tyrosyl radical, typically of width ~3 mT (full width half-maximum), is broadened by its weak interaction with a paramagnetic center, the oxygen evolving complex (OEC), a tetra-manganese cofactor located approximately ~7 Å away. In a similar fashion, the tyrosyl radical of the R2F subunit, is broaden by its interaction with a Mn−Mn dimer that is approximately ~8 Å away from the radical, (see Results 4.2 above). It is also noted that the 'split-tyrosyl radical' signal seen in PS II collapses at temperatures above ~90 K, i.e. the resolved 'splitting' (<10 mT peak-to-peak separation) seen at 5 K is lost upon warming to 90 K, where an unperturbed tyrosyl radical signal is then resolved.[63,64] This is nominally the same phenomenon as that observed for Mn-R2F (see Figure 8) and is the result of exchange narrowing.[46,65,66] At higher temperatures, the distinct 'split-tyrosyl radical' transitions of the spin manifold, which correspond to each line of the split signal pattern, interchange at frequencies exceeding the energy-level separation. Under these conditions a single average transition is observed, whose exact line shape depends upon the interchange frequencies within the spin manifold. The line shape of such signals appears as a broadened Lorentzian line.[66] The same line shape is observed at 77 K for the tyrosyl in Mn-R2F confirming that this signal is indeed an exchange narrowed species (Figure 8, traces A and B).

A similar coupled radical signal is observed for the metalloradical cofactor of the R2F subunit of *C. glutamicum*.[29]

(59) Koulougliotis, D.; Teutloff, C.; Sanakis, Y.; Lubitz, W.; Petrouleas, V. *Phys. Chem. Chem. Phys.* **2004**, *6*, 4859–4863.
(60) Havelius, K. G. V.; Su, J.-H.; Feyziyev, Y.; Mamedov, F.; Styring, S. *Biochemistry* **2006**, *45*, 9279–9290.
(61) Su, J. H.; Havelius, K. G. V.; Ho, F. M.; Han, G.; Mamedov, F.; Styring, S. *Biochemistry* **2007**, *46*, 10703–10712.
(62) Cox, N.; Ho, F. M.; Pewnim, N.; Steffen, R.; Smith, P. J.; Havelius, K. G. V.; Hughes, J. L.; Debono, L.; Styring, S.; Krausz, E.; Pace, R. J. *Biochim. Biophys. Acta* **2009**, *1787*, 882–889.
(63) Ioannidis, N.; Zahariou, G.; Petrouleas, V. *Biochemistry* **2008**, *47*, 6292–6300.
(64) Zahariou, G.; Ioannidis, N.; Sioros, G.; Petrouleas, V. *Biochemistry* **2007**, *46*, 14335–14341.
(65) Abragram, A.; Bleaney, B. *Electron Paramagnetic Resonance of Transition Metal Ions*; Clarendon Press: Oxford, 1970.
(66) Pake, G. E.; Estle, T. L. *The Physical Principles of Electron Paramagnetic Resonance*, 2nd ed.; Benjamin: Reading, MA, 1973.

However, the split-tyrosyl radical signal seen at X-band for this species is approximately half the spectral width seen in this study. This result is unusual considering the substantial sequence homology of the nrdF gene sourced from the two species. While we have not attempted a robust fitting of these spectra, we are confident that the spectra of *C. glutamicum* can be simulated using an identical spin Hamiltonian model presented in this work. The key difference between the two species could be the sign of the exchange interaction between the two Mn^{III} centers. For *C. ammoniagenes* the coupling between the two Mn centers is weakly ferromagnetic whereas the coupling between the two Mn centers of *C. glutamicum* is suspected to be weakly antiferromagnetic. This would redistribute the signal intensities of individual peaks in the split pattern. As the ground state for *C. glutamicum* is $S = 0$, the central line(s) of the split pattern ($g \approx 2$) appears more intense at low temperatures as compared to the wings of the split signal. Thus the split tyrosyl radical signal seen in *C. glutamicum* at low temperature (10 K)[29] should resemble the higher temperature spectra ($\geq$30 K) seen for *C. ammoniagenes* (Figure 9). It is noted that that the exchange coupling observed for metal dimer complexes, with virtually the same ligand sphere, is usually the same. However, a characteristic feature of the model $Mn^{III}Mn^{III}$ complexes of the type that match the structure of the metallocofactor of R2F (see next section) is the large variation in the Mn−Mn coupling between the two Mn centers. The magnetic coupling between the two Mn centers ranges from strongly antiferromagnetic (-100 cm^{-1}) to weakly ferromagnetic (10 cm^{-1}). Thus small perturbations in the ligand environment of the metallocofactor could dramatically change the Mn−Mn coupling and as a consequence, the observed split tyrosyl radical signal.

5.2. Oxidation State of the Metalloradical Cofactor: A $Mn^{III}Mn^{III}$ Dimer. The oxidation states of the two Mn centers can be deduced from a concomitant analysis of our EPR and crystallographic results. In particular, the structure of the 'split-tyrosyl radical' signal observed at X- and Q-band frequencies, reports on the energy levels of the Mn−Mn dimer system and thus the oxidation state of the two metal centers. The only oxidation states of the two Mn centers that are considered plausible are: Mn^{II}, Mn^{III} and Mn^{IV}. This allows for 5 possible Mn oxidation state configurations. Of these only the $Mn^{III}Mn^{III}$ oxidation state configuration is consistent with all crystallographic and EPR data. The arguments leading to this conclusion are as follows:

(i) The crystallographic data disfavor the $Mn^{II}Mn^{II}$ configuration. Earlier inactive structures in both *C. ammoniagenes* and *E. coli*,[26,50] which contained a $Mn^{II}Mn^{II}$ dimer, are structurally dissimilar to the metalloradical cofactor structure seen here. The active form contains an oxo/hydroxo-bridged Mn motif that is absent in the reduced ($Mn^{II}Mn^{II}$) structures. In addition, the bridging ligands between the two Mn centers resemble structural motifs of model complexes that contain at least one Mn center with oxidation number higher than two. The $Mn^{II}Mn^{II}$ oxidation state also does not provide a mechanism for radical formation.

(ii) The mixed valence $Mn^{II}Mn^{III}$ and $Mn^{III}Mn^{IV}$ configurations cannot readily explain the structure of the 'split tyrosyl radical' signal at X- or Q-band. Their spin manifolds only contain paramagnetic sublevels. As a consequence, a fitted exchange interaction between the Mn cluster and the tyrosyl radical cannot simultaneously explain both the unperturbed central line ($g \approx 2.00$) and the total width of the split signal (see Theory, and ref 52). It is also noted that mixed valence oxo/carboxylato bridged $Mn^{III}Mn^{IV}$ dimers exhibit antiferromagnetic exchange coupling of the order of about -100 cm^{-1} (refs 67−70 and references therein). Similarly, the crystallographic study of Högbom et al.[71] disfavors assigning the oxidation state of the metallocofactor to $Mn^{III}Mn^{II}$. In this earlier work, a purified apo-R2 subunit (*E. coli*) was loaded with Mn^{II} and oxidized to the $Mn^{II}Mn^{III}$ state via the exogenous addition of H_2O_2. This earlier structure is significantly different from the metallocofactor seen in R2F from *C. ammoniagenes* although the two metals have virtually the same co-ordination environment. In particular: (a) the Mn−Mn distance of 3.4 Å is 0.1 Å longer for the $Mn^{II}Mn^{III}$ dimer as compared to the Mn dimer seen in the R2F subunit; and (b) the Mn dimer lacks a μ-oxo bridge. The oxygen ligand to Mn_B is assigned as a monodentate water ligand. The bridging unit instead involves one of the terminal oxygens of a nearby glutamate residue. Thus, a $Mn^{II}Mn^{III}$ dimer as described by Högbom et al.[71] lies between the reduced $Mn^{II}Mn^{II}$ (Figure 6C) and the putative $Mn^{III}Mn^{III}$ structures (Figure 6B).

(iii) The $Mn^{IV}Mn^{IV}$ configuration is a plausible model based on the simple arguments above. However it does not as readily explain the structure or the temperature dependence of the 'split-tyrosyl radical' signal as do the $Mn^{III}Mn^{III}$ simulations (see Figures 9 and 10). It is noted that a $Mn^{IV}Mn^{IV}$ metallocofactor cannot be excluded based solely on the structural data presented. Some synthetic $Mn^{IV}Mn^{IV}$ analogues are likely to exhibit the same structural properties observed here for the metalloradical cofactor of R2F. Structural data have been reported for bis-μ-oxo-$Mn^{IV}Mn^{IV}$ complexes.[68] They generally have short Mn−Mn distances (2.5−2.9 Å), Mn−O−Mn bond angles between 91−102° and are strongly antiferromagnetically coupled (about -100 cm^{-1}) (ref 68 and references therein). A closer structural mimic of the metallocofactor of R2F lacks one of the μ-oxo linkages and instead has a carboxylato bridge. Unfortunately, there are no crystallographic data for μ-oxo-(mono/bis)μ-carboxylato $Mn^{IV}Mn^{IV}$ complexes in the current literature. However, it is noted though that $Mn^{III}Mn^{IV}$ to $Mn^{IV}Mn^{IV}$ conversion is electrochemically reversible for this structural motif,[67] suggesting the ligand environment is nominally the same for both oxidation states. An example of this μ-oxo-(mono/bis)μ-carboxylato $Mn^{III}Mn^{IV}$ complex is $LMn^{III}(\mu\text{-O})(\mu\text{-}CH_3CO_2)_2Mn^{IV}$ (L = *N*,*N*′,*N*″-trimethyl-1,4,7-triazacyclononane).[72] It has a Mn−Mn separation of ~3.2 Å, Mn−O bond length of ~1.8−1.9 Å and Mn−O−Mn bond length of ~120°. These bond lengths are approximately those seen for the metallocofactor of R2F (see results) albeit slightly shorter.

(iv) In contrast, the $Mn^{III}Mn^{III}$ configuration is consistent with all crystallographic and spectroscopic data. The best mimic of the Mn core structure seen in R2F are μ-oxo-(mono/bis)μ-carboxylato $Mn^{III}Mn^{III}$ complexes, which share the same structural and physical characteristics (ref 68 and references

(67) Wieghardt, K.; Bossek, U.; Nuber, B.; Weiss, J.; Bonvoisin, J.; Corbella, M.; Vitols, S. E.; Girerd, J. J. *J. Am. Chem. Soc.* **1988**, *110*, 7398–7411.
(68) Mukhopadhyay, S.; Mandal, S. K.; Bhaduri, S.; Armstrong, W. H. *Chem. Rev.* **2004**, *104*, 3981–4026.
(69) Schäfer, K. O.; Bittl, R.; Lendzian, F.; Barynin, V.; Weyhermüller, T.; Wieghardt, K.; Lubitz, W. *J. Phys. Chem. B* **2003**, *107*, 1242–1250.
(70) Schäfer, K.-O.; Bittl, R.; Zweygart, W.; Lendzian, F.; Haselhorst, G.; Weyhermüller, T.; Wieghardt, K.; Lubitz, W. *J. Am. Chem. Soc.* **1998**, *120*, 13104–13120.
(71) Högbom, M.; Andersson, M. E.; Nordlund, P. *J. Biol. Inorg. Chem.* **2001**, *6*, 315–323.
(72) Wieghardt, K.; Bossek, U.; Bonvoisin, J.; Beauvillain, P.; Girerd, J. J.; Nuber, B.; Weiss, J.; Heinze, J. *Angew. Chem., Int. Ed. Engl.* **1986**, *25*, 1030–1031.

therein). They generally have Mn−Mn distances of ~3.3 Å, Mn−O−Mn bond angles between 120−125° and exhibit weak Mn−Mn couplings (<10 cm^{-1}), favoring the ferromagnetic regime.[68] These values closely match the crystallographic data and fitted Mn−Mn exchange coupling seen for the R2F metalloradical cofactor of *C. ammoniagenes* studied here: The Mn−Mn distance of the metalloradical cofactor is 3.3 Å, the Mn−O−Mn bond angle is ~120° and the estimated exchange coupling is ~1 cm^{-1}.

It is noted that other synthetic $Mn^{III}Mn^{III}$ complexes involving biologically relevant ligands, do not in general show the same structural features.[68] The Mn−Mn coupling is strongly influenced by the bridging ligands between the two Mn ions. Both ferromagnetic and antiferromagnetic pathways exist in μ-oxo-bridged Mn complexes and the net coupling observed is dominantly dependent on the Mn−O−Mn bond angle (for full discussion see[67,73]). Bis-μ-oxo-$Mn^{III}Mn^{III}$ complexes typically have a Mn−Mn distance of ~2.7 Å, Mn−O−Mn bond angles of 92−95° and show strong antiferromagnetic coupling (−100 cm^{-1}) (ref 68 and references therein). Similarly, linear (~180°) Mn−O−Mn bridged complexes [$Mn_2O(5\text{-}NO_2saldien)_2$, etc], have a longer Mn−Mn distance (~3.5 Å) and display large antiferromagnetic coupling between the two Mn centers (J = −120 cm^{-1}).[74] The μ-oxo-(mono/bis)μ-carboxylato $Mn^{III}Mn^{III}$ complexes, as seen in R2F, represent a midpoint between these two limiting regimes. As the Mn−Mn bond length and Mn−O−Mn bond angle, seen for the bis-μ-oxo complexes increases, the ferromagnetic coupling between the two Mn increases to the extent that it approaches or becomes comparable to the antiferromagnetic pathway. It is in this range that the μ-oxo-(mono/bis)μ-carboxylato $Mn^{III}Mn^{III}$ complexes are found (see[67,73]). A further increase in the Mn−Mn distance and bond angle then reduced the ferromagnetic pathway contribution such that linear complexes exhibits similar properties that were seen for the bis-μ-oxo complexes. The balancing of the ferromagnetic and antiferromagnetic bonding pathways seen for μ-oxo-(mono/bis)μ-carboxylato $Mn^{III}Mn^{III}$ complexes should tune the redox chemistry. This could potentially stabilize the tyrosyl radical of the metalloradical cofactor, or alter the chemistry of higher valence states that would be involved in cofactor assembly.

Earlier ICP-MS and X-/Q-band EPR measurements had suggested that the metal site may contain a mononuclear Mn^{II} cluster.[25] Within the model presented in the current study, a Mn^{II} signal is probably reporting on a subfraction of R2F subunits that: (i) did not fully assembly an active metalloradical ($Mn^{III}Mn^{III}$) complex, the metal site may contain either one or two bound Mn^{II}; or (ii) contain nonspecifically bound Mn^{II} attached to the protein surface. As Mn^{II} ($S = {}^5/_2$) is a d^5 metal ion, it typically displays small zero-field splitting (a few 100 MHz) in ligand environments found in biological systems. As a consequence, it often appears as a structured signal, with six sharp lines separated by ~8 mT, centered at $g \approx 2$. These properties make it readily detectable using EPR. Thus only a small concentration of Mn^{II} needs to be present to observe a large signal.

The $Mn^{III}Mn^{III}$ (quenched radical) state of the R2F subunit, unlike Mn^{II}, is likely to be either invisible at low microwave frequencies (X- or Q-band) or sufficiently broad such that it would be difficult to identify outside of instrumental drift. The calculated simulation parameters for the fine structure tensors of both Mn are large ($D \approx 0.5$ cm^{-1}, $E/D > 0.1$), i.e. of the order of the microwave quanta at X and Q-band. No EPR signal would be expected to be observed using either perpendicular or parallel microwave polarizations for a $Mn^{III}Mn^{III}$ species using this parameter set. Thus we only observe the Mn dimer signal via its coupling with the tyrosine radical. It is also noted that as the coupling between the tyrosyl radical and $Mn^{III}Mn^{III}$ dimer is small, the 'metal signal', transitions that are dominantly Mn in character, should be approximately the same regardless of whether it is coupled to the tyrosyl radical or not.

5.3. Structural Similarities of RNR from *C. ammoniagenes* and *E. coli* (classes Ia and Ib). The Mn metalloradical cofactor of the R2F subunit obtained from *C. ammoniagenes* bears a strong resemblance to the corresponding diferric complex seen in class Ia RNR of *E. coli* (Fe-R2); the only obvious difference is that nature has chosen a different metal for the same catalytic function. The evidence for this is 4-fold: i) Earlier work, using UV/vis absorption spectroscopy, demonstrated that a tyrosyl radical is observed in *C. ammoniagenes*[28,75] and sequence alignment suggest that the tyrosine Y115 of the *C. ammoniagenes* NrdF[16] corresponds to the Y122 harboring the organic radical in *E. coli* Fe-R2[2]. ii) The crystal structure of the Mn containing, metalloradical cofactor is highly similar to the metal site of *E. coli* Fe-R2. The metal−metal distance is the same, the ligand field is virtually identical, and the tyrosine is nominally in the same position in both R2F subunits. Importantly, the structure shows that the two Mn centers of *C. ammoniagenes* are bridged by nonresidue derived oxygen(s), as seen for the Fe-R2 subunit of *E. coli*, which is known in the latter to form from the reaction of the reduced ferrous complex ($Fe^{II}Fe^{II}$) with O_2.[76] iii) Multifrequency EPR measurements and modeling demonstrate the R2F subunit contains a stable redox active tyrosyl, located near (~8 Å) an exchange coupled Mn dimer and support the assignment of the oxidation state of this dimer to $Mn^{III}Mn^{III}$, the same that is seen for the Fe-R2 subunit (active/met state) of *E. coli* ($Fe^{III}Fe^{III}Y^{\bullet}$).[2,5,76] It is noted that the two Fe^{III} centers of the Fe-R2 metalloradical cofactor are strongly antiferromagnetically coupled. The ground state of the $Fe^{III}Fe^{III}$ spin manifold is diamagnetic ($S = 0$) and thus an unperturbed tyrosyl radical signal is observed albeit with altered relaxation properties. The $Mn^{III}Mn^{III}Y^{\bullet}$ metalloradical cofactor signal is unique with regard to the field of RNR research to date.

5.4. Manganese and Iron Chemistry in Enzymatic Function. Several enzymes have been identified that use Fe or Mn interchangeably. In particular the oxidoreductase enzyme, superoxide dismutase (SOD), which catalyzes the dismutation of superoxide to O_2 and hydrogen peroxide, has evolved both monomeric Fe and Mn forms.[77] The catalytic site of these enzymes, regardless of the identity of the metal, contains a metal center ligated by three histidine residues and an asparate residue and this metallocofactor passes through the same redox states during its catalytic cycle.

(73) Hotzelmann, R.; Wieghardt, K.; Floerke, U.; Haupt, H. J.; Weatherburn, D. C.; Bonvoisin, J.; Blondin, G.; Girerd, J. J. *J. Am. Chem. Soc.* **1992**, *114*, 1681–1696.
(74) Kipke, C. A.; Scott, M. J.; Gohdes, J. W.; Armstrong, W. H. *Inorg. Chem.* **1990**, *29*, 2193–2194.
(75) Barckhausen, O. Doctoral Thesis, Universität Hannover, 2004.
(76) Atkin, C. L.; Thelander, L.; Reichard, P.; Lang, G. *J. Biol. Chem.* **1973**, *248*, 7464–7472.
(77) Meier, B.; Barra, D.; Bossa, F.; Calabrese, L.; Rotilio, G. *J. Biol. Chem.* **1982**, *257*, 13977–13980.

$$M^{III} - SOD + O_2^{\bullet -} \rightarrow M^{II} - SOD + O_2$$
$$M^{II} - SOD + O_2^{\bullet -} + 2H^+ \rightarrow M^{III} - SOD + H_2O_2$$

where M = Fe or Mn.

Another example of Fe and Mn cofactors that facilitate the same catalytic reaction are those found in the catalase enzymes, which catalyze the dismutation of hydrogen peroxide (H_2O_2) to O_2 and H_2O. Nature has independently evolved two types of catalases that contain either a heme Fe[78] or a dinuclear Mn cofactor.[36] It is thus not surprising that the same metal variation is seen in RNR.

Metalloradical cofactor formation in Fe containing class Ia RNR occurs via the reduction of O_2 and is thought to involve a peroxo-bridged di-iron intermediate with maximum oxidation state (Fe^{IV}).[79,80] A dimanganese complex should be able to move through a similar redox pathway. However, the $Mn^{II}Mn^{II}$ complex is unlikely to react with O_2 directly. The isolated apo-R2F protein sourced from *C. ammoniagenes* cannot be reactivated using Mn in the presence of O_2; while the protein binds Mn^{II}, no subsequent redox reaction takes place i.e. a tyrosyl radical is not observed.[26,50] Interestingly, the hydroxyrea quenched R2F protein can be reactivated by the addition of H_2O_2 (and a mediator), see Results 4.1. In this reaction the quenched Mn-cofactor, presumably ($Mn^{III}Mn^{III}Y$) is oxidized to a higher valence state ($Mn^{III}Mn^{IV}$, $Mn^{IV}Mn^{IV}$) both of which are of sufficient potential to oxidize the nearby Y115. It is presently not clear if the same conditions, the addition of H_2O_2 etc., can be used to reactivate the apo-R2F protein in the presence of Mn. This would require a precursory step, the oxidation of the bound $Mn^{II}Mn^{II}$ state to $Mn^{III}Mn^{III}$ as seen for the manganese catalase, which contains a $Mn^{II}Mn^{II}$ cofactor in its reduced state. Our reactivation result is similar to recent observations of Cotruvo and Stubbe,[32] performed *in vitro* using *E. coli* class Ib. They have identified an unusual flavodoxin (NrdI) that may be involved in metalloradical cofactor biosynthesis. They suggest its function may resemble that of flavoprotein oxidases, which catalyze H_2O_2 production from O_2 and thus supply the reduced metallocofactor with peroxide species *in vivo* (H_2O_2, HO_2^- etc).[32] The same subunit (NrdI) has also been identified in *C. ammoniagenes*, and may be common to all class Ib RNRs.[32]

5.5. Proposal for the Mechanism for the Metalloradical Cofactor ($Mn^{III}Mn^{III}Y^{\bullet}$) Generation. A possible mechanistic pathway for Mn metalloradical cofactor assembly has been proposed by Cotruvo and Stubbe[32] and involves two discrete oxidation steps using H_2O_2/HO_2^-.[81] The first step oxidizes the $Mn^{II}Mn^{II}$ dimer to $Mn^{III}Mn^{III}$ and resembles initially the Mn catalase H_2O_2 dismutation reaction mechanism.[34–36] The second step generates the 'intermediate X', a di-μ-oxo-bridged $Mn^{III}Mn^{IV}$ or $Mn^{IV}Mn^{IV}$ dimer,[82,83] with sufficient oxidizing power to extract an electron from the tyrosine Y115, as seen in

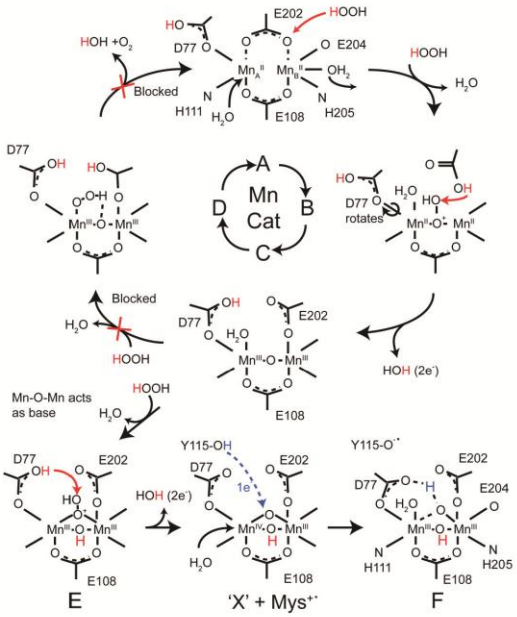

Figure 13. Proposed assembly pathway of the dimanganese metalloradical cofactor of R2F obtained from *C. ammoniagenes*. Structures A, B, C, and D correspond to the catalytic steps of the Mn-catalase H_2O_2 dismutation reaction. Structures E, X and F, correspond to the alternate pathway used to assemble the reactive 'intermediate X' that has a sufficient oxidizing potential to extract an electron from Y115. Pathway selectivity is governed by rotation of a glutamate residue (E202) that acts as an intermolecular base. Red denotes H_2O_2 proton movement; blue denotes Y115−H proton movement. For details see text.

di-iron class Ia type RNRs.[79,80] Our crystallographic and EPR data are broadly consistent with this reaction pathway and provides further details as to how protein conformational changes at the dimetal site direct the reaction mechanism, disfavoring alternate pathways i.e. H_2O_2 dismutation. Pathway selectivity appears to be governed by two carboxylate residues, the glutamate E202 and the aspartate D77.

It is first noted that the reduced ($Mn^{II}Mn^{II}$) R2F subunit of *C ammoniagenes* and of *E. coli* (Ib) is very similar to that of Mn catalase (Mn-Cat).[36] The ligand field of the two Mn centers in Mn-Cat contains only glutamates and histidines. An important structural feature is a glutamate residue that acts as an intermolecular base. An analogous glutamate residue (E202) is present in the reduced Mn-R2F metallocofactor; it caps the dimanganese cluster (Figure 6C, Figure 13A). The proposed reaction pathway for metalloradical cofactor assembly initially proceeds along the same mechanism as Mn-Cat (Figure 13A-C). H_2O_2 displaces a water ligand at the distal Mn (to the tyrosine Y115, Mn_B) forming a bridging hydroxoperoxide between the two Mn ions and protonating the E202. Subsequent protonation of the bridging peroxide species leads to two electron oxidation of the $Mn^{II}Mn^{II}$ complex and water release and results in a μ-oxo-bridged $Mn^{III}Mn^{III}$ complex termed here intermediate C (Figure 13C).

(78) Vainshtein, B. K.; Melik-Adamyan, W. R.; Barynin, V. V.; Vagin, A. A.; Grebenko, A. I.; Borisov, V. V.; Bartels, K. S.; Fita, I.; Rossmann, M. G. *J. Mol. Biol.* **1986**, *188*, 49–61.
(79) Burdi, D.; Willems, J.-P.; Riggs-Gelasco, P.; Antholine, W. E.; Stubbe, J.; Hoffman, B. M. *J. Am. Chem. Soc.* **1998**, *120*, 12910–12919.
(80) Willems, J.-P.; Lee, H.-I.; Burdi, D.; Doan, P. E.; Stubbe, J.; Hoffman, B. M. *J. Am. Chem. Soc.* **1997**, *119*, 9816–9824.
(81) Cotruvo and Stubbe suggest the likely oxidant for cofactor assembly is HO_2^- instead of H_2O_2. In the discussion of the metalloradical cofactor assembly we do not distinguish between the two species, all mechanistic arguments are equally valid for either reactive oxygen species.
(82) Sheats, J. E.; Czernuszewicz, R. S.; Dismukes, G. C.; Rheingold, A. L.; Petrouleas, V.; Stubbe, J.; Armstrong, W. H.; Beer, R. H.; Lippard, S. J. *J. Am. Chem. Soc.* **1987**, *109*, 1435–1444.
(83) Wieghardt, K.; Bossek, U.; Ventur, D.; Weiss, J. *J. Chem. Soc., Chem. Commun.* **1985**, 347–349.

If we assume the crystal structure of the metalloradical cofactor ($Mn^{III}Mn^{III}Y^{\bullet}$, Figure 6B) bears a resemblance to intermediate C (Figure 13C), we would suspect two important structural changes have occurred in the surrounding protein matrix: (i) the E202 has been displaced as a bridging bidentate ligand. It now appears as a monodentate carboxylate bound to the distal manganese Mn_B, with 4 Å separation to the proximal Mn_A; and (ii) the D77 has rotated ~180°, bringing its second oxygen into close proximity to the bridging Mn−O−Mn motif (Figure 13C).

The second H_2O_2 is thought to displace a water ligand at an open coordination site on the proximal Mn (Mn_A) as opposed to Mn_B. At this stage in the reaction pathway, E202 can no longer act as a base; it is too far away from the bridging peroxide (Figure 13D). This then prevents the completion of the dismutation cycle, trapping the high valence ($Mn^{III}Mn^{III}$) state. It is instead proposed that the μ-oxo-bridge acts as the proton acceptor (Figure 13E). While the basicity of μ-oxo-bridges between electron-withdrawing Mn ions is likely to be small, it could still act in this manner if we consider that the peroxide species is also ligated to the same metal center. Subsequent protonation of the bridging hydroxoperoxide leads to a second two-electron oxidation and water release (Figure 13X). The resulting $Mn^{IV}Mn^{IV}$ species may only form transiently and rapidly decay to a more stable $Mn^{III}Mn^{IV}$ species by oxidizing a nearby residue as is seen in class I Fe-R2 sourced *E. coli*. In this case, a nearby tryptophan radical is transiently formed during metalloradical cofactor synthesis.[84,85] A tryptophan residue has been identified in R2F from *C. ammoniagenes* in a similar structural position. In our preliminary reactivation experiments, it is suggested that the mediator methyl viologen possibly acts as a one-electron reductant. Regardless, a $Mn^{IV}Mn^{IV}$ or $Mn^{III}Mn^{IV}$ dimer (intermediate X) is of sufficient oxidizing potential to extract an electron from the tyrosine Y115, thus yielding the $Mn^{III}Mn^{III}Y^{\bullet}$ metalloradical cofactor (Figure 13F). It is noted that electron extraction from Y115 may be coupled to proton movement; our EPR measurements are consistent with the Y115 being deprotonated. The tyrosyl radical $Y115\text{-}OH^{+\bullet}$ may protonate the nearby D77, which could in turn participate in a hydrogen-bonding network around the Mn dimer (i.e. with D77). The lengths of the O bridges of the Mn dimer core are more consistent with hydroxo ligands with one bridging the two Mn centers, while the other forms a more asymmetric bridging unit, hydrogen bonded to the nearby D77 residue.

The same organization of residues about the metallocofactor, in particular D77, is not seen for R2F with an assembled $Fe^{III}Fe^{III}$ core in *C. ammoniagenes*.[26] This is perhaps not surprising as the mechanism of complex formation differs; the Fe dimer is assumed to move through an Fe−O−O−Fe peroxide intermediate[86] as opposed to the μ-oxo-bridged Mn dimer proposed above. The D77 residue, as suggested in our reaction mechanism (see above), potentially participates in a concerted proton−electron-coupled transfer and as a consequence, is required to be in close proximity to Mn_A. The same role is not suggested for D77 in Fe cofactor assembly. No reorganization of the D77 is required to assemble the Fe−Fe core, and thus D77 appears in approximately the same position in both the reduced $Fe^{II}Fe^{II}$ state and the oxidized (activated) $Fe^{III}Fe^{III}$ state (see Figure 6D).

5.6. Model for the Incorporation of Fe^{2+} into the Metal Binding Site of RNR from *C. ammoniagenes*. It was noted that the Fe-R2F metalloradical cofactor from *C. ammoniagenes* contains a solvent water molecule in close proximity (3.2 Å) to the tyrosine (Y115).[26] This feature is unique to this Fe-R2F subunit; an additional water molecule other than the water/hydroxo ligand to Mn_A^{III}/Fe_A^{III} has not been observed between the tyrosine and the metal dimer in all other oxidized R2/R2F subunits crystallized so far, including the structurally similar *S. typhimurium* (class Ib).[18] This additional solvent water molecule was considered part of the hydrogen-bonding network about the Y115 in Fe-R2F. The same water molecule is not present in the Mn-bound native system. This is due to the rotation of the phenylalanine residue (Phe172), and thus, this structure more closely resembles the typical environment seen for the redox active tyrosine of class I RNRs. Solvent access to the tyrosyl radical may lead to a faster decay of this radical species and, thus, to a decrease in activity when iron is incorporated into R2F from *C. ammoniagenes*. Preliminary results suggest this is the case in *C. ammoniagenes* and forms part of a continuing study. A similar effect is seen in *mouse* RNR. Its metalloradical cofactor site is more open than the corresponding site in *E. coli* RNR.[87] This appears to correlate with a drop in enzyme activity, i.e. radical stability. Thus incorrect metal binding, while causing minimal localized modification of the enzyme, may lead to global changes in how the protein interacts with the surrounding aqueous medium.

6. Conclusion

The multidisciplinary approach adopted in this study demonstrates conclusively that the native RNR enzyme derived from *C. ammoniagenes* predominantly uses Mn for tyrosyl radical generation and supports the assignment of this RNR to class Ib. The crystal structure of the R2F subunit shows that the metalloradical cofactor contains a bridged oxo/hydroxo Mn dimer in close proximity to a tyrosine (Y115) residue. Concomitant multifrequency EPR measurements confirm these findings and show that the R2F subunit contains a stable redox active tyrosyl radical, located near an exchange coupled Mn dimer (~8 Å), and support the assignment of the oxidation state of this dimer to $Mn^{III}Mn^{III}$ [51], the same that is seen for the Fe-R2 subunit (active/met state) of *E. coli*.[2,5,76]

A $Mn^{III}Mn^{III}$ metallocofactor is consistent with data from model Mn dimer complexes. The best mimic of the manganese core structure seen in R2F are μ-oxo-(mono/bis)μ-carboxylato $Mn^{III}Mn^{III}$ complexes, which share the same structural and physical characteristics (ref 68 and references therein). The μ-oxo-(mono/bis)μ-carboxylato $Mn^{III}Mn^{III}$ motif generally displays very small metal−metal exchange couplings. Here the antiferromagnetic and ferromagnetic coupling pathways effectively cancel each other; this structure type results in the minimum coupling seen between the two Mn^{III} centers. It is unclear why an effectively decoupled Mn dimer is required for tyrosyl radical generation or stabilization.

(84) Baldwin, J.; Krebs, C.; Ley, B. A.; Edmondson, D. E.; Huynh, B. H.; Bollinger, J. M. *J. Am. Chem. Soc.* **2000**, *122*, 12195–12206.
(85) Pötsch, S.; Lendzian, F.; Ingemarson, R.; Hörnberg, A.; Thelander, L.; Lubitz, W.; Lassmann, G.; Gräslund, A. *J. Biol. Chem.* **1999**, *274*, 17696–17704.
(86) Yun, D.; Garcia-Serres, R.; Chicalese, B. M.; An, Y. H.; Huynh, B. H.; Bollinger, J. M. *Biochemistry* **2007**, *46*, 1925–1932.
(87) Kauppi, B.; Nielsen, B. B.; Ramaswamy, S.; Larsen, I. K.; Thelander, K.; Thelander, L.; Eklund, H. *J. Mol. Biol.* **1996**, *262*, 706–720.

A mechanistic pathway for Mn metalloradical cofactor formation involving two discrete oxidation steps using H_2O_2/HO_2^- has been proposed. The initial step oxidizes the $Mn^{II}Mn^{II}$ dimer to $Mn^{III}Mn^{III}$ and resembles the first part of the Mn catalase H_2O_2 dismutation reaction mechanism.[34–36] The second step generates the 'intermediate X', a di-μ-oxo-bridged $Mn^{III}Mn^{IV}$ or $Mn^{IV}Mn^{IV}$ dimer, with sufficient oxidizing power to extract an electron from the tyrosine Y115,[82,83] as seen in di-iron class Ia type RNRs.[79,80] A comparison between our crystal structure of the active Mn-R2F subunit and earlier inactive structures that contain a $Mn^{II}Mn^{II}$ dimer provides further details as to how protein conformational changes at the dimetal site direct the reaction mechanism, disfavoring the completion of the H_2O_2 dismutation cycle, and allow the formation of a high-valence Mn state. Pathway selectivity appears to be governed by two carboxylate residues in the first coordination sphere, the glutamate E202 and the aspartate D77.

These new results in *C. ammoniagenes* in conjunction with the recent report of Cotruvo and Stubbe,[32] suggest that a Mn metalloradical cofactor may be ubiquitous in class Ib RNRs. Thus, the structure and mechanism of assembly presented here for the metalloradical cofactor of *C. ammoniagenes* may be representative of the native R2F subunit seem in all class Ib RNRs.

Protein Data Bank Accession Numbers

The coordinates and structure factor have been deposited in the PDB with accession number, 3MJO.

Acknowledgment. We thank Olaf Barckhausen (University of Hannover), Antonio Pierik (University of Marburg), Thomas Weyhermueller (MPI Mülheim), and Gudrun Klihm (MPI Mülheim) for their help and advice during the preparation of this manuscript. We also acknowledge the important contribution of our former colleague Peter Paul Schmidt (MPI Mülheim), who passed away before its completion. We dedicate this manuscript to his memory. We thank the staff of the beamline BL41XU at SPring-8 (Hyogo, Japan) and the beamline BL14.2 at BESSYII (Berlin, Germany) for their assistance during the data collection. This work was supported by the Max-Planck-Gesellschaft.

Supporting Information Available: Additional XRF data, additional X-band and high-field simulations, figures detailing solvent access channels, specific activities of selected RNRs, collated literature **g**-tensor data for tyrosyl radicals, and the complete authors list of ref 30. This material is available free of charge via the Internet at http://pubs.acs.org.

JA1036995

7.5 Publikation IV: Electron Paramagnetic Resonance (EPR) Spectroscopy of the Stable-Free Radical in the Native Metallo-Cofactor of the Manganese-Ribonucleotide Reductase (Mn-RNR) of *Corynebacterium glutamicum*

Eigenanteil:

Die an *C. ammoniagenes* gewonnenen Erkenntnisse wurden auf die Anreicherung einer aktiven R2F-Untereinheit bei einem Wildtyp des Aminosäureproduzenten *C. glutamicum* erfolgreich übertragen. Mit diesem modifizierten Reinigungsschema wurde erstmals homogenes Protein, mit einer im Vergleich zu einer vorhergehenden Dissertation (Abbouni, 1999) 6.000-fachen Steigerung der spezifischen Aktivität, erhalten. Dieses Vorgehen ermöglichte zum ersten Mal, dass spezifische 408 nm Absorptionssignals eines proteingebundenen Tyrosylradikals (Fig. 5) aus einem Wildtyp darzustellen.

Free Radical Research
2009, 1–8, iFirst article

informa
healthcare

Electron paramagnetic resonance (EPR) spectroscopy of the stable-free radical in the native metallo-cofactor of the manganese-ribonucleotide reductase (Mn-RNR) of *Corynebacterium glutamicum*

BOUZIANE ABBOUNI[1,2], WULF OEHLMANN[1], PATRICK STOLLE[1], ANTONIO J. PIERIK[3], & GEORG AULING[1]

[1]*Institut für Mikrobiologie, Leibniz Universität Hannover, Schneiderberg 50, D-30167 Hannover, Germany,* [2]*Université Djillali Liabes, Faculté des Sciences, Département de Biologie, BP 89 Cité Larbi Ben Mhidi, 22000-Sidi Bel Abbes, Algeria, and* [3]*Institut für Zytobiologie, Philipps Universität Marburg, Robert-Koch-Strasse 6, D-35037 Marburg, Germany*

(Received 30 March 2009; revised 20 June 2009)

Abstract
Ribonucleotide reductases (RNR; EC 1.17.4.1) provide the 2′-deoxyribonucleotides for DNA replication of proliferating cells by a uniform radical mechanism using diverse metals. The native metallo-cofactor of the *Corynebacterium glutamicum* RNR contains manganese and is sensitive to EDTA and radical scavengers. Hybrid holoenzymes, capable of ribonucleotide reduction, were composed of the small manganese-containing (R2F) and the large catalytic subunit (R1E) from either of the two corynebacterial RNRs. A synthetic peptide deduced from the C-terminal region of the *nrdF* gene inhibited the *C. glutamicum*-RNR non-competitively and cross-reacted with the *C. ammoniagenes*-RNR. The *C. glutamicum*-R2F has a saturable organic radical signal at $g = 2.005$ detected by electron paramagnetic resonance (EPR) spectroscopy and shows a distinct absorption at 408 nm indicative of a tyrosyl-like organic radical (Y·). Quantification of the metal content revealed 0.06 mol Fe but 0.8 mol Mn per mol R2F-monomer and would thus assign two manganese atoms bound to the dimeric metallo-cofactor, while a distinct enzymatic activity ($32\ \mu mol \times mg^{-1} \times min^{-1}$) was observed in the biochemical complementation assay. Divergence of the *C. glutamicum*-RNR studied here from the prototypical *Salmonella typhimurium* class 1b enzyme and the *Chlamydia trachomatis* class Ic enzyme is discussed below.

Keywords: Corynebacterium glutamicum, *manganese ribonucleotide reductase, tyrosyl radical, electron paramagnetic resonance*

Abbreviations: *RNR, ribonucleotide reductase; R1E, large catalytic; R2F, small subunit of the RNR from* C. glutamicum *and* C. ammoniagenes*; Y·, tyrosyl radical; HU, hydroxyurea;* nrd, n*ucleotide* r*eduction; R1, large catalytic, R2, small subunit of the class I Fe-RNR; CG1, CG2 = R1E and R2F of* C. glutamicum*; CA1, CA2 = R1E and R2F of* C. ammoniagenes*; ICP-MS, inductively coupled plasma-mass spectrometry; ATCC, American Type Culture Collection; I_{50} = value of 50% inhibition; TTP, thymidine triphosphate*

Introduction

The biochemical evolution from the ancient RNA world to the present-day DNA world created an universal *de novo* route of DNA precursor biosynthesis [1,2] which is potentially the rate limiting step in DNA replication. The key enzymes are ribonucleotide reductases (RNR) which catalyse the irreversible deoxygenation of ribonucleoside 5′- di- or triphosphates to the corresponding 2′-deoxyribonucleotides concomitant with the oxidation of a pair of sulphydryl groups to disulphide in thioredoxin or other small proteins with redox-active thiols [3]. Two redox

Correspondence: Professor Dr Georg Auling, Institut für Mikrobiologie, Leibniz Universität Hannover, Schneiderberg 50, D-30167 Hannover, Germany. Fax: 0511/762 5287. Email: auling@ifmb.uni-hannover.de

ISSN 1071-5762 print/ISSN 1029-2470 online
DOI: 10.1080/10715760903140568

equivalents, in most cases delivered from NADPH, are consumed for each substrate reduction and an organic free radical is required to activate the substrate before reduction. Expression of RNR-encoding genes occurs only in proliferating cells congruent with the central role of these enzymes in DNA formation and nucleotide metabolism. The same principle of allosteric regulation exists in all RNR and a monophyletic origin of ribonucleotide reduction was suggested first by Follmann [1]. On the other hand, trace elements like Co, Fe and Mn control growth and DNA formation in different prokaryotic and eukaryotic organisms [2,4,5]. These phenomena were traced back to a diverse array of metallo-cofactors which generate the transient radical for initiation of nucleotide reduction by RNR and serve for classification of these enzymes [6].

An early described prototype of manganese-containing enzymes [7] is the RNR of *Corynebacterium ammoniagenes* [8–10] which is encoded by *nrdEF* genes [11,12]. Highly similar *nrdEF* genes were cloned from the related species *C. glutamicum* [13]. However, the metal specificity cannot be delineated merely from DNA sequence. This paper presents the first biochemical characterization of the *C. glutamicum*-RNR with a focus on the manganese metallocofactor and its stable-free radical.

Materials and methods

Bacterial strains and culture conditions

The strains *Corynebacterium glutamicum* R163 [14], a derivative of the wild type strain ATCC 13032, and *Corynebacterium ammoniagenes* ATCC 6872 were grown in a complex medium (seed medium) at large scale according to Griepenburg et al. [15]. Strain R163 has wild type characteristics with respect to the *nrd*-genes.

Chemicals

2′,5′-ADP Sepharose 4B Superose 12, UNO^{TM} Q12 and phenylsuperose were obtained from Pharmacia LKB (Freiburg, Germany). [5-^{3}H]CDP, ammonium salt (10–30 Ci/mmol) and [8-^{3}H]GDP, ammonium salt (10–15 Ci/mmol) were purchased from Amersham-Buchler (Braunschweig, Germany). Visking® dialysis tubes were obtained from Serva Feinbiochemica GmbH & Co., KG (Heidelberg, Germany).

Assays of RNR activity

Ribonucleotide reduction was assayed in cell-free extracts with tritium-labelled CDP (GDP) as substrate and dATP (TTP) as positive effector according to Willing et al. [8] and the reactions products were separated by HPLC as modified by Plönzig and Auling [16]. Assaying the activity of sub-units resulting from either spontaneous or deliberate dissociation of the holoenzyme required biochemical complementation. For this purpose appropriate amounts of the large catalytic and the small (metal- and radical-containing) sub-unit were mixed and the capability to reduce ribonucleotides was assayed as described above. Basically the same procedure was used when hybrid holoenzymes were assayed for the restoration of the capability to reduce ribonucleotides. Inactivation of the enriched R2F protein (see below) was examined by a 10 min-preincubation at 10°C in the presence of increasing amounts of hydroxyurea, *p*-methoxyphenol or EDTA and subsequent biochemical complementation as above.

Preparation of RNR sub-units

In order to demonstrate heterologous biochemical complementation sub-units of corynebacterial RNR were obtained by affinity chromatography using 2′,5′-ADP Sepharose 4B (cf. flow scheme depicted in Figure 1 of Griepenburg et al. [15]). For molecular mass determination the *C. glutamicum* R2F was further enriched from the pass-through of the affinity chromatography by hydrophobic interaction chromatography using a Phenyl Superose HR 5/5 column (Pharmacia LKB, Freiburg, Germany). Prior to loading the protein was adjusted to 1.5 M ammonium sulphate in 85 mM potassium phosphate buffer with 2 mM DTT (pH 6.6) and eluted to zero with a 10 mL-gradient (gradient programmer GP-250 Plus, Pharmacia LKB, Freiburg, Germany). The three R2F protein-containing fractions were pooled for application to a Superose^{TM} 12 column, calibrated with reference proteins and molecular mass was determined exactly as described by Griepenburg et al. [15]. For inhibition studies the *C. glutamicum* R2F was further enriched from the pass-through of the affinity chromatography by Superdex G-200 gel filtration (flow rate: 0.8 ml/min, 2 ml fractions). The R2F protein-containing fraction nos 15–19 were

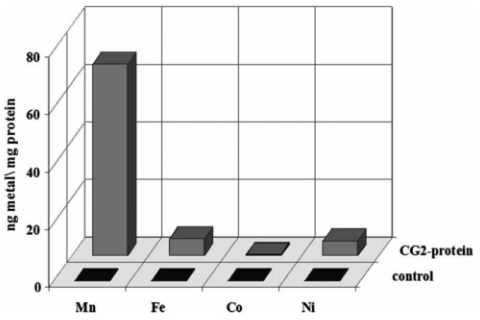

Figure 1. Metal content of the *C. glutamicum*-RNR. R2F of *C. glutamicum*, purified by gel filtration with Superdex G-200 and assayed by biochemical complementation, was analysed by ICP-MS as described by Griepenburg et al. [10].

pooled and concentrated with an Amicon-cell (PM 10 filter).

Synthetic heptapeptide and assay of its inhibitory action

The peptide Ac-EDDDWDF was obtained from SYNTEM (Nimes, France). In order to study its inhibitory effect on corynebacterial RNR the R1E protein of either *C. glutamicum* or *C. ammoniagenes* was pre-incubated in the presence of increasing concentrations of the synthetic peptide for 10 min at 0°C. Ribonucleotide reduction was assayed by biochemical complementation adding the respective R2F at 30°C as described above. Enzyme activity in the absence of the synthetic peptide was set as 100% and the value of 50% inhibition designated as I_{50}.

R2F preparation for detection of the radical signal

The active fraction from ammonium sulphate precipitation (40–60%) was dissolved in standard buffer (85 mM potassium phosphate buffer, pH 6.6 and 2 mM DTT) and the ionic strength was reduced by a 2-h dialysis against the same buffer. The resulting protein solution was applied to an UNO^{TM} Q12 column in buffer A (85 mM potassium phosphate buffer, pH 6.6, 2 mM DTT, 2 mM magnesium acetate). Unbound protein was isocratically eluted with 36 ml of buffer A. For enrichment of RNR holoenzyme a three-step linear gradient was applied: 48 ml of 10%, 36 ml of 35% and 48 ml of 65% buffer B (85 mM potassium phosphate buffer, pH 6.6, 2 mM DTT, 2 mM magnesium acetate and 1.5 M KCl). Finally, the column was re-equilibrated with 100% buffer A prior to application of new protein. The flow-rate was kept constant at 1.6 ml/min and 6 ml-fractions were collected. The active fractions eluted at 35% KCl were pooled, submitted to ammonium sulphate (70%) precipitation, concentrated by centrifugation (30 min, 40000 × g), dissolved and dialysed in buffer A as above and stored at −80°C prior to EPR measurements.

For detection of the UV/visible radical signal eluates from size exclusion chromatography (Superdex^{TM} 200, 16/60 prep grade, using 85 mM potassium phosphate buffer, pH 6.6, fractions in the range between 45–30 kDa) were pooled and submitted to a final anion exchange chromatography.

EPR spectroscopy

Freshly prepared partially purified ribonucleotide reductase (300 µl, 40 mg protein/ml) was transferred to EPR-tubes (Ilmasil-PN high purity quartz, 4.7 ± 0.2 mm outer diameter, 0.45 ± 0.05 mm wall thickness, 13 cm length, obtained from Quarzschmelze Ilmenau GmbH, Langewiesen, Germany) and immediately frozen and stored in liquid nitrogen. EPR spectra were recorded with an EMX-6/1 X-band spectrometer (Bruker, Karlsruhe, Germany) with a standard TE102 rectangular cavity and a variable temperature ESR-900 helium flow cryostat (Oxford instruments, Oxford, UK). Data acquisition was done with the software supplied by Bruker (WINEPR, version 2.3.1), data manipulation (determination of *g*-values, subtraction, baselining, integration and conversion to ASCII files for use with Microsoft EXCEL) was done with the WINEPR program version 2.11. For *g*-value determination the microwave frequency was measured with the built-in ER-041-1161 counter. The minor offset of the magnetic field as measured by the EMX-032T Hall probe was corrected using a strong pitch standard ($g = 2.0028$). A solution of 10 mM $CuSO_4$ in 2 M $NaClO_4$ and 10 mM HCl was used as standard for spin integration. Further EPR conditions are given in the legend to the Figure 4.

Other methods

Manganese and other transition metals of the R2F protein were determined by ICP-MS as described by Griepenburg et al. [10]. In the holoenzyme, enriched by UNO^{TM} Q12 anion exchange chromatography, the iron content was determined spectroscopically using the phenantroline method in comparison with a Fe standard (Merck Darmstadt), the Mn content by oxidation to MnO_4^- according to Jander et al. [17] and the UV/vis spectrum (380–450 nm) was recorded at 10°C in an Ultrospec^{TM} 3300pro (Amersham Biosciences) using quartz cuvettes (Suprasil®, Hellma, Mülheim, Germany). Protein concentrations were determined according to Lowry et al. [18].

Results

The RNR of C. glutamicum is a manganese enzyme and enzymatically active hybrid holoenzymes can be composed with the C. ammoniagenes Mn-RNR

From available DNA sequences [11–13] of the related bacterial species *C. ammoniagenes* and *C. glutamicum* similar corynebacterial RNR would be expected, i.e. holoenzymes with a large catalytic (R1E) and a small metal- and radical-containing subunit (R2F). In order to determine whether the metallo-cofactor of the *C. glutamicum*-RNR contains manganese or iron its R2F protein was prepared by affinity chromatography and gel filtration. A high manganese content was found by ICP-MS, whereas the level of iron was close to that of the buffer control (Figure 1). The molecular mass of the R2F protein was determined to 34 kDa ± 5 kDa matching the 38 kDa-value calculated for the 334 amino acid residues derived from its *nrdF* gene.

A specific heptapeptide corresponding to the C-terminus of the small sub-unit of the RNR of *C. glutamicum* was synthesized. This heptapeptide

distinctly inhibited the activity of the *C. glutamicum*-RNR when the concentrations of both sub-units (R1E and R2F) were held constant while concentrations of the CDP substrate and heptapeptide were varied. Double-reciprocal plots of velocity vs total CDP at five levels of heptapeptide yielded a family of lines intersecting on the ordinate (Figure 2). The pattern is consistent with a non-competitive type of inhibition. For a test of functional similarity the Mn-RNR of *C. ammoniagenes* was also assayed with the C-terminal *C. glutamicum*-R2F heptapeptide. A distinct cross-inhibition albeit at a reduced level (I_{50}-value: 37 μM vs 94 μM) was observed.

An additional proof for similarity of the two corynebacterial RNRs was to generate hybrid enzymes by heterologous biochemical complementation. For this purpose, large and small sub-units of the two corynebacterial RNRs were deliberately separated by affinity chromatography with 2′, 5′-ADP Sepharose 4B and combined to yield heterologous holoenzymes. Remarkably, these hybrid enzymes were capable to reduce ribonucleotides (Figure 3). Compared to the value from homologous complementation the highest activity was observed when R2F of the *C. glutamicum*-RNR was complemented with R1E of the *C. ammoniagenes*-RNR.

The radical in the metallo-cofactor of the C. glutamicum-RNR

It was of interest to examine if the enzyme from *C. glutamicum* would be a target for known inhibitors of the *C. ammoniagenes* Mn-RNR, namely EDTA [8] and the radical scavengers *p*-methoxyphenol [10] and hydroxyurea [11,15]. Compared to the *C. ammoniagenes* enzyme the *C. glutamicum*-RNR was significantly more sensitive to EDTA and *p*-methoxyphenol and had a similar sensitivity towards hydroxyurea (Table I). The remarkable sensitivity towards the

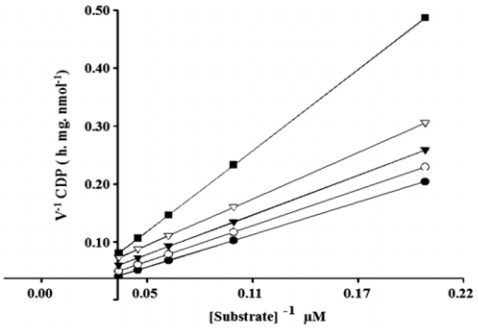

Figure 2. Double-reciprocal plot of velocity versus CDP concentration (5, 10, 15, 20, 25 μM) during cytidine nucleotide reduction catalysed by *C. glutamicum* RNR in the standard biochemical complementation assay (30°C, pH 6.6, 0.1 mM dATP, 6 mM dithithreitol) in the presence of increasing heptapeptide concentrations: 0 μM (●), 5 μM (○), 25 μM (▼), 35 μM (△), 50 μM (■).

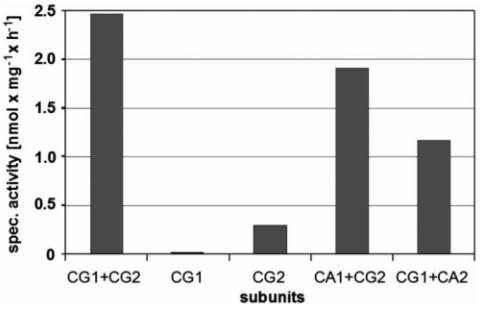

Figure 3. Specific activity of hybrid ribonucleotide reductase holoenzymes upon heterologous biochemical complementation of the sub-units prepared from *C. glutamicum* and *C. ammoniagenes*. RNR sub-units alone are not ribonucleotide reduction proficient. Abbreviations: CG1, CG2 = R1E and R2F of *C. glutamicum*; CA1, CA2 = R1E and R2F of *C. ammoniagenes* (specific activity of 3.6 nmol × mg^{-1} × h^{-1} as holoenzyme).

radical scavengers prompted us to search for a putative radical by EPR. However, detection of a radical signal was a challenge for two reasons: (I) the radical in the metallo-cofactor of the *C. glutamicum*-RNR appeared to be less stable than its counterpart in the related species *C. ammoniagenes* [15] with its reported half-life time of only 1.5 h, and (II) a wild type strain containing an estimated amount of RNR less than 1/1000th of its total protein content is currently the only available enzyme source. As lengthy chromatographic procedures would reduce the actual spin concentration it was decided to apply active protein from the ammonium sulphate precipitation (40–60%) to a trimethylammonium based anion exchange column (UNO™ Q12). A sample of holoenzyme enriched as described in the Materials and methods section allowed to detect an EPR signal of the *C. glutamicum* RNR (Figure 4, traces recorded at various temperatures and at non-saturating conditions) for the first time. The spin concentration of this clear organic radical signal at $g = 2.005$ was determined to 2 μM. Unlike the tyrosyl radical in various binuclear iron centres containing RNR, the signal here had an isotropic appearance and did not show partially resolved proton-hyperfine coupling in X-band EPR at various experimental conditions (i.e. field modulation of 0.3 mT, 10–150 K). The low concentration of the radical species did not allow extensive EPR characterization by multi-frequency or pulsed experiments. This EPR signal is saturable (not

Table I. Efficacy of specific inhibitors towards RNRs from *Corynebacterium* species.

Inhibitors	I_{50}- *C. glutamicum*	I_{50}- *C. ammoniagenes*
Hydroxyurea	1.7 mM	2.5 mM [8]
p-methoxyphenol	0.5 mM	5.3 mM [10]
EDTA	2.4 mM	10.0 mM [8]

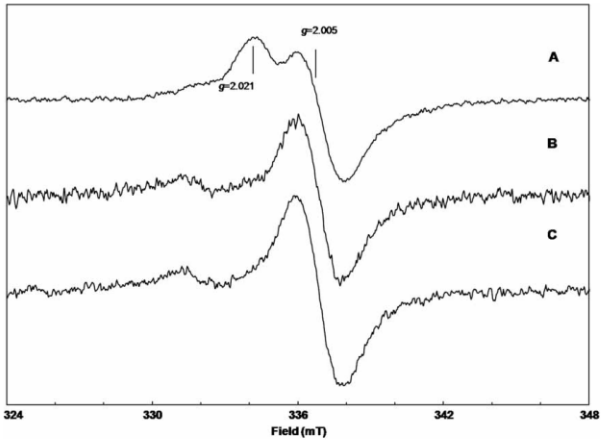

Figure 4. EPR spectra of the organic radical of *C. glutamicum* RNR (holoenzyme, 40 mg/ml, equivalent to 2.5 μM R2F monomer) in 85 mM potassium phosphate buffer, pH 6.6, containing 2 mM DTT at different temperatures and microwave power. EPR parameters: modulation amplitude, 1.2 mT; modulation frequency, 100 kHz; microwave frequency 9458±1 MHz. The temperature and (non-saturating) microwave power was 10 K, 0.80 μW (trace A); 35 K, 12.7 μW (trace B); 80 K, 50.5 μW (trace C), respectively. For comparison the amplitudes were corrected to trace C (gain, number of scans, microwave power and Curie Law).

shown) and the microwave power at half-saturation at 80 K was ≈ 0.3 mW. The blurred lineshape and saturation behaviour indicate the presence of a nearby paramagnetic metal ion (Mn^{2+}), a coupled binuclear centre with paramagnetic ground state or a weakly coupled binuclear centre with thermally populated paramagnetic excited state(s) which appear(s) as binuclear Mn^{2+}. Since no other EPR signals could be detected the type of coupling partner remains to be elucidated. Further purification of the active fractions by anion exchange chromatography (to be described elsewhere) allowed us to detect a sharp visible signal at 408 nm (Figure 5). Its absorption maximum is characteristic of tyrosyl radicals in other ribonucleotide reductases [19]. The purified *C. glutamicum*-R2F had a high ribonucleotide reductase activity (32 $\mu mol \times mg^{-1}$ protein $\times min^{-1}$) in the biochemical complementation assay. Chemical analysis revealed a low iron (0.08 μg Fe/mg R2F), but a high manganese (1.16 μg Mn/mg R2F) content in the purified metallo-cofactor.

Discussion

Corynebacterium glutamicum has been intensively studied with respect to large-scale production of amino acids and its underlying metabolism [20], while the metal dependence of its DNA precursor biosynthesis is completely unknown. The work presented here (Figure 1) suggests that we were studying a manganese-containing ribonucleotide reductase in *C. glutamicum* with a high manganese but a low iron content as reported for the *C. ammoniagenes* R2F [10]. Thus, the RNRs from both corynebacteria contain manganese and lack iron when obtained as native enzymes from the original source.

The above data and sequence information [11–13] place the two corynebacterial RNRs side-by-side. However, an amino acid exchange between the two corynebacterial R2F proteins [11] would explain the lower efficacy of the synthetic heptapeptide, while similar efficacy [21] is due to sequence identity of the C-terminal region of *C. glutamicum* and *M. tuberculosis* (Table II). Our data in Figure 2 are consistent with other reports on competition of synthetic peptides for R2 binding in RNRs [22–25]. Furthermore,

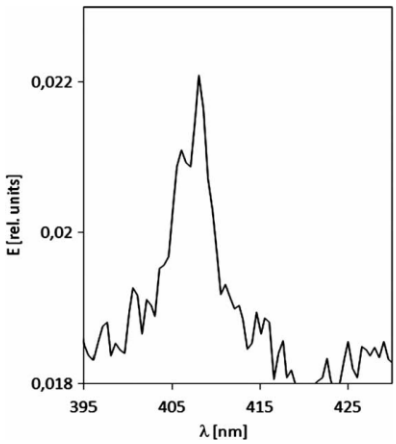

Figure 5. The 408 nm tyrosyl-like signal of the *C. glutamicum*-Mn-RNR in the UV/visible difference spectrum (absorption of HU-treated protein subtracted from native sample) from the purified R2F sample.

Table II. Inhibition of RNRs from high-GC Gram-positive bacteria (Actinobacteria) by a specific heptapeptide derived from the C-terminal region of the *C. glutamicum nrdF* gene.

C-terminal sequence	I_{50}	Source of target RNRs	Reference
E-D-D-D-W-D-F	37 μM	*C. glutamicum*	This work
T-D-D-D-W-D-F	94 μM	*C. ammoniagenes*	This work
E-D-D-D-W-D-F	20 μM	*M. tuberculosis* (R2-2)	[21]

the non-competitive mode of inhibition of the *C. glutamicum*-RNR points to a common binding region of R2F and its terminal heptapeptide distant from the active centre of R1E and suggests a long-range electron transfer from the radical-bearing R2F to the catalytic R1E well known from the class Ia RNR [19].

The tendency of RNRs to dissociate into large catalytic and small metal-containing sub-units facilitates generation of hybrid enzymes and evaluation of their capability for reduction of ribonucleotides. The successful biochemical complementation of R1E and R2F from *C. glutamicum* or *C. ammoniagenes* to active holoenzymes (Figure 3) confirmed the similarity of the two corynebacterial RNRs. It is noteworthy that previous attempts for generation of hybrid enzymes composed of sub-units from the *C. ammoniagenes* Mn-RNR and the *E. coli*-Fe-RNR failed [8]. This indicates diversity of the latter enzymes in spite of an analogous sub-unit structure.

On the other hand, the two corynebacterial Mn-RNRs have many properties in common, e.g. inhibition by EDTA and the radical scavengers hydroxyurea and *p*-methoxyphenol. EPR spectroscopy revealed a saturable organic radical in the *C. glutamicum* RNR. The $g_{average}$-value is in the range reported for tyrosyl radicals in other RNRs (Table III). However, the use of an average *g*-value to prove the nature of the radical-bearing moiety has limitations, especially since the presence of a nearby coupling partner or a second underlaying radical species could shift the *g*-value. It is known that the *g*-anisotropy and linewidth of radicals strongly depend on the local environment (i.e. hydrophobicity, hydrogen bonds, β-methylene dihedral angles) [26,27]. A factor which complicates the definitive assignment to a tyrosyl radical is the variable relaxation behaviour of tyrosyl radicals in RNRs; i.e. *E. coli* RNR has a $P_{1/2}$ of 12 mW (77 K), *S. typhimurium* RNR (Fe-substituted) of 3.7 mW (95 K), *C. glutamicum* RNR of 1.3 mW (95 K), *M. tuberculosis* RNR of 0.72 mW (77 K) and *C. ammoniagenes* RNR of 0.5 mW (77 K). Differences in the relative orientation of the tyrosyl radical with respect to the binuclear centre and in the coupling constants of the binuclear centres cause this variation.

Table III. Values of $g_{average}$ factors of selected tyrosyl radicals in biological systems.

Tyrosyl radical sources	$g_{average}$ value	References
R2, *E. coli*	2.0047*	[30]
	2.0053	[31]
R2F, *S. typhimurium*	2.0047	[32]
	2.0051	[33]
R2F, *C. ammoniagenes*	2.004	[15]
R2F, *C. ammoniagenes*	2.005	[34]
R2F, *C. glutamicum*	2.005	This work
R2F, *M. tuberculosis*	2.0053	[26]
	2.0056	[35]

*In this first report on a tyrosyl radical of RNR a doublet centred at $g = 2.0047$ was reported as the only signal detected.

As for tyrosyl radicals of RNRs from Gram-positive bacteria [15], the radical of the *C. glutamicum* enzyme shows a saturation behaviour which is characteristic of a weak magnetic interaction. Both the visible 408 nm Y·-radical signal observed here (Figure 5) and the conserved Y_{120} suggest that a tyrosyl radical exists in the *C. glutamicum*-R2F. Assignment of the featureless EPR signal (Figure 4) to a tyrosyl radical broadened by coupling is tempting, but will have to await site-directed mutagenesis of Tyr_{120} or multiple frequency EPR studies using R2F with enriched spin concentration from homologous expression. Noteworthily, our results were obtained with the wild type of *C. glutamicum* grown in complex medium without any perturbation of trace element nutrition. Thus, the manganese detected here by different methods is intrinsic to the *C. glutamicum* RNR. Chemical quantification of the metal content in the purified sample revealed 0.06 mol Fe but 0.8 mol Mn per mol R2F-monomer and would thus assign two manganese atoms bound to the dimeric metallo-cofactor of the *C. glutamicum* RNR. Options which are compatible with this observation are: (1) R2F contains a mononuclear manganese centre, (2) our preparations contain apo-protein and the metallo-cofactor is a binuclear Mn centre and (3) R2F has a binuclear centre with Mn and a second metal ion other than Mn or Fe.

The corresponding *nrdEF* genes represent the only RNR in the genome of *C. glutamicum* ATCC 13032 [28]. Therefore, this genomic information and our finding of a Mn-type of RNR exclude a class Ia RNR in *C. glutamicum* since the type of metal centre defines the class of the RNR [6].

Finally, the *C. glutamicum* metallo-cofactor is also remarkably different from the recently described unconventional manganese(IV)/iron(III) cofactor in the *Chlamydia trachomatis* ribonucleotide reductase

[29] due to the presence of a tyrosyl radical (Figures 4 and 5).

Acknowledgements

We thank A. Walter for contributing initial data on hybrid enzymes, H. Plattner for advice during protein chromatography, S. Straßburg and G. Wünsch (Institut für Anorganische Chemie der Universität Hannover, Germany) for help with ICP-MS, and R. K. Thauer (MPI Terrestrische Mikrobiologie, Marburg) for free access to the EPR spectrometer. This work was supported by the grant Au62/4-3 from the Deutsche Forschungsgemeinschaft to G. Auling.

References

[1] Follmann H. Deoxyribonucleotide synthesis and the emergence of DNA in molecular evolution. Naturwissenschaften 1982;69:75–81.

[2] Follmann H. Deoxyribonucleotides: the unusual chemistry and biochemistry of DNA precursors. Chem Soc Rev 2004; 33:225–233.

[3] Reichard P. From RNA to DNA, why so many ribonucleotide reductases? Science 1993;260:1773–1777.

[4] Hogenkamp HP. Nature and properties of the bacterial ribonucleotide reductases. Pharmacol Ther 1983;23: 393–405.

[5] Lammers M, Follmann H. The ribonucleotide reductases a unique group of metalloenzymes essential for cell proliferation. Structure & Bonding 1983;54:27–91.

[6] Stubbe J, van der Donk WA. Ribonucleotide reductases: radical enzymes with suicidal tendencies. Chem Biol 1995;2:793 801.

[7] Schimpff-Weiland G, Follmann H, Auling G. A new manganese-activated ribonucleotide reductase found in gram-positive bacteria. Biochem Biophys Res Commun 1981;102: 1276–1282.

[8] Willing A, Follmann H, Auling G. Ribonucleotide reductase of *Brevibacterium ammoniagenes* is a manganese enzyme. Eur J Biochem 1988;170:603–611.

[9] Auling G, Follmann H. Manganese-dependent ribonucleotide reduction and overproduction of nucleotides in coryneform bacteria. In: H Sigel, A Sigel, editors. Metal ions in biological systems. New York: Marcel Dekker Inc;30; 1994. p 132–161.

[10] Griepenburg U, Blaszczyk K, Kappl R, Hüttermann J, Auling G. A divalent metal site in the small subunit of the manganese-dependent ribonucleotide reductase of *Corynebacterium ammoniagenes*. Biochemistry 1998;37:7992 7996.

[11] Oehlmann W, Griepenburg U, Auling G. Cloning and sequencing of the nrdF gene of *Corynebacterium ammoniagenes* ATCC 6872 encoding the functional metallo-cofactor of the manganese-ribonucleotide reductase (Mn-RRase). Biotechnol Lett 1998;20:483 488.

[12] Fieschi F, Torrents E, Toulokhonova L, Jordan A, Hellman U, Barbe J, Gibert I, Karlsson M, Sjöberg BM. The manganese-containing ribonucleotide reductase of *Corynebacterium ammoniagenes* is a class Ib enzyme. J Biol Chem 1998;273: 4329–4337.

[13] Oehlmann W, Auling G. Ribonucleotide reductase (RNR) of *Corynebacterium glutamicum* ATCC 13032-genetic characterization of a second class IV enzyme. Microbiology 1999;145: 1595–1604.

[14] Liebl W, Schein B. Isolation of restriction deficient mutants of *Corynebacterium glutamicum*. In: Behrens D, Krämer J, editors. DECHEMA Biotechnology conference. 1990. pp 323 327, VCH Verlagsgemeinschaft, Weinheim.

[15] Griepenburg U, Lassmann G, Auling G. Detection of a stable free radical in the B2 subunit of the manganese ribonucleotide reductase (Mn-RRase) of *Corynebacterium ammoniagenes*. Free Radic Res 1996;24:473–481.

[16] Plönzig J, Auling G. Manganese deficiency impairs ribonucleotide reduction but not replication in *Arthrobacter* species. Arch Microbiol 1987;146:396–401.

[17] Jander G, Blasius E, Strähle J, Schweda E. Lehrbuch der analytischen und präparativen anorganischen chemie. Stuttgart: Hirzel; 2002.

[18] Lowry OH, Rosebrough NJ, Farr AL, Randall RJ. Protein measurement with the Folin phenol reagent. J Biol Chem 1951;193:265 275.

[19] Sjöberg B-M. Ribonucleotide reductases—a group of enzymes with different metallosites and a similar reaction mechanism. Structure & Bonding 1997;88:139–173.

[20] Leuchtenberger W, Huthmacher K, Drauz K. Biotechnological production of amino acids and derivatives: current status and prospects. Appl Microbiol Biotechnol 2005;69:1 8.

[21] Yang F, Curran SC, Li LS, Avarbock D, Graf JD, Chua MM, Lu G, Salem J, Rubin H. Characterization of two genes encoding the *Mycobacterium tuberculosis* ribonucleotide reductase small subunit. J Bacteriol 1997;179:6408–6415.

[22] Laplante SR, Aubry N, Liuzzi M, Thelander L, Ingemarson R, Moss N. The critical C-terminus of the small-subunit of *Herpes-simplex* virus ribonucleotide reductase is mobile and conformationally similar to the C-terminal peptides. Int J Pept Protein Res 1994;44:549–555.

[23] Cohen EA, Gaudreau P, Brazeau P, Langelier Y. Specific inhibition of herpesvirus ribonucleotide reductase by a non-apeptide derived from the carboxy terminus of subunit-2. Nature 1986;321:441–443.

[24] Dutia BM, Frame MC, Subaksharpe JH, Clark WN, Marsden HS. Specific inhibition of herpesvirus ribonucleotide reductase by synthetic peptides. Nature 1986;321:439–441.

[25] Yang FD, Spanevello RA, Celiker I, Hirschmann R, Rubin H, Cooperman BS. The carboxyl terminus heptapeptide of the R2 subunit of mammalian ribonucleotide reductase inhibits enzyme activity and can be used to purify the R1 subunit. FEBS Lett 1990;272:61–64.

[26] Liu A, Pötsch S, Davydov A, Barra AL, Rubin H, Gräslund A. The tyrosyl free radical of recombinant ribonucleotide reductase from *Mycobacterium tuberculosis* is located in a rigid hydrophobic pocket. Biochemistry 1998;37:16369–16377.

[27] Ivancich A, Mattioli TA, Un S. Effect of protein microenvironment on tyrosyl radicals. A high-field (285 GHz) EPR, resonance raman, and hybrid density functional study. J Am Chem Soc 1999;121:5743–5753.

[28] Kalinowski J, Bathe B, Bartels D, Bischoff N, Bott M, Burkovski A, Dusch N, Eggeling L, Eikmanns BJ, Gaigalat L, Goesmann A, Hartmann M, Huthmacher K, Kramer R, Linke B, McHardy AC, Meyer F, Mockel B, Pfefferle W, Puhler A, Rey DA, Ruckert C, Rupp O, Sahm H, Wendisch VF, Wiegrabe I, Tauch A. The complete *Corynebacterium glutamicum* ATCC 13032 genome sequence and its impact on the production of L-aspartate-derived amino acids and vitamins. J Biotechnol 2003;104:5–25.

[29] Jiang W, Yun D, Saleh L, Barr EW, Xing G, Hoffart LM, Maslak MA, Krebs C, Bollinger JM, Jr. A manganese(IV)/iron(III) cofactor in *Chlamydia trachomatis* ribonucleotide reductase. Science 2007;316:1188–1191.

[30] Ehrenberg A, Reichard P. Electron spin resonance of iron-containing protein B2 from ribonucleotide reductase. J Biol Chem 1972;247:3485–3488.

[31] Gerfen GJ, Bellew BF, Un, S, Bollinger JM, Stubbe J, Griffin RG, Singel DJ. High-frequency (139.5 GHZ) EPR spectroscopy of the tyrosyl radical in *Escherichia coli*

ribonucleotide reductase. J Am Chem Soc 1993;115: 6420 6421.

[32] Jordan A, Pontis E, Atta M, Krook M, Gibert I, Barbe J, Reichard PA. second class I ribonucleotide reductase in Enterobacteriaceae: characterization of the *Salmonella typhimurium* enzyme. Proc Natl Acad Sci U S A 1994;91: 12892–12896.

[33] Allard P, Barra AL, Andersson KK, Schmidt PP, Atta M, Gräslund A. Characterization of a new tyrosyl free radical in *Salmonella typhimurium* ribonucleotide reductase with EPR at 9.45 and 245 GHz. J. Amer. Chem. Soc. 1996;118:895–896.

[34] Huque Y, Fieschi F, Torrents E, Gibert I, Eliasson R, Reichard P, Sahlin M, Sjöberg BM. The active form of the R2F protein of class Ib ribonucleotide reductase from *Corynebacterium ammoniagenes* is a diferric protein. J Biol Chem 2000;275:25365–25371.

[35] Elleingand E, Gerez C, Un S, Knupling M, Lu G, Salem J, Rubin H, Sauge-Merle S, Laulhere JP, Fontecave M. Reactivity studies of the tyrosyl radical in ribonucleotide reductase from *Mycobacterium tuberculosis* and *Arabidopsis thaliana*–comparison with *Escherichia coli* and mouse. Eur J Biochem 1998;258:485–490.

This paper was first published online on iFirst on 20 August 2009.

Diskussion

Die in dieser Arbeit vorgestellte interdisziplinäre Bearbeitung der nativen R2F Proteine von *C. ammoniagenes* und *C. glutamicum* klärt endgültig, dass diese Enzyme Mangan für die Generation des Tyrosylradikals in ihrem Metallocofaktor verwenden. Damit erwies sich die heterologe Expression des *nrdF*-Gens von *C. ammoniagenes* im phylogenetisch entfernten *E. coli*-Hintergrund (Högbom et al., 2002; Huque et al., 2000) als Irrweg für die Analyse des Metallocofaktors dieser R2F-Proteine. Eine immer größere Zahl an Präzedenzfällen zeigt, dass die heterologe Expression von Genen, die Metalloproteine kodieren, oft nicht die korrekte Antwort auf die Frage nach dem physiologisch relevanten Metall liefert (Hidalgo et al., 2004; Kennedy et al., 1998). In der Einleitung zu dieser Arbeit (vergl. 5.1, S.13ff.) wurde ausdrücklich auf die große Bedeutung akzessorischer Proteine bei der Assemblierung von Metalloproteinen hingewiesen (Mulrooney & Hausinger, 2003a). Eine Rolle von Mangan für die Genregulation des *nrd*-Operons in *C. ammoniagenes* (Torrents et al., 2003) bleibt davon unbenommen, hat aber keinen Einfluss auf die hier präsentierten Ergebnisse, da die homologe Überexpression des *nrdF*-Gens unter der Kontrolle des *tac*-Promotors erfolgte (Barckhausen, 2004), der in Corynebakterien gut abgelesen wird (Paik & Lee, 2003; Stolle et al., 2010a). Die hier etablierte Methode der Reinigung des R2F-Proteins liefert hochaktives und homogenes Protein. Nach zusätzlicher Ultrafiltration können die für physikalische Messungen benötigten Konzentrationen ebenfalls bereitgestellt werden. Der entscheidende Schritt zur Abtrennung unspezifischer eisenhaltiger Proteine fand in der Gelfiltration an einer Superdex 200 Säule statt. Auffallend ist, dass nach homologer Expression die Elution von nativem R2F bei 38 kDa (Monomer) erfolgt, während vorherige Versuche zur Anreicherung von R2F aus dem Wildtyp *von C. ammoniagenes* als 80 kDa Dimer beschrieben (Fieschi et al., 1998; Griepenburg et al., 1998; Willing et al., 1988b). Der hier ermittelte molare Extinktionskoeffizient entspricht mit $\varepsilon_{280} = 76280 \times M^{-1} cm^{-1}$ nahezu perfekt dem erwarteten theoretischen Wert für das Monomer. Die Annahme eines in der Gelfiltration ungewöhnlich migrierenden, maskierten Dimers würde diesen Wert halbieren. Dies ist unwahrscheinlich. Das hier beobachtete unterschiedliche Elutionsverhalten des R2F-Proteins kann durch die gesteigerte Expression des *nrdF*-Gens in *C. ammoniagenes* pOCA2 erklärt werden. Das resultierende Ungleichgewicht zwischen R2F und R1E deutet darauf hin, dass stöchiometrische Mengen der beiden Untereinheiten für eine R2F-Dimerisierung erforderlich sind. In der Erstbeschreibung wurde die Mn-RNR mit einer $\alpha\beta_2$ Struktur beschrieben (Willing

et al., 1988b). Es ist daher nicht verwunderlich, dass die Messung der spezifischen R2F-Aktivität nach biochemischer Komplementation nur im Verhältnis 2 Teile R2F zu 1 Teil R1E mit Erfolg durchgeführt werden konnte. Verglichen mit *E. coli*-R2 (Larsson et al., 1996), *S. typhimurium* Fe-R2F (Huque et al., 2000), *C. ammoniagenes* Fe-R2F (Huque et al., 2000) ist die hier präsentierte spezifische Aktivität des nativen *C. ammoniagenes*-R2F aus homologer Expression (69 µmol × mg^{-1} × min^{-1}) sehr hoch (6.00, 0.60, 0.05 µmol × mg^{-1} × min^{-1}). Eine Ausnahme bildet die etwa gleich hohe Aktivität (32 µmol × mg^{-1} × min^{-1}) der *C. glutamicum* RNR (Abbouni et al., 2009). Damit ist keine nachträgliche *in-vitro* Aktivierung des Metallocofaktors im hier vorgestellten *C. ammoniagenes* R2F-Protein mit Hilfe akzessorischer Faktoren nötig, wie sie für das *E. coli* Ib Enzym durch NrdI beschrieben wurde (Cotruvo & Stubbe, 2010). Jedoch ist eine Beteiligung von NrdI an der *in-vivo* Assemblierung des R2F-Proteins in *C. ammoniagenes* nicht ausgeschlossen. Dieser Organismus hat auch ein *nrdI*-Gen in seinem *nrd*-Operon (vergl. Abb. 7, S. 14). Andererseits lieferten sämtliche hier durchgeführten Metallbestimmungen eine Stöchiometrie von 1,4 Mn pro R2F-Dimer. Diese lässt sich mit der Annahme erklären, dass R2F zwar gereinigt wurde, aber bezüglich der Metallbesetzung inhomogen ist, dergestalt, dass ein Teil voll besetzt ist (4 Mn) und der Rest in der inaktiven Apoform vorliegt. Eine Unterbesetzung des für Klasse I RNRs typischen dinuclearen Metallocofaktors in der hier benutzten R2F-Präparation liegt vor, da bei dem hier kalkulierten Mangan- (0,74 Mol/Mol) und Radikalgehalt (0,18 Mol/Mol) der R2F-Monomere nur 25 % im vollbesetzten und damit aktiven Zustand vorliegen. Es ist denkbar, dass eine Coexpression von NrdF und NrdI eine höhere Besetzung der Metallbindeplätze im R2F-Protein ermöglichen würde (vergl. oben). Die hohe Manganspezifität des hier vorgestellten R2F-Metallocofaktors wurde durch ausgewählte Induktionsversuche belegt. Bei dem standardisierten Protokoll der Induktion werden dem Anzuchtmedium üblicherweise 185 µM $MnCl_2$ zur Generierung des Mn-R2F zugesetzt. Die gleichzeitige Zugabe äquimolarer Mengen Mn^{2+}, Fe^{2+} und Zn^{2+} veränderte weder den Metallstatus R2F-Cofaktors noch dessen Radikalgehalt. Bei einer Induktion allein mit Fe^{2+} wurde nur die Apoform von R2F erhalten.

Über die Kristallstruktur wurde ein oxo/hydroxo verbrücktes Mangandimer in direkter Nachbarschaft (8 Å) zu einem Tyrosin (Y115) gezeigt (Ogata et al., 2009). Weiterführende Multi-Frequenz EPR Messungen, kombiniert mit biochemischen Analysen, zeigten, dass hierbei ein stabiles, redoxaktives Tyrosylradikal in räumlicher Nähe, und damit in Kopplung zu einem Mangan-Dimer vorlag, dessen Oxidationszustand als $Mn^{III}Mn^{III}$, vergleichbar dem

des Eisencofaktors der Klasse Ia RNR von *E. coli* ist (Atkin et al., 1973; Nordlund et al., 1990; Sjöberg, 1997). Das native R2F von *C. ammoniagenes* zeigt in der EPR ein gekoppeltes Radikalsignal (split signal). Solche Signale wurden zuvor schon in anderen biologischen Systemen mit redoxaktiven Tyrosinen, z.B. dem Photosystem II beschrieben (Cox et al., 2009; Havelius et al., 2006; Koulougliotis et al., 2004; Su et al., 2007). Im PSII wird das üblicherweise ~3 mT breite Tyrosylsignal aufgrund einer schwachen Wechselwirkung mit dem 7 Å entfernten, paramagnetischen Tetra-Manganzentrum des „oxygen evolving complex" (vergl. 5.2, S.18), verbreitert. Damit Vergleichbar ist die Signalverbreiterung des in R2F lokalisierten Tyrosylradikals, das 8 Å entfernt vom Mn-Mn Dimer liegt (Ogata et al., 2009). Auch der in dieser Arbeit untersuchte Metallocofaktor des *C. glutamicum* R2F-Proteins (Abbouni et al., 2009) zeigt ein ähnliches gekoppeltes Radikalsignal. Es fällt aber auf, dass sich ihre EPR Spektren sowie die Temperaturabhängigkeit unterscheiden. Die g-Werte beider Radikale liegen im Normbereich für Tyrosylradikale, dennoch ist die Signalbreite des *C.g.*-Metallocofaktors in der X-Band EPR, verglichen mit dem *C.a.*-Metallocofaktor, halbiert. Der Hauptunterschied der beiden Cofaktoren ist, das die Kopplung des Mangandimers von *C. ammoniagenes* schwach ferromagnetisch, die Kopplung zwischen den beiden Manganzentren von *C. glutamicum* aber wahrscheinlich schwach antiferromagnetisch ist (Cox et al., 2010). Darüber hinaus stimmt der hier vorgeschlagene $Mn^{III}Mn^{III}$-Metallocofaktor mit den Eigenschaften eine μ-oxo-(mono/bis)μ-carboxylato $Mn^{III}Mn^{III}$-Modellkomplexes (Stolle et al., 2010b) sehr gut überein. Der Hauptunterschied zum *E. coli* R2 ist, dass die Evolution hier ein anderes Metall für die gleiche katalytische Aufgabe verwendet hat. Jeweils ein zusätzliches Wassermolekül wurde im Bindungsnetzwerk des R2-(Nordlund et al., 1990) und des R2F-Metallocofaktors (Högbom et al., 2002) postuliert, das auf einen leichteren Zugang zum Metallzentrum schließen lässt. Ein entsprechendes Wassermolekül kommt im nativen R2F von *C. ammoniagenes* nicht vor (Ogata et al., 2009). Die daraus resultierende dichtere Struktur des R2F-Proteins erklärt die höhere Stabilität dieses Metallocofaktors auch gegenüber EDTA (Willing et al., 1988b).

Ein neuer Aspekt ist, dass das im Metallocofaktor lokalisierte Tyrosylradikal direkt an der Ribonucleotidreduktion beteiligt ist. In dem hier entwickelten neuen Enzymtest konnte über die Löschung des Radikalsignals gezeigt werden, dass 0,4 nmol $Y^{\bullet}$ an der Bildung von 0,2 nmol dCDP (Produkt) beteiligt sind (Fig. 3b, Stolle et al., 2010a). Das während der Katalyse zum Tyrosin reduzierte Tyrosylradikal verbleibt in diesem Zustand. Das Fehlen von DTT im

alternativen Test führt dazu, dass die R1E-Disulfide nach der Reaktion nicht wieder reduziert werden können. Zumindest in der Theorie kann deshalb von einer „single-turnover"-Reaktion ausgegangen werden. In diesem Enzymtest führt eine standardmäßig betriebene Schutzmaßnahme allerdings zu einem geringen Eintrag eines künstlichen Reduktionsäquivalents. Bei der Affinitätschromatographie des R1E Proteins wird das Reduktionsmittel Dithiothreitol (2 mmol) eingesetzt, um die Thiolgruppen der Cysteine während der Reinigung vor Oxidation zu schützen. Dadurch sollten die Cysteine in R1E nach der Anreicherung in der reduzierten Form vorliegen. Weil so kleine Mengen DTT mit R1E in den Assay eingebracht werden. Dies führt zu einer Regeneration eines geringen Anteils der bei Katalyse oxidierten Cysteine von R1E, was die Produktausbeute durch einen erneuten Turnover geringfügig erhöhen dürfte (< 10 %). Der hier neu entwickelte Test zeigte sich als geeignet als Screeningverfahren zur Suche nach RNR-Inhibitoren. In einem gezielten Versuch, konnte die Interaktion der R1E und R2F Untereinheiten wirkungsvoll unterbrochen werden, erkennbar am Erhalt des Tyrosylsignals wie auch an der fehlenden Produktbildung (Stolle et al., 2010b).

Die hier präsentierte Reaktivierung des Tyrosylradikals im Metallocofaktor des R2F Protein nach Quenchen mit Hydroxyharnstoff weist auf die Beteiligung von H_2O_2 bei der Oxidation des Metallclusters hin (Fig. 13, Cox et al., accepted). Verglichen mit der Ausgangskonzentration wurde dabei ein 30 % höherer Radikalgehalt erhalten. Dabei ist nicht ganz klar, ob diese zusätzliche Radikalausbeute dem während der Reinigung reduziertem Anteil entspricht oder mit einem Anteil neu aus der Apoform assemblierter Cofaktoren zu begründen ist. In diesem Zusammenhang ist interessant, dass kürzlich die Beteiligung eines zusätzlichen Flavodoxins, NrdI, für die Aktivierung des Klasse Ib Mn-Metallocofaktors von *E. coli* vorgeschlagen wurde (Cotruvo & Stubbe, 2010). Für die hier benutzten R2F-Präparationen konnte die Anwesenheit eines vergleichbaren akzessorischen Proteins (*C. ammoniagenes*-NrdI, PDB 069272) über ESI-QTOF Massenspektrometrie ausgeschlossen werden. Im von Cotruvo und Stubbe vorgeschlagenen Mechanismus zur Assemblierung des Mn-Metallocofaktors der *E. coli* Klasse Ib RNR wird in einem ersten Schritt, der an die H_2O_2 Deprotonierungreaktion der Mn-Katalase erinnert, das $Mn^{II}Mn^{II}$-Dimer zu $Mn^{III}Mn^{III}$ oxidiert (Barynin et al., 2001; Boelrijk & Dismukes, 2000; Dismukes, 1996). Der zweite Schritt generiert daraufhin ein di-μ-oxo-verbrücktes $Mn^{III}Mn^{IV}$ oder $Mn^{IV}Mn^{IV}$ Dimer (Sheats et al., 1987; Wieghardt et al., 1985), welches ein Elektron vom Tyrosin (Y115) abstrahiert und das für die Ribonucleotidreduktion essentielle Tyrosylradikal generiert. Bezogen auf die ersten

Schritte des Reaktionsmechanismus (vergl. Abb. 13, (Cox et al., 2010)) stimmen sowohl die publizierte R2F-Kristallstruktur (vergl. Ogata et al., 2009; PDB 3MJO) als auch Multifrequenz-EPR Analysen (Cox et al., 2010; Stolle et al., 2010a) mit dem obigen Modell überein. Beide Ansätze liefern aber auch weitere Details, insbesondere welche Konformationsänderungen des Mn-Mn Ligandenfeldes (vergl. Fig. 6B, (Cox et al., 2010)) den Reaktionsmechanismus begleiten. Diese neuen Informationen zur Rolle von Glu202 & Asp77 werden in der vorliegenden Arbeit berücksichtigt und führen zu einer Änderung im Mechanismus (vergl. Abb. 13, (Cox et al., 2010)). Damit werden die letzten Schritte des obigen von (Cotruvo & Stubbe, 2010) vorgeschlagenen Mechanismus abgelehnt.

Die in der vorliegenden Dissertation erzielten Erkenntnisse über die R2F-Metallocofaktoren von *C. ammoniagenes* und *C. glutamicum* in Verbindung mit der Arbeit von (Cotruvo & Stubbe, 2010) an der Aktivierung der Klasse Ib RNR von *E. coli* legen den Schluss nahe, dass Mangan das wichtigste Metall für sämtliche RNRs dieser Klasse ist. Die hier präsentierte Struktur sowie der Mechanismus der Cofaktorassemblierung (vergl. Abb. 13, (Cox et al., 2010)) können repräsentativ für alle Klasse Ib Ribonucleotid-Reduktasen sein.

Literaturverzeichnis

Abbouni B, Oehlmann W, Stolle P, Pierik AJ, Auling G (2009) Electron paramagnetic resonance (EPR) spectroscopy of the stable-free radical in the native metallo-cofactor of the manganese-ribonucleotide reductase (Mn-RNR) of *Corynebacterium glutamicum*. *Free Radic Res* **43:** 943-950

Abreu IA, Cabelli DE (2010) Superoxide dismutases-a review of the metal-associated mechanistic variations. *Biochim Biophys Acta* **1804:** 263-274

Ahn BE, Cha J, Lee EJ, Han AR, Thompson CJ, Roe JH (2006) Nur, a nickel-responsive regulator of the Fur family, regulates superoxide dismutases and nickel transport in *Streptomyces coelicolor*. *Mol Microbiol* **59:** 1848-1858

Andreini C, Bertini I, Cavallaro G, Holliday GL, Thornton JM (2008) Metal ions in biological catalysis: from enzyme databases to general principles. *J Biol Inorg Chem* **13:** 1205-1218

Arino J, Ramos J, Sychrova H (2010) Alkali metal cation transport and homeostasis in yeasts. *Microbiol Mol Biol Rev* **74:** 95-120

Arosio P, Ingrassia R, Cavadini P (2009) Ferritins: A family of molecules for iron storage, antioxidation and more. *Biochimica et Biophysica Acta (BBA) - General Subjects* **1790:** 589-599

Atkin CL, Thelander L, Reichard P, Lang G (1973) Iron and free radical in ribonucleotide reductase. Exchange of iron and Mossbauer spectroscopy of the protein B2 subunit of the *Escherichia coli* enzyme. *J Biol Chem* **248:** 7464-7472

Auling G (1980) Nucleotidstoffwechsel in *Brevibacterium ammoniagenes* und *Micrococcus sodonensis*. *Institut für Mikrobiologie*

Auling G, Follmann H (1994) Manganese dependent ribonucleotide reduction and overproduction of nucleotides in coryneform bacteria. pp 131-161. New York: Marcel Dekker Inc

Auling G, Thaler M, Diekmann H (1980) Parameters of unbalanced growth and reversible inhibition of deoxyribnucleic acid synthesis in *Brevibacterium ammoniagenes* ATCC 6872 induced by depletion of Mn^{2+}. Inhibitor studies on the reversibility of deoxyribonucleic acid synthesis. *Arch Microbiol* **127:** 105--114

Baichoo N, Helmann JD (2002) Recognition of DNA by Fur: a reinterpretation of the Fur box consensus sequence. *J Bacteriol* **184:** 5826-5832

Baichoo N, Wang T, Ye R, Helmann JD (2002) Global analysis of the *Bacillus subtilis* Fur regulon and the iron starvation stimulon. *Mol Microbiol* **45:** 1613-1629

Barber J, Nield J, Morris EP, Zheleva D, Hankamer B (1997) The structure, function and dynamics of photosystem two. *Physiol Plant* **100:** 817-827

Barckhausen O (2004) Nachweis eines mononuclearen Mangan (II)-Zentrums in der Ribonucleotid-Reduktase aus *Corynebacterium ammoniagenes* ATCC 6872 nach Überexpression des den Metallocofaktor codierenden *nrdF*-Gens im Originalstamm. *Universität Hannover*

Barynin VV, Whittaker MM, Antonyuk SV, Lamzin VS, Harrison PM, Artymiuk PJ, Whittaker JW (2001) Crystal structure of manganese catalase from *Lactobacillus plantarum*. *Structure* **9:** 725-738

Becker A, Fritz-Wolf K, Kabsch W, Knappe J, Schultz S, Volker Wagner AF (1999) Structure and mechanism of the glycyl radical enzyme pyruvate formate-lyase. *Nat Struct Biol* **6:** 969-975

Boekema EJ, Hankamer B, Bald D, Kruip J, Nield J, Boonstra AF, Barber J, Rogner M (1995) SUPRAMOLECULAR STRUCTURE OF THE PHOTOSYSTEM-II COMPLEX FROM GREEN PLANTS AND *CYANOBACTERIA*. *P Natl Acad Sci USA* **92:** 175-179

Boelrijk AE, Dismukes GC (2000) Mechanism of hydrogen peroxide dismutation by a dimanganese catalase mimic: dominant role of an intramolecular base on substrate binding affinity and rate acceleration. *Inorg Chem* **39:** 3020-3028

Booker S, Stubbe J (1993) Cloning, sequencing, and expression of the adenosylcobalamin-dependent ribonucleotide reductase from *Lactobacillus leichmannii*. *Proc Natl Acad Sci U S A* **90:** 8352--8356

Boston T, Atlung T (2003) FNR-mediated oxygen-responsive regulation of the *nrdDG* operon of *Escherichia coli*. *J Bacteriol* **185:** 5310-5313

Brown NC, Reichard P (1969a) Ribonucleoside diphosphate reductase. Formation of active and inactive complexes of proteins B1 and B2. *J Mol Biol* **46:** 25-38

Brown NC, Reichard P (1969b) Role of effector binding in allosteric control of ribonucleoside diphosphate reductase. *J Mol Biol* **46:** 39-55

Bsat N, Herbig A, Casillas-Martinez L, Setlow P, Helmann JD (1998) *Bacillus subtilis* contains multiple Fur homologues: identification of the iron uptake (Fur) and peroxide regulon (PerR) repressors. *Mol Microbiol* **29:** 189-198

Cech TR (2004) Self-splicing and enzymatic activity of an intervening sequence RNA from Tetrahymena. *Biosci Rep* **24:** 362-385

Changela A, Chen K, Xue Y, Holschen J, Outten CE, O'Halloran TV, Mondragon A (2003) Molecular basis of metal-ion selectivity and zeptomolar sensitivity by CueR. *Science* **301:** 1383-1387

Chivers PT, Sauer RT (2000) Regulation of high affinity nickel uptake in bacteria. Ni^{2+}-Dependent interaction of NikR with wild-type and mutant operator sites. *J Biol Chem* **275:** 19735-19741

Chivers PT, Sauer RT (2002) NikR repressor: high-affinity nickel binding to the C-terminal domain regulates binding to operator DNA. *Chem Biol* **9:** 1141-1148

Christianson DW (1997) Structural chemistry and biology of manganese metalloenzymes. *Prog Biophys Mol Biol* **67:** 217-252

Corbett MC, Hu Y, Fay AW, Ribbe MW, Hedman B, Hodgson KO (2006) Structural insights into a protein-bound iron-molybdenum cofactor precursor. *Proc Natl Acad Sci U S A* **103:** 1238-1243

Cotruvo JA, Jr., Stubbe J (2008) NrdI, a flavodoxin involved in maintenance of the diferric-tyrosyl radical cofactor in *Escherichia coli* class Ib ribonucleotide reductase. *Proc Natl Acad Sci U S A* **105:** 14383-14388

Cotruvo JA, Stubbe J (2010) An Active Dimanganese(III)-Tyrosyl Radical Cofactor in *Escherichia coli* Class Ib Ribonucleotide Reductase. *Biochemistry* **49:** 1297-1309

Cox N, Ho FM, Pewnim N, Steffen R, Smith PJ, Havelius KG, Hughes JL, Debono L, Styring S, Krausz E, Pace RJ (2009) The S(1) split signal of photosystem II; a tyrosine-manganese coupled interaction. *Biochim Biophys Acta* **1787:** 882-889

Cox N, Ogata H, Stolle P, Reijerse E, Auling G, Lubitz W (2010) A Tyrosyl–Dimanganese Coupled Spin System is the Native Metalloradical Cofactor of the R2F Subunit of the

Ribonucleotide Reductase of *Corynebacterium ammoniagenes*. *Journal of the American Chemical Society* **132:** 11197-11213

Curatti L, Hernandez JA, Igarashi RY, Soboh B, Zhao D, Rubio LM (2007) In vitro synthesis of the iron-molybdenum cofactor of nitrogenase from iron, sulfur, molybdenum, and homocitrate using purified proteins. *Proc Natl Acad Sci U S A* **104:** 17626-17631

Daly MJ, Gaidamakova EK, Matrosova VY, Vasilenko A, Zhai M, Venkateswaran A, Hess M, Omelchenko MV, Kostandarithes HM, Makarova KS, Wackett LP, Fredrickson JK, Ghosal D (2004) Accumulation of Mn(II) in *Deinococcus radiodurans* facilitates gamma-radiation resistance. *Science* **306:** 1025-1028

Daly MJ, Ouyang L, Fuchs P, Minton KW (1994) In vivo damage and *recA*-dependent repair of plasmid and chromosomal DNA in the radiation-resistant bacterium *Deinococcus radiodurans*. *J Bacteriol* **176:** 3508-3517

Dau H, Haumann M (2007) Eight steps preceding O-O bond formation in oxygenic photosynthesis--a basic reaction cycle of the Photosystem II manganese complex. *Biochim Biophys Acta* **1767:** 472-483

Delany I, Pacheco ABF, Spohn G, Rappuoli R, Scarlato V (2001) Iron-dependent transcription of the *frpB* gene of *Helicobacter pylori* is controlled by the *fur* repressor protein. *J Bacteriol* **183:** 4932-4937

Delany I, Rappuoli R, Scarlato V (2004) Fur functions as an activator and as a repressor of putative virulence genes in *Neisseria meningitidis*. *Mol Microbiol* **52:** 1081-1090

Dismukes GC (1996) Manganese enzymes with binuclear active sites. *Chem Rev* **96:** 2909-2926

Dixon NE, Gazzola C, Blakeley RL, Zerner B (1975) JACK-BEAN UREASE (EC 3.5.1.5) - METALLOENZYME - SIMPLE BIOLOGICAL ROLE FOR NICKEL. *Journal of the American Chemical Society* **97:** 4131-4133

Dosanjh NS, Michel SL (2006) Microbial nickel metalloregulation: NikRs for nickel ions. *Curr Opin Chem Biol* **10:** 123-130

Drechsel H, Winkelmann G (1997) *Iron Chelation and Siderophores*, Vol. 1, Amsterdam: Harwood academic publishers.

Eklund H, Uhlin U, Farnegardh M, Logan DT, Nordlund P (2001) Structure and function of the radical enzyme ribonucleotide reductase. *Prog Biophys Mol Biol* **77:** 177-268

Eriksson M, Jordan A, Eklund H (1998) Structure of *Salmonella typhimurium nrdF* ribonucleotide reductase in its oxidized and reduced forms. *Biochemistry* **37:** 13359-13369

Eriksson M, Uhlin U, Ramaswamy S, Ekberg M, Regnstrom K, Sjöberg BM, Eklund H (1997) Binding of allosteric effectors to ribonucleotide reductase protein R1: reduction of active-site cysteines promotes substrate binding. *Structure* **5:** 1077-1092

Fieschi F, Torrents E, Toulokhonova L, Jordan A, Hellman U, Barbe J, Gibert I, Karlsson M, Sjöberg BM (1998) The manganese-containing ribonucleotide reductase of *Corynebacterium ammoniagenes* is a class Ib enzyme. *J Biol Chem* **273:** 4329-4337

Finney LA, O'Halloran TV (2003) Transition metal speciation in the cell: insights from the chemistry of metal ion receptors. *Science* **300:** 931-936

Follmann H. (2001) BMBF Abschlussbericht - Förderkennzeichen 1481194. Marburg.

Follmann H (2004) Deoxyribonucleotides: the unusual chemistry and biochemistry of DNA precursors. *Chem Soc Rev* **33:** 225-233

Frey PA, Hegeman AD, Reed GH (2006) Free radical mechanisms in enzymology. *Chem Rev* **106:** 3302-3316

Furukawa Y, Torres AS, O'Halloran TV (2004) Oxygen-induced maturation of SOD1: a key role for disulfide formation by the copper chaperone CCS. *Embo J* **23:** 2872-2881

Gaballa A, Helmann JD (1998) Identification of a zinc-specific metalloregulatory protein, Zur, controlling zinc transport operons in *Bacillus subtilis*. *J Bacteriol* **180:** 5815-5821

Gaballa A, Wang T, Ye RW, Helmann JD (2002) Functional analysis of the *Bacillus subtilis zur* regulon. *J Bacteriol* **184:** 6508-6514

Ge R, Watt RM, Sun X, Tanner JA, He QY, Huang JD, Sun H (2006) Expression and characterization of a histidine-rich protein, Hpn: potential for Ni^{2+} storage in *Helicobacter pylori*. *Biochem J* **393:** 285-293

George SJ, Igarashi RY, Piamonteze C, Soboh B, Cramer SP, Rubio LM (2007) Identification of a Mo-Fe-S cluster on NifEN by Mo K-edge extended X-ray absorption fine structure. *J Am Chem Soc* **129:** 3060-3061

Griepenburg U, Blasczyk K, Kappl R, Hüttermann J, Auling G (1998) A divalent metal site in the small subunit of the manganese-dependent ribonucleotide reductase of *Corynebacterium ammoniagenes*. *Biochemistry* **37:** 7992-7996

Griepenburg U, Lassmann G, Auling G (1996) Detection of a stable free radical in the B2 subunit of the manganese ribonucleotide reductase (Mn-RRase) of *Corynebacterium ammoniagenes*. *Free Radic Res* **24:** 473-481

Grotzinger J, Jordan TH, Press F, Siever R (2007) *Press/Siever - Allgemeine Geologie*, Vol. 5, Heidelberg: Spektrum Akademischer Verlag.

Guedon E, Moore CM, Que Q, Wang T, Ye RW, Helmann JD (2003) The global transcriptional response of *Bacillus subtilis* to manganese involves the MntR, Fur, TnrA and sigmaB regulons. *Mol Microbiol* **49:** 1477--1491

Haddy A (2007) EPR spectroscopy of the manganese cluster of photosystem II. *Photosynth Res* **92:** 357-368

Hantke K (2001) Iron and metal regulation in bacteria. *Curr Opin Microbiol* **4:** 172-177

Havelius KG, Su JH, Feyziyev Y, Mamedov F, Styring S (2006) Spectral resolution of the split EPR signals induced by illumination at 5 K from the S1, S3, and S0 states in photosystem II. *Biochemistry* **45:** 9279-9290

Herbig AF, Helmann JD (2001) Roles of metal ions and hydrogen peroxide in modulating the interaction of the *Bacillus subtilis* PerR peroxide regulon repressor with operator DNA. *Mol Microbiol* **41:** 849-859

Hernandez JA, Igarashi RY, Soboh B, Curatti L, Dean DR, Ludden PW, Rubio LM (2007) NifX and NifEN exchange NifB cofactor and the VK-cluster, a newly isolated intermediate of the iron-molybdenum cofactor biosynthetic pathway. *Mol Microbiol* **63:** 177-192

Hidalgo A, Betancor L, Moreno R, Zafra O, Cava F, Fernandez-Lafuente R, Guisan JM, Berenguer J (2004) *Thermus thermophilus* as a cell factory for the production of a thermophilic Mn-dependent catalase which fails to be synthesized in an active form in *Escherichia coli*. *Appl Environ Microbiol* **70:** 3839-3844

Högbom M, Huque Y, Sjöberg B-M, Nordlund P (2002) Crystal structure of the di-iron/radical protein of ribonucleotide reductase from *Corynebacterium ammoniagenes*. *Biochemistry* **41:** 1381-1389

Högbom M, Stenmark P, Voevodskaya N, McClarty G, Graslund A, Nordlund P (2004) The radical site in chlamydial ribonucleotide reductase defines a new R2 subclass. *Science* **305:** 245-248

Hu Y, Corbett MC, Fay AW, Webber JA, Hodgson KO, Hedman B, Ribbe MW (2006a) FeMo cofactor maturation on NifEN. *Proc Natl Acad Sci U S A* **103:** 17119-17124

Hu Y, Corbett MC, Fay AW, Webber JA, Hodgson KO, Hedman B, Ribbe MW (2006b) Nitrogenase Fe protein: A molybdate/homocitrate insertase. *Proc Natl Acad Sci U S A* **103:** 17125-17130

Huber C, Wachtershauser G (1997) Activated acetic acid by carbon fixation on (Fe,Ni)S under primordial conditions. *Science* **276:** 245-247

Huque Y, Fieschi F, Torrents E, Gibert I, Eliasson R, Reichard P, Sahlin M, Sjöberg BM (2000) The active form of the R2F protein of class Ib ribonucleotide reductase from *Corynebacterium ammoniagenes* is a diferric protein. *J Biol Chem* **275:** 25365-25371

Irving H, Williams RJP (1948) Order of Stability of Metal Complexes. *Nature* **162:** 746-747

Iwig JS, Rowe JL, Chivers PT (2006) Nickel homeostasis in *Escherichia coli*; the *rcnR-rcnA* efflux pathway and its linkage to NikR function. *Mol Microbiol* **62:** 252-262

Jakubovics NS, Jenkinson HF (2001) Out of the iron age: new insights into the critical role of manganese homeostasis in bacteria. *Microbiology* **147:** 1709-1718

Jakubovics NS, Valentine RA (2009) A new direction for manganese homeostasis in bacteria: identification of a novel efflux system in *Streptococcus pneumoniae*. *Mol Microbiol* **72:** 1-4

Jiang W, Hoffart LM, Krebs C, Bollinger JM, Jr. (2007a) A manganese(IV)/iron(IV) intermediate in assembly of the manganese(IV)/iron(III) cofactor of *Chlamydia trachomatis* ribonucleotide reductase. *Biochemistry* **46:** 8709-8716

Jiang W, Yun D, Saleh L, Barr EW, Xing G, Hoffart LM, Maslak MA, Krebs C, Bollinger JM, Jr. (2007b) A manganese(IV)/iron(III) cofactor in *Chlamydia trachomatis* ribonucleotide reductase. *Science* **316:** 1188-1191

Jitrapakdee S, Nezic MG, Cassady AI, Khew-Goodall Y, Wallace JC (2002) Molecular cloning and domain structure of chicken pyruvate carboxylase. *Biochem Biophys Res Commun* **295:** 387-393

Jordan A, Pontis E, Aslund F, Hellman U, Gibert I, Reichard P (1996) The ribonucleotide reductase system of *Lactococcus lactis*. Characterization of an NrdEF enzyme and a new electron transport protein. *J Biol Chem* **271:** 8779-8785

Jordan A, Pontis E, Atta M, Krook M, Gibert I, Barbe J, Reichard P (1994) A second class I ribonucleotide reductase in Enterobacteriaceae: characterization of the *Salmonella typhimurium* enzyme. *Proc Natl Acad Sci U S A* **91:** 12892-12896

Jordan A, Reichard P (1998) Ribonucleotide reductases. *Annu Rev Biochem* **67:** 71-98

Kanyo ZF, Scolnick LR, Ash DE, Christianson DW (1996) Structure of a unique binuclear manganese cluster in arginase. *Nature* **383:** 554-557

Kennedy M, Yu L, Lima MJ, Ascenso CS, Czaja C, Moura I, Moura JJG, Rusnak F (1998) Metal binding to the tetrathiolate motif of desulforedoxin and related polypeptides. *J Biol Inorg Chem* **3:** 643-649

Khalimonchuk O, Rodel G (2005) Biogenesis of cytochrome c oxidase. *Mitochondrion* **5:** 363-388

Khangulov SV, Gladyshev VN, Dismukes GC, Stadtman TC (1998) Selenium-containing formate dehydrogenase H from *Escherichia coli*: a molybdopterin enzyme that catalyzes formate oxidation without oxygen transfer. *Biochemistry* **37:** 3518-3528

Kok B, Forbush B, McGloin M (1970) Cooperation of charges in photosynthetic O_2 evolution-I. A linear four step mechanism. *Photochem Photobiol* **11:** 457-475

Koulougliotis D, Teutloff C, Sanakis Y, Lubitz W, Petrouleas V (2004) *Phys Chem Chem Phys* **6:** 4859-4863

Kranz RG, Richard-Fogal C, Taylor JS, Frawley ER (2009) Cytochrome c biogenesis: mechanisms for covalent modifications and trafficking of heme and for heme-iron redox control. *Microbiol Mol Biol Rev* **73:** 510-528, Table of Contents

Larsson A, Climent I, Nordlund P, Sahlin M, Sjöberg BM (1996) Structural and functional characterization of two mutated R2 proteins of *Escherichia coli* ribonucleotide reductase. *Eur J Biochem* **237:** 58-63

Licht S, Gerfen GJ, Stubbe J (1996) Thiyl radicals in ribonucleotide reductases. *Science* **271:** 477-481

Logan DT, Andersson J, Sjöberg BM, Nordlund P (1999) A glycyl radical site in the crystal structure of a class III ribonucleotide reductase. *Science* **283:** 1499-1504

May JJ, Wendrich TM, Marahiel MA (2001) The *dhb* operon of *Bacillus subtilis* encodes the biosynthetic template for the catecholic siderophore 2,3-dihydroxybenzoate-glycine-threonine trimeric ester bacillibactin. *Journal of Biological Chemistry* **276:** 7209-7217

McEvoy JP, Gascon JA, Batista VS, Brudvig GW (2005) The mechanism of photosynthetic water splitting. *Photochem Photobiol Sci* **4:** 940-949

McHugh JP, Rodriguez-Quinones F, Abdul-Tehrani H, Svistunenko DA, Poole RK, Cooper CE, Andrews SC (2003) Global iron-dependent gene regulation in *Escherichia coli*. A new mechanism for iron homeostasis. *J Biol Chem* **278:** 29478-29486

Merchant S, Dreyfuss BW (1998) POSTTRANSLATIONAL ASSEMBLY OF PHOTOSYNTHETIC METALLOPROTEINS. *Annu Rev Plant Physiol Plant Mol Biol* **49:** 25--51

Monje-Casas F, Jurado J, Prieto-Alamo MJ, Holmgren A, Pueyo C (2001) Expression analysis of the *nrdHIEF* operon from *Escherichia coli*. Conditions that trigger the transcript level in vivo. *J Biol Chem* **276:** 18031-18037

Moore CM, Helmann JD (2005) Metal ion homeostasis in *Bacillus subtilis*. *Curr Opin Microbiol* **8:** 188-195

Moore CM, Nakano MM, Wang T, Ye RW, Helmann JD (2004) Response of *Bacillus subtilis* to nitric oxide and the nitrosating agent sodium nitroprusside. *J Bacteriol* **186:** 4655-4664

Mulliez E, Ollagnier S, Fontecave M, Eliasson R, Reichard P (1995) Formate is the hydrogen donor for the anaerobic ribonucleotide reductase from *Escherichia coli*. *Proc Natl Acad Sci U S A* **92:** 8759-8762

Mulrooney SB, Hausinger RP (2003a) Metal ion dependence of recombinant *Escherichia coli* allantoinase. *J Bacteriol* **185:** 126-134

Mulrooney SB, Hausinger RP (2003b) Nickel uptake and utilization by microorganisms. *FEMS Microbiol Rev* **27:** 239-261

Nelson N, Ben-Shem A (2005) The structure of photosystem I and evolution of photosynthesis. *Bioessays* **27:** 914-922

Nordlund P, Reichard P (2006) Ribonucleotide reductases. *Annu Rev Biochem* **75:** 681-706

Nordlund P, Sjöberg BM, Eklund H (1990) Three-dimensional structure of the free radical protein of ribonucleotide reductase. *Nature* **345:** 593--598

Nygaard P (1993) Purine and Pyrimidine Salvage Pathways. *Bacillus Subtilis and Other Gram-Positive Bacteria: Biochemistry, Physiology, and Molecular Genetics*: 359-378

Oehlmann W (1998) Klonierung der Gene der Ribonucleotid Reduktasen von *Corynebacterium ammoniagenes* und *Corynebacterium glutamicum*. *Dissertation*

Ogata H, Stolle P, Stehr M, Auling G, Lubitz W (2009) Crystallization and preliminary X-ray analysis of the small subunit (R2F) of native ribonucleotide reductase from *Corynebacterium ammoniagenes*. *Acta Crystallogr Sect F Struct Biol Cryst Commun* **65:** 878-880

Paik JE, Lee BR (2003) Isolation of transcription initiation signals from *Corynebacterium ammoniagenes* and comparison of their gene expression levels in *C. ammoniagenes* and *Escherichia coli*. *Biotechnol Lett* **25:** 1311-1316

Pal BC, Regan JD, Hamilton FD (1975) Separation of bases, ribonucleosides and deoxyribonucleosides by anion-exclusion and partition chromatography on cation-exchange resin: application to the assay of ribonucleotide reductase, deaminase and nucleosidase. *Anal Biochem* **67:** 625-633

Panagou D, Orr MD, Dunstone JR, Blakley RL (1972) A monomeric, allosteric enzyme with a single polypeptide chain. Ribonucleotide reductase of *Lactobacillus leichmannii*. *Biochemistry* **11:** 2378-2388

Pelmenschikov V, Cho KB, Siegbahn PE (2004) Class I ribonucleotide reductase revisited: the effect of removing a proton on Glu441. *J Comput Chem* **25:** 311-321

Pirson A (1937) Ernährungs- und stoffwechselphysiologische Untersuchungen an Fontinalis und Chlorella. *Z Bot* **31:** 193-267

Pufahl RA, Singer CP, Peariso KL, Lin SJ, Schmidt PJ, Fahrni CJ, Culotta VC, Penner-Hahn JE, O'Halloran TV (1997) Metal ion chaperone function of the soluble Cu(I) receptor Atx1. *Science* **278:** 853-856

Que Q, Helmann JD (2000) Manganese homeostasis in *Bacillus subtilis* is regulated by MntR, a bifunctional regulator related to the diphtheria toxin repressor family of proteins. *Mol Microbiol* **35:** 1454-1468

Reichard P (1993) From RNA to DNA, why so many ribonucleotide reductases? *Science* **260:** 1773-1777

Reichard P (2010) Ribonucleotide reductases: substrate specificity by allostery. *Biochem Biophys Res Commun* **396:** 19-23

Renger G, Renger T (2008) Photosystem II: The machinery of photosynthetic water splitting. *Photosynth Res* **98:** 53-80

Rigby Duncan KE, Stillman MJ (2006) Metal-dependent protein folding: metallation of metallothionein. *J Inorg Biochem* **100:** 2101-2107

Riggs-Gelasco PJ, Mei R, Penner-Hahn JE (1995) Structural characterization of manganese redox enzymes - Results from X-ray absorption spectroscopy. In *Mechanistic Bioinorganic Chemistry*, Thorp HH, Pecoraro VL (eds), Vol. 246, pp 219-248. Washington: Amer Chemical Soc

Rodrigue A, Effantin G, Mandrand-Berthelot MA (2005) Identification of *rcnA* (*yohM*), a nickel and cobalt resistance gene in *Escherichia coli*. *J Bacteriol* **187:** 2912-2916

Roshick C, Iliffe-Lee ER, McClarty G (2000) Cloning and characterization of ribonucleotide reductase from *Chlamydia trachomatis*. *J Biol Chem* **275:** 38111-38119

Rouhier N, Couturier J, Johnson MK, Jacquot JP (2010) Glutaredoxins: roles in iron homeostasis. *Trends Biochem Sci* **35:** 43-52

Rubio LM, Ludden PW (2008) Biosynthesis of the iron-molybdenum cofactor of nitrogenase. *Annu Rev Microbiol* **62:** 93-111

Schleif R (1988) DNA binding by proteins. *Science* **241:** 1182-1187

Schneider R, Hantke K (1993) Iron-Hydroxamate Uptake Systems in *Bacillus subtilis* - Identification of a Lipoprotein as Part of a Binding Protein-Dependent Transport-System. *Mol Microbiol* **8:** 111-121

Sharp RE, Chapman SK (1999) Mechanisms for regulating electron transfer in multi-centre redox proteins. *Biochim Biophys Acta* **1432:** 143-158

Sheats JE, Czernuszewicz RS, Dismukes GC, Rheingold AL, Petrouleas V, Stubbe J, Armstrong WH, Beer RH, Lippard SJ (1987) Binuclear manganese(III) complexes of potential biological significance. *Journal of the American Chemical Society* **109:** 1435-1444

Sjöberg B-M (1997) Ribonucleotide reductases - a group of enzymes with different metallosites and a similar reaction mechanism. *Structure & Bonding* **88:** 139-173

Soboh B, Igarashi RY, Hernandez JA, Rubio LM (2006) Purification of a NifEN protein complex that contains bound molybdenum and a FeMo-Co precursor from an *Azotobacter vinelandii* Delta*nifHDK* strain. *J Biol Chem* **281:** 36701-36709

Sofia HJ, Chen G, Hetzler BG, Reyes-Spindola JF, Miller NE (2001) Radical SAM, a novel protein superfamily linking unresolved steps in familiar biosynthetic pathways with radical mechanisms: functional characterization using new analysis and information visualization methods. *Nucleic Acids Res* **29:** 1097-1106

Stehr M, Schneider G, Aslund F, Holmgren A, Lindqvist Y (2001) Structural basis for the thioredoxin-like activity profile of the glutaredoxin-like NrdH-redoxin from *Escherichia coli. J Biol Chem* **276:** 35836-35841

Stolle P, Barckhausen O, Oehlmann W, Knobbe N, Vogt C, Pierik AJ, Cox N, Schmidt PP, Reijerse EJ, Lubitz W, Auling G (2010a) Homologous expression of the *nrdF* gene of *Corynebacterium ammoniagenes* strain ATCC 6872 generates a manganese-metallocofactor (R2F) and a stable tyrosyl radical (Y(*)) involved in ribonucleotide reduction. *FEBS J* **277:** 4849-4862

Stolle P, Nitzsche T, Auling G (2010b) Studies on potential drug targets in Gram-positive bacteria – a manganese Metallo-cofactor in the native Ribonucleotide Reductase (RNR) from *Bacillus subtilis. Gemeinsame Jahrestagung der Vereinigung für Allgemeine und Angewandte Mikrobiologie (VAAM) und Deutsche Gesellschaft für Hygiene und Mikrobiologie eV (DGHM)* **Abstractband:** 30

Stubbe J (2003) Di-iron-tyrosyl radical ribonucleotide reductases. *Curr Opin Chem Biol* **7:** 183-188

Stubbe J, Ator M, Krenitsky T (1983) Mechanism of ribonucleoside diphosphate reductase from *Escherichia coli*. Evidence for 3'-C--H bond cleavage. *J Biol Chem* **258:** 1625-1631

Stubbe J, Nocera DG, Yee CS, Chang MC (2003) Radical initiation in the class I ribonucleotide reductase: long-range proton-coupled electron transfer? *Chem Rev* **103:** 2167-2201

Stubbe J, Riggs-Gelasco P (1998) Harnessing free radicals: formation and function of the tyrosyl radical in ribonucleotide reductase. *Trends Biochem Sci* **23:** 438-443

Stubbe J, van Der Donk WA (1998) Protein Radicals in Enzyme Catalysis. *Chem Rev* **98:** 705-762

Su JH, Havelius KG, Ho FM, Han G, Mamedov F, Styring S (2007) Formation spectra of the EPR split signals from the S0, S1, and S3 states in photosystem II induced by monochromatic light at 5 K. *Biochemistry* **46:** 10703-10712

Sumner JB (1926) The Isolation and Crystallaization of the Enzyme Urease: Preliminary Paper. *J Biol Chem* **69:** 435-441

Tamarit J, Gerez C, Meier C, Mulliez E, Trautwein A, Fontecave M (2000) The activating component of the anaerobic ribonucleotide reductase from *Escherichia coli*. An iron-sulfur center with only three cysteines. *J Biol Chem* **275:** 15669-15675

Torrents E, Aloy P, Gibert I, Rodriguez-Trelles F (2002) Ribonucleotide reductases: divergent evolution of an ancient enzyme. *J Mol Evol* **55:** 138-152

Torrents E, Grinberg I, Gorovitz-Harris B, Lundstrom H, Borovok I, Aharonowitz Y, Sjöberg BM, Cohen G (2007) NrdR controls differential expression of the *Escherichia coli* ribonucleotide reductase genes. *J Bacteriol* **189:** 5012-5021

Torrents E, Roca I, Gibert I (2003) *Corynebacterium ammoniagenes* class Ib ribonucleotide reductase: transcriptional regulation of an atypical genomic organization in the *nrd* cluster. *Microbiology* **149:** 1011-1020

Torrents E, Sjöberg BM (2010) Antibacterial activity of radical scavengers against class Ib ribonucleotide reductase from *Bacillus anthracis*. *Biol Chem* **391:** 229-234

Tottey S, Harvie DR, Robinson NJ (2005) Understanding how cells allocate metals using metal sensors and metallochaperones. *Acc Chem Res* **38:** 775-783

Waldron KJ, Rutherford JC, Ford D, Robinson NJ (2009) Metalloproteins and metal sensing. *Nature* **460:** 823-830

Watson J (1987) Evolution of catalytic function. In *Cold Spring Harbor Symposia on Quantitative Biology*, Watson J (ed), p 955pp.

Whittaker JW (2010) Metal uptake by manganese superoxide dismutase. *Biochim Biophys Acta* **1804:** 298-307

Wieghardt K, Bossek U, Ventur D, Weiss J (1985) Assembly and structural characterization of binuclear μ-oxo-di-μ-acetato bridged complexes of manganese(III). Analogues of the di-iron(III) center in hemerythrin. *J Chem Soc*: 347-349

Willing A, Follmann H, Auling G (1988a) Nucleotide and thioredoxin specificity of the manganese ribonucleotide reductase from *Brevibacterium ammoniagenes*. *Eur J Biochem* **175:** 167--173

Willing A, Follmann H, Auling G (1988b) Ribonucleotide reductase of *Brevibacterium ammoniagenes* is a manganese enzyme. *Eur J Biochem* **170:** 603-611

Yamashita MM, Almassy RJ, Janson CA, Cascio D, Eisenberg D (1989) Refined atomic model of glutamine synthetase at 3.5 A resolution. *J Biol Chem* **264:** 17681-17690

Zhao D, Curatti L, Rubio LM (2007) Evidence for *nifU* and *nifS* participation in the biosynthesis of the iron-molybdenum cofactor of nitrogenase. *J Biol Chem* **282:** 37016-37025

Zheng L, White RH, Cash VL, Jack RF, Dean DR (1993) Cysteine desulfurase activity indicates a role for NIFS in metallocluster biosynthesis. *Proc Natl Acad Sci U S A* **90:** 2754--2758

Publikationsverzeichnis

STOLLE, P., Barckhausen, O., Oehlmann, W., Knobbe, N., Vogt, C., Pierik, A., Schmidt, P.P., Reijerse, E.J., Lubitz, W., Auling, G. Homologous Expression of the *nrdF* Gene of *Corynebacterium ammoniagenes* Strain ATCC 6872 generates a Manganese-Metallocofactor (R2F) and a Stable Tyrosyl Radical (Y·) involved in Ribonucleotide Reduction. FEBS J. 2010 Dec;277(23):4849-486. PMID: 20977673

Cox, N., Ogata, H., STOLLE,P., Reijerse, E., Pierik, A., Auling, G., Lubitz, W. The Native Metalloradical Complex of the Ribonucleotide Reductase in *Corynebacterium ammoniagenes*: Evidence of a Tyrosyl-Dimanganese Coupled Spin System. J Am Chem Soc. 2010 Aug 18;132(32):11197-213. PMID: 20698687

Ogata, H., STOLLE, P., Stehr, M., Auling, G. and Lubitz, W. Crystallization and preliminary X-ray analysis of the native small subunit (R2F) of ribonucleotide reductase from *Corynebacterium ammoniagenes*. Acta Crystallogr Sect F Struct Biol Cryst Commun. 2009 Sep 1;65(Pt 9):878-80. PMID: 19724122

Abbouni, B., Oehlmann,W., STOLLE, P., Pierik A.J. and Auling, G. Electron paramagnetic resonance (EPR) spectroscopy of the stable-free radical in the native metallo-cofactor of the manganese-ribonucleotide reductase (Mn-RNR) of *Corynebacterium glutamicum*. Free Radic Res. 2009 Aug 25:1-8. PMID: 19707921

STOLLE, P. (2007) „Anreicherung coryneformer Ribonucleotid-Reduktasen nach gentechnischer Überproduktion aus *Corynebacterium ammoniagenes* pOCA2". Diplomarbeit, Leibniz Universität Hannover

Tagungsbeiträge

Vorträge

STOLLE, P.*, Reijerse, E.J., Lubitz, W., Auling, G. (2008) Highfield-EPR (244 GHz) of a New Type of Tyrosyl-Manganese (II) Radical-Metal Center. Joint Annual Conference of the Association for General and Applied Microbiology and the German Society for Biochemistry and Molecular Biology, Frankfurt am Main, Deutschland.

STOLLE, P., Auling, G. (2007) Biophysical characterization of the unique Ribonucleotide Reductase from *C. ammoniagenes* – an EXAFS approach. BIOXAS-Workshop, EMBL-Outstation, Deutsches Elektronen-Synchrotron DESY, Hamburg, Deutschland.

Abstracts

STOLLE, P.*, Nitzsche, T., Auling, G. (2010) Studies on potential drug targets in Gram-positive bacteria – a manganese Metallo-cofactor in the native Ribonucleotide Reductase (RNR) from *Bacillus subtilis*. Gemeinsame Jahrestagung der Vereinigung für Allgemeine und Angewandte Mikrobiologie (VAAM) und Deutsche Gesellschaft für Hygiene und Mikrobiologie e.V. (DGHM), Hannover, Deutschland.

Cox, N., Ogata, H., STOLLE, P., Reijerse, E., Auling, G., Lubitz, W. (2010) A Tyrosyl-Dimanganese Coupled Spin System in Ribonucleotide Reductase of *C. ammoniagenes* Studied by Multifrequency EPR Spectroscopy and X-ray Chrystallography. Multi-Frequency EPR: A Perspective for the Biosciences. Lorentz Center, Leiden, Niederlande.

Nick Cox, Hideaki Ogata, Peter Paul Schmidt, Edward Reijerse, Wolfgang Lubitz, PATRICK STOLLE, Georg Auling (2010) The Native Metalloradical Complex of the RNR in *Corynebacterium ammoniagenes*: Evidence for a Tyrosyl-Dimanganese Coupled Spin System. Fachbeiratkonferenz des Max Planck Instituts für Bioanorganische Chemie, Mülheim a. d. Ruhr, Deutschland.

Hideaki Ogata, PATRICK STOLLE, Matthias Stehr, Georg Auling and Wolfgang Lubitz (2010) Protein Crystallography III, MAD Methods Revealed a Di-Manganese Cluster in the Native Ribonucleotide Reductase R2F Small Subunit of *Corynebacterium ammoniagenes*. Fachbeiratkonferenz des Max Planck Instituts für Bioanorganische Chemie, Mülheim a. d. Ruhr, Deutschland.

Gomaa, M., STOLLE, P., Dräger, G., Auling, G. (2009) Separation and Characterization of Pumilacidin Isoforms Produced by *Bacillus pumilus*. Joint Annual Conference of the Association for General and Applied Microbiology and the German Society for Biochemistry and Molecular Biology, Dortmund, Deutschland.

Rathmann, C., Herrmann, M., STOLLE, P., Ackermann, M., Pust, J., Auling, G. (2009) Influence of lake trophic status on pelagic microbial community composition and microbial and viral abundance. Joint Annual Conference of the Association for General and Applied Microbiology and the German Society for Biochemistry and Molecular Biology, Dortmund, Deutschland.

Rathmann, C., STOLLE, P., Auling, G. (2008) Microbial Ecology Revised due to New Methods for Quantification of Bacteriophages. RAISEBIO-HIGRADE Summerschool, Chemicals in Soil: Interactions, Availability and Residue Formation, Leibzig, Deutschland.

Erklärung zur vorliegenden Dissertation

Gemäß §6(1) der Promotionsordnung der Naturwissenschaftlichen Fakultät der Gottfried Wilhelm Leibniz Universität Hannover für die Promotion zum Dr. rer. nat.

Hierdurch erkläre ich, dass ich meine Dissertation mit dem Titel

Nachweis eines neuartigen Tyrosyl–$Mn^{III}Mn^{III}$ gekoppelten Spinsystems in der Mn-Ribonucleotid-Reduktase von *Corynebacterium ammoniagenes* und *Corynebacterium glutamicum*

selbständig verfasst und die benutzten Hilfsmittel und Quellen sowie gegebenenfalls zu Hilfeleistungen herangezogenen Institutionen vollständig angegeben habe.

Die Dissertation wurde nicht schon als Masterarbeit, Diplomarbeit oder andere Prüfungsarbeit verwendet.

Hannover, den 15. Juni 2010

_____

Patrick Stolle

Patrick Stolle

Gottfried Wilhelm Leibniz Universität Hannover
Naturwissenschaftliche Fakultät
Institut für Mikrobiologie
Schneiderberg 50
D-30167 Hannover
Telefon : +49 (0) 511 762 4792
Fax : +49 (0) 511 762 5287
E-Mail : patrick.stolle@ifmb.uni-hannover.de

Studium / Wissenschaftliche Qualifizierung

Seit 09/2010	Projektleiter der gentechnischen Anlagen Institut für Mikrobiologie, LUH	30167 Hannover
07/2009 – 08/2010	Beauftragter für biologische Sicherheit Institut für Mikrobiologie, LUH	30167 Hannover
Seit 10/2008	Strahlenschutzbeauftragter Institut für Mikrobiologie, LUH	30167 Hannover
10/2008	Fachkunde 4.1 Strahlenschutz Gewerbeaufsichtsamt Hannover	30177 Hannover
09/2008	FB-Lehrgang - Gene Technology, Biosafety and Biosecurity Dept. for Biosafety, Medizinische Hochschule (MHH)	30625 Hannover
11/2007	Strahlenschutzlehrgang (4.1) Zentrum für Strahlenschutz und Radioökologie, LUH	30167 Hannover
07/2007	BioXAS Workshop EMBL Outstation & DESY	22607 Hamburg
06/2005	FELASA Kategorie C Stiftung Tierärztliche Hochschule	30559 Hannover
09 - 11/2005	Laborpraktikum Institut für Mikrobiologie, LUH	30167 Hannover
05/2005 - 07/2005	Laborpraktikum Institut für med. Mikrobiologie, MHH	30625 Hannover
10/2001 - 02/2007	Abgeschlossenes Biologiestudium Fachprüfungen in Mikrobiologie, Biophysik & Versuchstierkunde Thema der Diplomarbeit: „Anreicherung coryneformer Ribonucleotid-Reduktasen nach gentechnischer Überproduktion aus *Corynebacterium ammoniagenes* pOCA2“ Leibniz Universität Hannover	30167 Hannover
08/1992 - 05/1999	Gymnasium, Abitur Ratsgymnasium	31655 Stadthagen